UNIVERSIDADE DE SÃO PAULO
FACULDADE DE ZOOTECNIA E ENGENHARIA DE ALIMENTOS

GISELLE VALLIM CORRÊA RAMOS

Modificação dupla do amido de mandioca para estabilização de emulsões de *Pickering* e produção de géis carregados: sistemas de encapsulação de curcumina à base de amido

Pirassununga
2023

GISELLE VALLIM CORRÊA RAMOS

Modificação dupla do amido de mandioca para estabilização de emulsões de *Pickering* e produção de géis carregados: sistemas de encapsulação de curcumina à base de amido

(Versão Corrigida)

Tese de doutorado apresentado à Faculdade de Zootecnia e Engenharia de Alimentos da Universidade de São Paulo, como requisito para obtenção do título de Doutora no programa de Ciências e Engenharia de Materiais

Área de Concentração: Desenvolvimento, caracterização e aplicação de materiais voltados à agroindústria.

Orientadora: Profa. Dra. Izabel Cristina Freitas Moraes

Pirassununga

2023

Ficha catalográfica elaborada pelo
Serviço de Biblioteca e Informação, FZEA/USP,
com os dados fornecidos pelo(a) autor(a)

Ramos, Giselle Vallim Correa
R175m Modificação dupla do amido de mandioca para estabilização de emulsões de Pickering e produção de géis carregados / Giselle Vallim Correa Ramos ; orientadora Izabel Cristina Freitas Moraes. -- Pirassununga, 2023.
156 f.

Tese (Doutorado - Programa de Pós-Graduação em Engenharia e Ciência de Materiais) -- Faculdade de Zootecnia e Engenharia de Alimentos, Universidade de São Paulo.

1. amido. 2. emulsões Pickering. 3. géis carregados de emulsão. 4. curcumina. 5. nanoprecipitação. I. Moraes, Izabel Cristina Freitas , orient. II. Título.

Autor: Giselle Vallim Corrêa Ramos

Título: Modificação dupla do amido de mandioca para estabilização de emulsões de *Pickering* e produção de géis carregados: sistemas de encapsulação de curcumina à base de amido

Natureza: Tese de doutorado apresentado à Faculdade de Zootecnia e Engenharia de Alimentos da Universidade de São Paulo, como requisito para obtenção do título de Doutora no programa de Ciências e Engenharia de Materiais. Área de Concentração: Desenvolvimento, caracterização e aplicação de materiais voltados à agroindústria.

Data da aprovação: 11/10/2023

Banca examinadora:

Profª. Drª. Izabel Cristina Freitas Moraes
Instituição: Faculdade de Zootecnia e Engenharia de Alimentos (FZEA/USP)
Presidente da Banca Examinadora

Profª. Drª. Samantha Cristina de Pinho
Instituição: Faculdade de Zootecnia e Engenharia de Alimentos (FZEA/USP)

Profª. Drª Maria Teresa Pedrosa Silva Clerici
Universidade Estadual de Campinas (FEA/UNICAMP)

Prof. Dr Germán Ayala Valencia
Universidade Federal de Santa Catarina (UFSC)

Drª Jéssica Thaís do Prado Silva
Instituição: Faculdade de Zootecnia e Engenharia de Alimentos (FZEA/USP)

Agradecimentos

Agradeço primeiramente a Deus, por guiar meus caminhos.

À professora Izabel Cristina Freitas Moraes por toda a orientação nesses anos de pós-graduação (mestrado e doutorado), pela amizade e pela confiança para a realização desta tese. Ao professor Paulo José do Amaral Sobral, professora Samantha Cristina de Pinho, professora Milena Martelli Tosi e professora Alessandra Lopes de Oliveira, que permitiram a realização de parte dos experimentos em seus laboratórios e pelo uso de equipamentos fundamentais à realização deste trabalho.

Aos laboratórios de Tecnologia de Alimentos (LTA/ZEA), Laboratório de Análise de Alimentos (Bromatologia/ZAZ) e Laboratório de Multiusuários de Caracterização de Materiais (ZEB) da Faculdade de Zootecnia e Engenharia de Alimentos (USP) pelo uso de equipamentos e realização de análises. Ao Instituto Nacional de Ciência e Tecnologia de Fotônica Aplicada à Biologia Celular (INFABIC), ao Laboratório de Engenharia de Processos (LEP) e ao Laboratório de Desenvolvimento de Processos Biotecnológicos da Universidade Estadual de Campinas (UNICAMP), pelo uso de equipamentos, bem como pelo apoio e auxílio técnico.

Ao Departamento de Engenharia de Alimentos (ZEA) e ao Laboratório de Tecnologia de Biopolímeros (BIOPOLITEC), pela disponibilização do laboratório e da área para realização da fase experimental deste trabalho.

Aos técnicos, Alan Cleber Borim, Marcelo Thomazini, Nilson Ferreira, Ana Mônica Bittante, Rodrigo Vinicius Lourenço e Carla Alves Monaco Lourenço pela colaboração em diferentes análises e no auxílio do uso de equipamentos.

Aos meus amigos, Lía Velásquez Castillo, Santiago López, Yves Souza Santos, Jéssica Thais do Prado Silva, Júlio Souza e Deyvisson Rocha, pela troca de experiências e momentos de descontração e amizade, que certamente me tornaram mais forte durante essa jornada.

À minha família, em especial ao meu esposo Paulo, por toda a paciência, carinho e apoio incondicional em todos os momentos, aos meus pais Celina e Edson, pela minha formação pessoal e por sempre apoiarem minhas decisões, aos meus sogros Dona Dita e Sr. Sebastião pela compreensão e incentivo

sempre que precisei e aos meus filhos de 4 patas, Frodo e Amy, pelos momentos de carinho e diversão incansáveis.

Ao projeto CAPES pelo apoio financeiro para a realização desta pesquisa. O presente trabalho foi realizado com apoio da Coordenação de Aperfeiçoamento de Pessoal de Nível Superior – Brasil (CAPES) – Código de Financiamento 001.

“There can be no triumph without loss. No victory without suffering. No freedom without sacrifice.”

J.R.R. Tolkien

RESUMO

RAMOS, G. V. C. **Modificação dupla do amido de mandioca para estabilização de emulsões de *Pickering* e produção de géis carregados: sistemas de encapsulação de curcumina à base de amido.** 2023. 156 f. Tese de doutorado – Faculdade de Zootecnia e Engenharia de Alimentos, Universidade de São Paulo, Pirassununga, 2023.

Os géis carregados com emulsão (EFG) representam uma classe inovadora e promissora de materiais, capazes de encapsular bioativos lipofílicos e hidrofóbicos em sua matriz. Porém, é importante ressaltar que há pouca literatura relacionada ao estudo deste biomaterial, principalmente quando se considera a utilização da emulsão *Pickering* nas formulações de EFG. Assim, os objetivos deste estudo foram o desenvolvimento e caracterização de gel à base de amido de quinoa carregado com emulsão *Pickering*, visando o encapsulamento da curcumina. Os amidos de mandioca nativos e modificados, por meio de tratamento de calor e umidade (HMT) ou ultrassom (US), foram empregados para a produção de nanopartículas de amido (SNP) pelo método antissolvente. As SNP obtidas de amido nativo (NSNP) e amidos modificados por HMT (HSNP) ou US (USNP) foram caracterizadas e avaliadas como agentes estabilizantes na produção de emulsões *Pickering*. A microscopia eletrônica de varredura (MEV) mostrou que as SNP obtidas dos amidos modificados (HSNP ou USNP) apresentaram formato de placa com superfícies rugosas. As partículas apresentaram tamanhos menores (~63-674 nm) para o HSNP em comparação com o NSNP e o USNP. O potencial zeta (-1,4 a -3,4 mV) e os valores de cristalinidade relativa (2,2 – 3,7%) foram baixos, com estrutura tipo V. A baixa cristalinidade das SNP foi confirmada através de análise de espectroscopia no infravermelho (FTIR) e análise térmica (DSC). As medidas de capacidade de absorção de óleo e ângulo de contato demonstraram aumento na hidrofobicidade das SNP após a modificação do amido, seguindo ordem crescente (NSNP<USNP<HSNP). Nas condições de processo aplicadas na produção de SNP, apenas o HSNP (4% em massa) foi capaz de estabilizar a emulsão (7 dias, 20 ºC). As NSNP e USNP, nesta concentração, apresentaram separação de

fases. A emulsão estabilizada com 4 g de HSNP/100 g de emulsão foi escolhida para encapsulamento de curcumina. O valor da tensão interfacial para sistemas com e sem curcumina foi de ~40 mN/m e atingiu o equilíbrio rapidamente. O potencial zeta das emulsões foi baixo (-5,39 mV) indicando baixa atividade das partículas. O CSLM mostrou a presença de partículas na interface das gotas, sugerindo que as partículas foram adsorvidas na interface óleo-água. As análises de distribuição de tamanho de gotas, índice de cremeação e viscosidade aparente indicaram que as emulsões de *Pickering* carregada com curcumina apresentaram melhor estabilidade que as emulsões sem o bioativo. A análise quantitativa da curcumina revelou 100% de retenção por até 60 dias. O EFG foi desenvolvido substituindo a água do gel de amido de quinoa pela emulsão *Pickering*, em diferentes proporções emulsão:água (100:0; 75:25; 50:50, 25:0 e 0:100). A tonalidade, obtida na análise de cor, de todos os géis carregados com emulsão foi predominantemente amarela (h°~73-80), e os géis formulados com 50% e 75% de emulsão permaneceram sem alterações significativas de cor por 14 dias. Os EFG formulados com 25% e 50% de emulsão exibiram tamanhos de gotas menores e mais uniformes e os géis com maiores proporções de emulsão (75% e 100%) apresentavam uma estrutura mais compacta com poros de tamanhos menores. O aumento na quantidade de emulsão usada na formulação dos EFG aumentou o módulo de *Young* e a dureza dos géis, e também os módulos viscoelásticos, sugerindo que a emulsão funcionou como uma partícula ativa de enchimento, com interação entre as cadeias de amido e as gotas de óleo. Todos os EFG apresentaram comportamento de gel fraco (G'>G”), com características de materiais elásticos ($\tan(\delta) < 0,12$). O teste de fluência e recuperação mostrou que os EFG são mais elásticos, enquanto o gel sem emulsão é mais viscoso. Assim, os resultados deste estudo contribuíram para o avanço dos sistemas de encapsulamento bioativos, utilizando a emulsão *Pickering* estabilizada apenas por nanopartículas de amido, bem como o gel carregado com emulsão. Os resultados dessa tese indicaram que é possível utilizar apenas SNP na estabilização de emulsões por mais de 60 dias. Essas emulsões podem ser utilizadas para desenvolver EFG à base de amido, que podem ser utilizados na encapsulação (ou como veículos de transporte) de bioativos com diferentes estruturas para aplicação em indústrias alimentícia ou farmacêutica.

Palavras-chave: amido de quinoa, nanopartículas de amido, nanoprecipitação, EFG, ultrassom, HMT, CLSM, Creep e recuperação.

ABSTRACT

RAMOS, G. V. C. **Double modification of cassava starch for stabilization of Pickering emulsions and production of filled gels: starch-based curcumin encapsulation systems**. 2023. 156 f. Doctoral thesis – Faculty of Animal Science and Food Engineering, University of São Paulo, Pirassununga, 2023.

Emulsion-filled gels (EFG) represent an innovative and promising class of materials, capable of encapsulation lipophilic and hydrophobic bioactive within their matrix. However, it is important to note that there is still a lack of literature related to the study of this biomaterial, particularly when considering the use of Pickering emulsion in EFG formulations. So, the objectives of this study were the development and characterization of quinoa starch-based gel filled with Pickering emulsion, aiming at the encapsulation of curcumin. Native and modified cassava starches, through heat-moisture treatment (HMT) or ultrasound (US), were employed for the production of nanoparticles (SNP) using the anti-solvent method. The SNP obtained from native starch (NSNP) and starches modified by HMT (HSNP) or US (USNP) were characterized and evaluated as stabilizing agents in the production of Pickering emulsions. Scanning electron microscopy (SEM) showed that the dual modification (HSNP or USNP) resulted in plate-shaped particles with rough surfaces. The particles had smaller sizes (~63-674 nm) for HSNP than NSNP and USNP. The zeta potential (-1.4 a -3.4 mV) and relative crystallinity values (2.2 – 3.7%) were low, with a V-type structure. The low crystallinity of SNP was confirmed through infrared spectroscopy analysis (FTIR) and thermal analysis (DSC). Oil absorption capacity and contact angle measurements demonstrated an increase in the hydrophobicity of the SNP after starch modification, following an ascending order (NSNP<USNP<HSNP). Under the process conditions applied in SNP production, only HSNP (4wt%) stabilized the emulsion (7 days, 20 ºC). NSNP and USNP at this concentration showed phase separation. The emulsion stabilized with 4 g de HSNP/ 100 g of emulsion was chosen for curcumin encapsulation. The interfacial tension value for systems with and without curcumin was ~40 mN/m and reached equilibrium quickly. The zeta potential of the emulsions was low (-5.39 mV), indicating low particle activity. Confocal scanning laser microscopy (CSLM) showed the presence of particles at

the drop interface, suggesting that the particles were adsorbed at the oil-water interface. Droplet size distribution analysis, creaming index, and apparent viscosity indicated that Pickering emulsions loaded with curcumin exhibited better stability than emulsions without the bioactive. Quantitative analysis of curcumin revealed 100% retention for up to 60 days. The EFG was developed by replacing water in quinoa starch gel with Pickering emulsion, in different emulsion:water ratios (100:0; 75:25; 50:50, 25:0 e 0:100). The color analysis revealed predominantly yellow tones (h°~73-80) for all gels loaded with emulsion, and the gels formulated with 50% and 75% emulsion remained without significant color changes for 14 days. The EFG formulated with 25% and 50% emulsion exhibited smaller and more uniform droplet sizes, while gels with higher emulsion proportions (75% and 100%) had a more compact structure with smaller pores. The increase in the amount of emulsion used in the EFG formulation increased the Young's moduli and hardness of the gels, as well as the viscoelastic moduli, suggesting that the emulsion functioned as an active filling particle with interaction between starch chains and oil droplets. All EFG showed weak gel behavior (G'>G”), with elastic material characteristics (tan(δ) < 0.12). The creep and recovery tests showed that EFG are more elastic, while the gel without emulsion is more viscous. Thus, the results of this study contributed to the advancement of bioactive encapsulation systems, using Pickering emulsion stabilized only by starch nanoparticles, as well as emulsion-filled gel. The findings indicated that it is possible to use only SNP for emulsion stabilization for more than 60 days. These emulsions can be used to develop starch-based EFG, which can be employed for the encapsulation (or as carrier vehicles) of bioactive with different structures for applications in the food or pharmaceutical industries

Keywords: quinoa starch, nanoparticles, nanoprecipitation, EFG, ultrasound, HMT, CLSM, Creep-recovery.

SUMÁRIO

1. CAPÍTULO 1: INTRODUÇÃO

1.1. Introdução

Os géis carregados de emulsão são caracterizados por estruturas de gel com gotas de óleo aprisionadas em uma matriz de biopolímero (DICKINSON, 2012). Moléculas lipofílicas, como aromatizantes, óleos essenciais ou medicamentos, apresentam desafios consideráveis quando incorporados em alimentos, produtos farmacêuticos e outras aplicações de materiais *soft* (macio), devido à sua insolubilidade parcial ou total em água (GEREMIAS-ANDRADE *et al.*, 2017). Por causa disso e de sua suscetibilidade à oxidação, a maioria desses compostos são difíceis de gerir (MCCLEMENTS, 2015; MWANGI *et al.*, 2020). Uma ampla gama de abordagens baseadas em emulsão foi desenvolvida para encapsular moléculas solúveis em óleo, como emulsões convencionais, nanoemulsões, emulsões duplas e géis de emulsão (ZHANG *et al.*, 2015; MWANGI *et al.*, 2020; ZHAO *et al.*, 2023).

É raro encontrar géis carregados com polissacarídeos tanto na interface (emulsificantes) quanto na fase contínua (agentes gelificantes). Os amidos podem ser modificados para obter capacidades de emulsificação e gelificação e, assim, podem formar géis carregados contendo gotas ativas (ZHANG *et al.*, 2021; MU *et al.*, 2023). Os amidos são polímeros naturais, importante fonte de carboidrato renovável e de baixo custo. Suas propriedades variam de acordo com a fonte vegetal e suas características como biocompatibilidade, biodegradabilidade, bioadesividade e não-toxicidade permitem aplicação cada vez maior em formulações de cosméticos, de medicamentos tópicos, de alimentos entre outras (LAPASIN; PRICL, 1995; TORRES *et al.*, 2017).

No entanto, o amido nativo apresenta limitações para algumas aplicações industriais como: baixa resistência, decomposição térmica e alta tendência à retrogradação (HERMANSSON; SVEGMARK, 1996; ALI; DASH; ROUTRAY, 2020). A modificação física dos grânulos tem sido uma alternativa promissora, relacionada com o emergente conceito de “tecnologia verde”. Estas modificações não empregam reagentes químicos ou enzimas e não exigem tratamento de resíduos, além de apresentarem menores custos quando

comparados aos métodos químicos e enzimáticos tradicionais (SANTOS, 2016; QIU *et al.*, 2019). O tratamento por calor e umidade (HMT) e por ultrassom são métodos físicos importantes usados para modificar o amido empregando processos simples e ambientalmente seguros, a baixo custo e sem subprodutos de reagentes químicos (ADEBOWALE; AFOLABI; OLU-OWOLABI, 2005; ALI; DASH; ROUTRAY, 2020; MANIGLIA *et al.*, 2021).

A nanoprecipitação é um outro método de modificação do amido, também considerado uma tecnologia “verde”, recente e promissora para a produção de nanopartículas de amido (SNP) de tamanho controlado (CHIN; PANG; TAY, 2011; QIU *et al.*, 2019). Essa técnica consiste em um procedimento simples, que não requer equipamentos especializados, nem condições operacionais complexas e produz um alto rendimento, sem poluição. No entanto, poucos estudos relatam a preparação de SNP por precipitação com antissolvente, como o etanol, por exemplo (CHANG *et al.*, 2017a; QIU *et al.*, 2019; LIMA *et al.*, 2021).

As nanopartículas de amido tem grande potencial para aplicações, como reforços para nanocompósitos, sistemas de entrega para drogas, nanoencapsulações de ingredientes e aditivos alimentares, adsorventes para íons de metais pesados, além de estabilizantes em emulsões *Pickering* (CORRE; ANGELLIER-COUSSY, 2014; KIM; PARK; LIM, 2015). As emulsões *Pickering* são estabilizadas por partículas sólidas em substituição aos surfactantes clássicos (químicos), o que torna essas emulsões adequadas para formulações de alimentos, pois são livres dos efeitos adversos dos emulsificantes sintetizados quimicamente (HERNÁNDEZ-SORIANO; PEÑA; MINGORANCE, 2010; ZHU, 2019).

A curcumina, composto extraído da cúrcuma, possui várias propriedades medicinais, como antioxidante, anti-inflamatória, antibacteriana, antifúngica, entre outras, podendo, além disso, suprir a necessidade de substituição de corantes artificiais amarelos por corantes naturais (RAVIADARAN *et al.*, 2018; LEE; TARTÉ; ACEVEDO, 2021). Porém, a integração desse composto em matrizes é complexa devido à sua hidrofobicidade. As emulsões podem ser uma solução para a incorporação e entrega deste composto, encapsulando, protegendo e distribuindo de forma mais controlada o bioativo (GHOSH; BANERJEE; SIL, 2015; FENG *et al.*, 2020).

Tendo em vista o que foi exposto anteriormente, a justificativa para esse trabalho foi a motivação pelo estudo emergente de técnicas de produção de novos materiais, como a produção de géis carregados à base de amido em ambas as matrizes (gel e emulsão), com um bioativo hidrofóbico encapsulado (curcumina). Esse novo material, por ser resultante de técnicas de produção “verdes” e de uso de materiais biocompatívies, que pode ser considerado para aplicações em cosméticos, medicamentos e principalmente, em matrizes de alimentos mais saudáveis. Assim, os objetivos desse trabalho foram a produção de nanopartículas de amido para a estabilização de emulsões *Pickering* e o desenvolvimento de géis carregados à base de amido com curcumina encapsulada em emulsão *Pickering*.

1.2. Objetivos

1.2.1. Objetivo geral

Os objetivos desse trabalho foram produzir nanopartículas de amido para a estabilização de emulsões *Pickering* e desenvolver géis carregados de emulsão à base de amido com curcumina encapsulada em emulsão *Pickering*.

1.2.2. Objetivos específicos

Os objetivos específicos desse trabalho foram:

- Produzir nanopartículas (SNP) de amidos de mandioca nativo e modificados, pelo tratamento de umidade e temperatura (HMT) ou por ultrassom (US), seguido pelo método antissolvente.
- Caracterizar as SNP de amido, quanto a morfologia, propriedades estruturais e físico-químicas e capacidade de estabilização de emulsão.
- Desenvolver emulsões com diferentes concentrações e tipos de SNP. Selecionar a SNP com capacidade de estabilização de emulsão na menor concentração necessária para estabilizar uma emulsão O/A (com 20% de fase óleo) e encapsular a curcumina.

- Caracterizar as emulsões e avaliar a estabilidade da curcumina encapsulada.
- Quantificar a curcumina nas emulsões produzidas e avaliar a estabilidade durante o tempo de armazenamento.
- Produzir e caracterizar géis carregados de emulsão à base de amido, substituindo a água dos hidrogéis pela emulsão *Pickering* com curcumina. Avaliar o efeito da quantidade de emulsão no gel sobre a estabilidade da curcumina, capacidade de retenção de água, morfologia, propriedades mecânicas e reológicas.

1.3. Estrutura da tese

Esta tese está dividida em 6 capítulos independentes, descritos a seguir. Os capítulos 3, 4 e 5 estão apresentados no formato de artigos submetidos ou sob processo de submissão.

Capítulo 1: contextualização, motivação e objetivos deste trabalho.

Capítulo 2: revisão da literatura sobre amido, emulsões de *Pickering* estabilizadas por amido e géis à base de amido carregados de emulsão.

Capítulo 3: Modificação do amido de mandioca por ultrassom e tratamento por calor e umidade para produção de nanopartículas com propriedades físico-químicas e tecnológicas promissoras para aplicação como estabilizantes em emulsões do tipo *Pickering*.

Capítulo 4: estudo da influência da concentração e do tipo de nanopartícula de amido na estabilização de emulsões *Pickering* e encapsulação da curcumina.

Capítulo 5: avaliação do efeito da quantidade de emulsão na morfologia, propriedades mecânicas e reológicas de géis à base de amido carregados com emulsão *Pickering* e na estabilidade da curcumina.

Capítulo 6: considerações finais e resumo das principais conclusões obtidas ao longo do desenvolvimento desta tese. Atividades futuras relacionadas a esta área de pesquisa são indicadas.

A Figura 1 apresenta a sequência de etapas desenvolvidas ao longo da pesquisa, delineando o progresso desta tese de doutorado.

Figura 1 – Fluxograma das etapas que foram desenvolvidas durante o andamento da pesquisa.

Fonte: autoria própria

Referências

ADEBOWALE, K. O.; AFOLABI, T. A.; OLU-OWOLABI, B. I. Hydrothermal treatments of Finger millet (Eleusine coracana) starch. **Food hydrocolloids**, v. 19, p. 974–983, 2005.

ALI, N. A.; DASH, K. K.; ROUTRAY, W. Physicochemical characterization of modified lotus seed starch obtained through acid and heat moisture treatment. **Food Chemistry**, v. 319, p. 126513, 30 jul. 2020.

CHANG, Y. *et al.* Influence of ultrasonic treatment on formation of amylose nanoparticles prepared by nanoprecipitation. **Carbohydrate Polymers**, v. 157, p. 1413–1418, 2017.

CHIN, S. F.; PANG, S. C.; TAY, S. H. Size controlled synthesis of starch nanoparticles by a simple nanoprecipitation method. **Carbohydrate Polymers**, v. 86, n. 4, p. 1817–1819, 15 out. 2011.

CORRE, D. Le; ANGELLIER-COUSSY, H. Reactive & Functional Polymers Preparation and application of starch nanoparticles for nanocomposites : A review. **Reactive & Functional Polymers**, v. 85, p. 97–120, 2014.

DICKINSON, E. Food Hydrocolloids Emulsion gels : The structuring of soft solids with protein-stabilized oil droplets. **Food hydrocolloids**, v. 28, n. 1, p. 224–241, 2012.

FENG, T. *et al.* Emulsion-based delivery systems for curcumin: Encapsulation and interaction mechanism between debranched starch and curcumin. **International Journal of Biological Macromolecules**, v. 161, p. 746–754, 15 out. 2020.

GEREMIAS-ANDRADE, I. M. *et al.* Rheological and mechanical characterization of curcumin-loaded emulsion-filled gels produced with whey protein isolate and xanthan gum. **Lwt**, v. 86, p. 166–173, 2017

GHOSH, S.; BANERJEE, S.; SIL, P. C. The beneficial role of curcumin on inflammation, diabetes and neurodegenerative disease: A recent update. **Food and Chemical Toxicology**, v. 83, p. 111–124, 2015.

HERMANSSON, A. M. .; SVEGMARK, K. Developments in the understanding of starch functionality. **Trends in Food Science and Technology**, v. 7, p. 345–53, 1996.

HERNÁNDEZ-SORIANO, M. del C.; PEÑA, A.; MINGORANCE, M. D. Release of Metals from Metal-Amended Soil Treated with a Sulfosuccinamate Surfactant: Effects of Surfactant Concentration, Soil/Solution Ratio, and pH. **journal of environmental quality**, v. 39, n. 4, p. 1298–1305, 2010.

KIM, H.; PARK, S. S.; LIM, S. Colloids and Surfaces B : Biointerfaces Preparation , characterization and utilization of starch nanoparticles. **Colloids and Surfaces B: Biointerfaces**, v. 126, p. 607–620, 2015.

LAPASIN, R.; PRICL, S. Rheology of Industrial Polysaccharides Theory and Applications. In: **Blackie Academic and Processional, Chapman & Hall**. p. 620.

LEE, Y. S.; TARTÉ, R.; ACEVEDO, N. C. Curcumin encapsulation in Pickering emulsions co-stabilized by starch nanoparticles and chitin nanofibers. **RSC Advances**, v. 11, n. 27, p. 16275–16284, 2021.

LIMA, K. T. dos S. *et al.* Physicochemical Properties of Modified Starches Obtained by Anti-Solvent Precipitation Containing Anthocyanins from Jambolan (Syzygium cumini) Fruit. **Starch/Stärke**, v. 73, n. 3–4, 2021.

MCCLEMENTS, D. Encapsulation, protection, and release of hydrophilic active components: Potential and limitations of colloidal delivery systems. **Advances in Colloid and Interface Science**, v. 219, p. 27–53, 2015.

MWANGI, W. W. *et al.* Food-grade Pickering emulsions for encapsulation and delivery of bioactives. **Trends in Food Science & Technology**, v. 100, p. 320–332, 1 jun. 2020.

QIU, C. *et al.* A review of green techniques for the synthesis of size-controlled starch-based nanoparticles and their applications as nanodelivery systems. **Trends in Food Science & Technology**, v. 92, n. October 2018, p. 138–151, 2019.

RAVIADARAN, R. *et al.* Optimization of palm oil in water nano-emulsion with curcumin using microfluidizer and response surface methodology. **Lwt**, v. 96, n. March, p. 58–65, 2018.

SANTOS, T. P. R. dos. **Efeitos de modificações físicas sobre as propriedades de amido de tuberosas**. 2016. 146f.; Tese (Doutorado); Universidade Estadual Paulista, 2016.

TORRES, O. *et al.* Novel starch based emulsion gels and emulsion microgel particles : Design , structure and rheology. **Carbohydrate Polymers**, v. 178, n. September, p. 86–94, 2017.

ZHANG, Y. *et al.* Physical properties and salt release of potato starch-based emulsion gels with OSA starch-stabilized oil droplets. **LWT**, v. 141, p. 110929, 2021.

ZHANG, Z. *et al.* Designing hydrogel particles for controlled or targeted release of lipophilic bioactive agents in the gastrointestinal tract. **European Polymer Journal**, v. 72, p. 698–716, 2015.

ZHAO, X. *et al.* Role of gelation temperature in rheological behavior and microstructure of high elastic starch-based emulsion-filled gel. **Food Hydrocolloids**, v. 135, n. July 2022, p. 108208, 2023

ZHU, F. Starch based Pickering emulsions: Fabrication, properties, and applications. **Trends in Food Science & Technology**, v. 85, p. 129–137, 2019.

2. CAPÍTULO 2: REVISÃO BIBLIOGRÁFICA

2.1. Amido: composição, estrutura e propriedades

O amido é um polímero natural, biodegradável, extremamente abundante na natureza e atóxico. Ele pode ser obtido de diversas fontes vegetais, tais como cereais, raízes e tubérculos, além de frutas e legumes e é a principal reserva de energia das plantas, armazenado na forma de granulos (OLADEBEYE *et al.*, 2013). Os dois principais componentes macromoleculares do amido são a amilose e a amilopectina (Fig. 1) (DENARDIN; SILVA, 2009; PÉREZ; BALDWIN; GALLANT, 2009).

Figura 1 - Representação esquemática das moléculas de amilose e amilopectina.

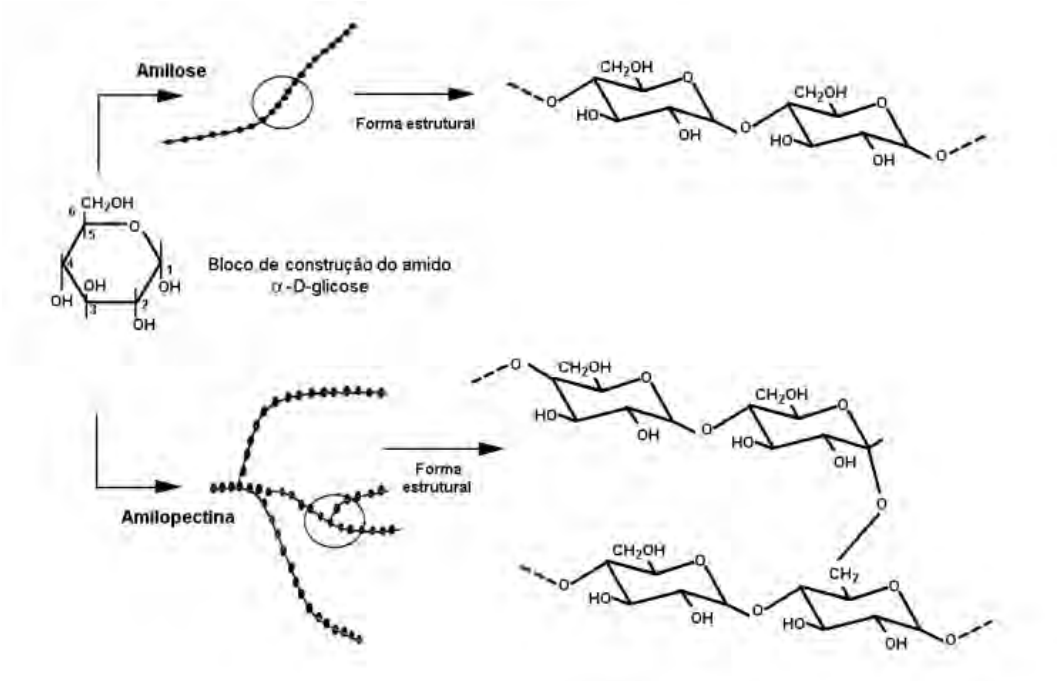

Fonte: Beninca (2008).

A amilose possui uma estrutura essencialmente linear, formada por unidades de glicose com ligações α-(1→4), formando majoritariamente a região amorfa do grânulo (WURZBURG, 1986). As cadeias de α-D-Glicose presentes na amilose geralmente formam estruturas espirais, devido à facilidade de formação de ligações de hidrogênio entre os grupos hidroxila, adquirindo uma

conformação helicoidal. O interior da hélice é hidrofóbico, admitindo a formação de complexos com ácidos graxos livres, alguns álcoois e com o iodo (TESTER, 1997). A amilose apresenta massa molar da ordem de $1,5.10^5$ a 10^6 Daltons e tamanho médio de 103 unidades de glicose (XIE; LIU; CUI, 2005).

Já a amilopectina, predominantemente ramificada, é formada por unidades de glicose através de ligações α-(1→4) e α-(1→6) e é a principal responsável pela região cristalina do grânulo de amido (WURZBURG, 1986; PÉREZ; BALDWIN; GALLANT, 2009). O grau de polimerização dessa macromolécula é da ordem de 10^4 a 10^5 unidades de glicose e apresenta massa molar de 0,5 x 10^8 a 10^9 Daltons e possui comprimento de ramificações variável, geralmente de 20 a 30 unidades de glicose (XIE; LIU; CUI, 2005).

As propriedades funcionais do amido variam principalmente de acordo com a razão entre amilose / amilopectina presente no grânulo, assim como sua organização física na estrutura (WURZBURG, 1986). Diferentes fontes botânicas, assim como o grau de maturação da planta pode interferir na proporção dessas macromoléculas (VAN SOEST; VLIEGENTHART, 1997).

O grânulo de amido apresenta uma estrutura hierárquica, parcialmente cristalina, se organizando em regiões amorfas e cristalinas (Fig. 2). Os grânulos de amido são formados por camadas concêntricas cristalinas e amorfas alternadas, formadas a partir de anéis de crescimento semicristalinos, compostos de bloquetes (20-50 nm) que incluem lamelas amorfas e cristalinas (9 nm) (GALLANT; BOUCHET; BALDWIN, 1997). Os anéis de crescimento são formados a partir de um centro de nucleação, conhecido como “*hillum*”, onde pode se observar a “Cruz de Malta” em amidos nativos, sob luz polarizada, devido à birrefringência do grânulo (GALLANT; BOUCHET; BALDWIN, 1997).

Figura 1 - (A) anéis de crescimento semicristalinos e amorfos dentro dos grânulos de amido, (B) pequenos e grandes bloquetes, (C) lamelas cristalinas e amorfas, (D) estrutura da amilopectina formando as regiões amorfas e cristalinas no grânulo de amido.

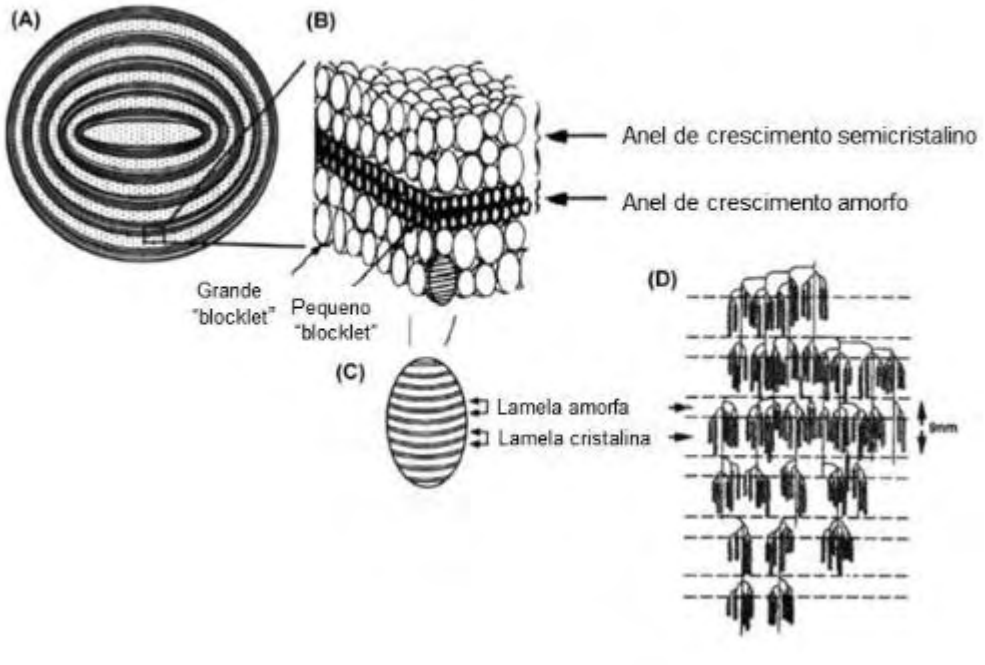

Fonte: Kim, Kim e Baik (2012).

As regiões cristalinas dos grânulos apresentam padrões específicos de difração de raios X, que variam de acordo com a fonte botânica do grânulo (ZOBEL, 1964). O padrão A é característico de amidos de cereais, o padrão B de amidos de tubérculos e grãos com elevada concentração de amilose, o padrão C é intermediário entre o A e o B, característico de amido de leguminosas e o tipo V provém de moléculas de amilose co-cristalizadas com compostos como iodo, álcoois ou ácidos graxos (BULÉON *et al.*, 1998; TESTER; KARKALAS; QI, 2004).

Os formatos dos grânulos de amido podem ser regulares ou irregulares, se apresentando em formas geométricas arredondadas, ovais e até mesmo poliédricas e triangulares e seus diâmetros variam geralmente de 1 a 100 μm, dependendo da fonte botânica (XIE; LIU; CUI, 2005; LEONEL, 2007).

O amido nativo é praticamente insolúvel em água fria, no entanto, quando há excesso de água e aquecimento, os grânulos de amido sofrem um inchamento irreversível, produzindo uma pasta viscosa, fenômeno conhecido como gelatinização. O fenômeno da gelatinização pode ser caracterizado pela

perda da ordem cristalina (birrefringência), inchamento dos grânulos, lixiviação da amilose e ruptura da estrutura dos grânulos (HOOVER, 2001). A temperatura de gelatinização pode variar de 55 a 70 ºC, dependendo da fonte do amido (ATWELL *et al.*, 1983; LAGARRIGUE *et al.*, 2008).

Quando resfriadas, as pastas de amido tendem a formar géis e as moléculas de amido tendem a se rearranjar, formando estruturas fortemente unidas e ordenadas, incidindo na perda de seus sítios reativos, fenômeno conhecido como retrogradação (KOKSEL *et al.*, 2008). Fatores importantes que podem influenciar o fenômeno da retrogradação são a fonte do amido, a concentração, as condições de aquecimento / resfriamento, pH, presença de solutos (lipídeos e açúcares) e, um dos mais importantes, a proporção de amilose no grânulo, sendo que quanto maior for o teor de amilose, maior será a tendência de reassociação ou retrogradação (DENARDIN; SILVA, 2009).

2.1.1. Amido de mandioca

No mundo, são produzidas mais de 256 milhões de toneladas de mandioca (*Manihot esculenta Crantz*) por ano. O Brasil é o terceiro maior produtor de mandioca à nível mundial, sendo que o tubérculo é cultivado nas mais diversas regiões do país (EMBRAPA, 2018). Essa tuberosa é uma importante fonte energética para cerca de 800 milhões de pessoas da África, América do Sul, Ásia e Ilhas do Pacífico e importante fonte de extração do amido (IYER; MATTINSON; FELLMAN, 2010). A sua produção tem sido dirigida tanto para consumo direto quanto para indústria de transformação, onde é utilizada na elaboração de diversos produtos como fécula ou amido, farinha de mesa, raspas, farinha de raspas e polvilho azedo (LEITE, 2016).

O amido é o principal componente da mandioca e pode representar até 80% do peso seco da raiz (OLOMO; AJIBOLA, 2003). Há uma grande variação de genótipos desse tubérculo cultivados hoje, assim, sua composição química e conteúdo de amilose também têm uma larga faixa de valores encontrados na literatura: cinzas, proteínas, lipídios, fósforo, fibras e amilose podem variar de 0,03–0,29%, 0,06–0,75%, 0,01–1,2%, 0,0029–0,0095%, 0,11–1,9% e 0-30,3%, respectivamente (ZHU, 2015). Em comparação com outros amidos

comerciais (batata, trigo, feijão, milho), o amido de mandioca contém uma quantidade muito menor de fósforo, além de menos lipídeos quando comparado aos amidos de cereais (KASEMSUWAN *et al.*, 1995).

A composição centesimal do amido, bem como o conteúdo de amilose, de lipídeos e o tamanho dos grânulos influenciam diretamente nas propriedades térmicas do amido, como a temperatura de gelatinização, que para o amido de mandioca varia de no intervalo de 55-75 ºC (PÉREZ; BERTOFT, 2010; ZHU, 2015). A morfologia do amido de mandioca, consiste em um grânulo de formato oval, truncado e arredondado, com tamanho variando de ~2 a 32 μm, e apresenta um padrão cristalino tipo A ou C, com cristalinidade relativa que varia de ~15 a 49% (ZHU, 2015).

2.1.2. Amido de quinoa

A quinoa (*Chenopodium quinoa*), um pseudoceral (dicotiledônea), é um grão originário das regiões andinas, sendo considerada um dos alimentos mais completos do mundo, pois é rico em nutrientes, com padrão único de aminoácidos e alto conteúdo de ácidos graxos poli-insaturados e minerais (OGUNGBENLE, 2003). A composição do grão de quinoa contém, aproximadamente, 65% de carboidratos (~60% amido), 15% de proteínas, 6% de gordura, 7% de fibra e 3% de cinzas (OGUNGBENLE, 2003). Os grãos se apresentam em três principais colorações: brancos, vermelhos ou pretos (FLEMING; GALWEY, 1995).

O amido de quinoa, fonte de amido não convencional, apresenta baixo conteúdo de amilose (3,5-22,5 %) e alto teor de amilopectina, com cadeias curtas e super longas, o que lhe confere baixas temperaturas de gelatinização e retrogradação lenta (LI; ZHU, 2018). Quanto à morfologia, o amido de quinoa possui grânulos pequenos, entre 0,5-3 μm, com formatos hexagonais (ARAUJO-FARRO, 2008; LI; ZHU, 2018). O padrão cristalino é do tipo A, com cristalinidade relativa variando de 21,5 a 43% e temperaturas de gelatinização na faixa de 45 a 60 ºC (ATWELL *et al.*, 1983).

2.1.3. Nanopartículas de amido

As partículas de amido na escala nano podem ser divididas em dois tipos: nanocristais de amido (NC), que resultam da ruptura de domínios amorfos de grânulos de amido; e nanopartículas à base de amido (SNP), que são produzidas a partir de amido gelatinizado, onde há a quebra da estrutura cristalina do grânulo (BUZEA; PACHECO; ROBBIE, 2007; QIU *et al.*, 2019; VELÁSQUEZ-CASTILLO *et al.*, 2020; LIMA *et al.*, 2021).

Devido às suas pequenas dimensões, as nanopartículas apresentam características específicas. Essas diferenças são atribuídas principalmente à dois efeitos: o pequeno tamanho e a alta relação superfície / volume (BUZEA; PACHECO; ROBBIE, 2007). A dimensão das nanopartículas proporciona propriedades físico-químicas e fisiológicas diferentes de partículas maiores, como dispersão de luz reduzida, estabilidade melhorada para separação gravitacional e agregação, taxas de difusão mais rápidas, solubilidades mais altas e taxas de penetração mais altas através de barreiras biológicas (JOYE; MCCLEMENTS, 2013).

Recentemente, as nanopartículas de amido ganharam muita atenção devido às suas características de liberação controlada, melhor solubilidade e biodisponibilidade em água e melhor entrega de vários ingredientes ativos em alimentos e medicamentos (QIU *et al.*, 2019; LIMA *et al.*, 2021), podendo ser aplicadas como carreadores de medicamentos, substituto de surfactantes, substituto do acetato polivinílico, embalagens hidrossolúveis para inseticidas, embalagens biodegradáveis (JOYE; MCCLEMENTS, 2013; QIU *et al.*, 2019; WIGATI *et al.*, 2023).

Existem várias técnicas para a produção de nanopartículas e nanocristais de amido, que podem ser classificadas em métodos *top-down* (hidrólise ácida, homogeneização, ultrassonicação, extrusão reativa, irradiação gama, etc.) e *bottom-up* (automontagem ou nanoprecipitação) (BUZEA; PACHECO; ROBBIE, 2007; JOYE; MCCLEMENTS, 2013; QIU *et al.*, 2019; LIMA *et al.*, 2021). Um dos métodos convencionais que tem sido usado por muito tempo para preparar NC é a hidrólise ácida, no entanto, este método incide em um impacto ambiental negativo, já que se faz uso de HCl ou H_2SO_4 para que haja a quebra da região

amorfa dos grânulos, além de apresentar um baixo rendimento e exigir um longo tempo de reação (3-7 dias) (KAUR *et al.*, 2018).

Algumas técnicas verdes ou físicas para a produção de nanopartículas têm sido estudadas como alternativas. A nanoprecipitação é exemplo de método recente e promissor para a produção de SNP de tamanho controlado, sendo um método simples, que não requer equipamento especializado nem condições operacionais complexas e produz um alto rendimento sem poluição (QIU *et al.*, 2019; LIMA *et al.*, 2021). Esse método é considerado uma tecnologia verde na obtenção de nanopartículas de amido amorfo (ASCHENBRENNER *et al.*, 2013) e também tem sido amplamente utilizado na indústria para produzir nanopartículas para fins farmacêuticos (JOYE; MCCLEMENTS, 2013).

O tamanho das nanopartículas pode ser controlado ajustando-se a concentração inicial do substrato, a razão solvente:não-solvente, velocidade de titulação, velocidade de agitação e outros parâmetros. No entanto, poucos estudos relatam a preparação de SNP por precipitação com um não solvente (CHACON *et al.*, 2019; QIU *et al.*, 2019; GUIDA, 2021; LIMA *et al.*, 2021).

No método de precipitação com não-solvente, o amido é gelatinizado em uma determinada concentração, em seguida, um não-solvente (etanol, metanol, n-propanol, isopropanol ou n-butanol, entre outros) é adicionado gota a gota à solução gelatinizada (CHACON *et al.*, 2019; LIMA *et al.*, 2021). A precipitação pode ser alcançada pela supersaturação, seguida por crescimento de partículas de amido coloidal de tamanho nanométrico (QIU *et al.*, 2019).

Lima *et al.* (2021) produziram nanopartículas de amido de mandioca e batata pelo método de precipitação antissolvente, utilizando suspensões de amido com concentrações de 5 ou 10% (p/v) em água, gelatinizando por 30 min a 90 ºC e precipitando as SNP com etanol acidificado (100:1 v/v, etanol: HCl 37%) através de gotejamento. Os autores utilizaram proporção água:etanol de 1:1 (v/v), e mantiveram as SNP sob agitação por 12 h com o antissolvente, obtendo nanopartículas com tamanhos inferiores a 900 nm e estruturas amorfas, com pequenos picos em um padrão de difração do tipo V e cristalinidade relativa variando de 1-2,5%.

Já Chacon *et al.* (2019) utilizaram o método de nanoprecipitação para produzir SNP de amido de batata. Foram feitas concentrações de 5 e 10% (p/v) de amido em solução de NaOH 1,5% m/m, sendo aquecidas a 90 ºC por 30 min.

Em seguida, etanol absoluto 1:1 (v/v) foi gotejado, promovendo a precipitação das SNP, que foram mantidas sob agitação por 6 h em contato com o antissolvente. Os autores relataram que as SNP exibiram tamanho de 50 a 150 nm e a cristalinidade relativa diminuiu em comparação com o amido nativo (de 25,4 para 23,5%).

2.1.4. Métodos combinados para produção de SNP de amido

A nanoprecipitação pode ser realizada com ou sem técnicas assistentes. Algumas técnicas assistentes à produção de SNP ou NC relatadas na literatura empregam: ultrassom (CHANG *et al.*, 2017b), micro-ondas (JUNA *et al.*, 2014), tratamento por calor e umidade (HMT) (JI *et al.*, 2015; PARK *et al.*, 2016; KIM *et al.*, 2017), uso de surfactantes (CHIN; PANG; TAY, 2011), ácidos fracos (AGI *et al.*, 2019; LIMA *et al.*, 2021), acetona (OLIVEIRA *et al.*, 2018), enzimas (KIM; LIM, 2009), entre outras.

Os métodos combinados são utilizados para produzir SNP de amido com propriedades aprimoradas e geralmente são utilizados durante a produção das nanopartículas ou imediatamente após sua formação. Estratégias alternativas para preparar nanopartículas de amido incluem combinação simultânea com tratamento físico ou tratamento enzimático. Essas estratégias visam superar as limitações do procedimento tradicional, como baixo rendimento e tamanhos de partículas muito grandes (KIM; PARK; KIM, 2017; VELÁSQUEZ-CASTILLO *et al.*, 2020). Estudos recentes têm avaliado o efeito da pré-modificação do amido para a produção de nanocristais (PINTO *et al.*, 2021). Métodos de pré-modificação do amido foram utilizados neste trabalho de doutorado para produzir nanopartículas por nanoprecipitação.

2.1.4.1. Modificação por HMT

O tratamento por calor e umidade (HMT ou *heat-moisture treatment)* é um método físico de modificação do amido que envolve o aquecimento de grânulos de amido em baixos níveis de umidade (<35% p/p), a temperaturas acima da transição vítrea, porém, abaixo da temperatura de gelatinização (84 -140 °C), por

um período de tempo definido (15 min - 16 h) (HOOVER, 2010). O HMT causa mudanças estruturais nas regiões amorfas e / ou cristalinas dos grânulos, resultando em mudanças no comportamento de intumescimento granular, cristalinidade, lixiviação de amilose, propriedades de transição térmica, estabilidade térmica e comportamento de pasta (KIM; PARK; KIM, 2017; WANG *et al.*, 2018; PIECYK; DOMIAN, 2021; ACEVEDO *et al.*, 2022).

Poucos estudos relacionados à utilização da técnica de HMT combinada à nanoprecipitação de amido está disponível na literatura, sendo, em sua maioria, estudos relacionando o HMT à hidrólise ácida do amido para produção de nanocristais (NC) (PINTO *et al.*, 2021). A modificação dos grânulos de amido usando métodos combinados, por exemplo o HMT e a hidrólise ácida, pode induzir a alterações na estrutura granular e molecular do amido (KIM; PARK; KIM, 2017).

Ji *et al.* (2015) produziram SNP de amido de milho ceroso, através de gelatinização em hidrogenofosfato dissódico e solução tampão de ácido cítrico (pH 5,0) e hidrólise enzimática, com adição de pullulanase. Posteriormente, eles modificaram esse material utilizando a técnica HMT, em temperaturas de 90 e 110 ºC por 4 h e umidade de 20% e 30%. Esses autores observaram que a modificação por HMT aumentou significativamente as propriedades térmicas das SNP, alterou o padrão de cristalinidade do tipo B para o tipo A, porém, sem mudanças na morfologia.

Kim, Park e Kim (2017) e Park *et al.* (2016) utilizaram condições levemente ácidas, com ácido sulfúrico até 0,2N e 0,1M, amido de milho ceroso e amido de milho normal, para cada trabalho, respectivamente, suspensão de amido de 10% (m/v), em alíquotas de solução de ácido:suspensão de amido de 6:150 (v/v), hidrolisando os grânulos de amido. Posteriormente, submeteram o amido já seco ao processo de HMT e adicionaram etanol para a precipitação dos nanocristais (NC). Para a modificação por HMT, os autores mantiveram a temperatura em 130 ºC, umidade a 20% e variaram o tempo (3, 5 e 8 h). Esses autores relataram que as condições ácidas durante o HMT podem hidrolisar preferencialmente as regiões amorfas dos grânulos de amido, resultando em grânulos de amido frágeis com aumento da cristalinidade, além de redução no tempo de produção e aumento do rendimento dos NC.

Pinto *et al.* (2021) estudaram o efeito do pré-tratamento por HMT no amido de pinhão para posterior produção de NC de amido por hidrólise ácida. Esses autores utilizaram como parâmetros a umidade do amido ajustada em 22%, sendo equilibrado a 4 ºC por 4 dias, aquecimento a 100 ºC por 60 min. Foi reportado um aumento no rendimento (de 10,2% para 14,7%), porém com uma redução de aproximadamente 8,3% na cristalinidade (CR) dos NC em comparação ao amido nativo (CR do amido nativo: 28,5% e modificado por HMT: 20,2%).

2.1.4.2. Modificação por ultrassom

Outro método de modificação física é o ultrassom, considerado uma tecnologia verde, pois seu uso emergente nas indústrias de alimentos mostra baixo impacto no meio ambiente e melhoria na qualidade higiênica dos alimentos (SHABANA *et al.*, 2019). Os efeitos físicos e químicos causados pelo ultrassom são geralmente atribuídos à cavitação, que é o colapso das microbolhas que se rompem e se propagam como uma onda sonora através da solução (GORDON, 1969; PRICE; SMITH, 1993). As forças de cisalhamento criadas devido ao colapso das bolhas podem quebrar ligações covalentes em materiais poliméricos (FARZI *et al.*, 2011; ZHANG *et al.*, 2013), podendo ocasionar redução da massa molar e/ou prevenir a agregação (AGI *et al.*, 2019).

As nanopartículas têm forte tendência a se agregar, especialmente na forma de pó seco, devido à atração entre as suas superfícies. e o ultrassom é uma técnica que pode ser considerada uma boa opção para melhorar essa limitação (DUFRESNE, 2008). Na literatura, encontram-se mais estudos relacionando o ultrassom à hidrólise ácida para se obter nanocristais de amido (PINTO *et al.*, 2021). No entanto, poucos trabalhos têm sido realizados sobre a modificação do amido por ultrassom seguido de produção de nanopartículas pelo método de nanoprecipitação (CHANG *et al.*, 2017b, 2017a), o que foi estudado nessa presente tese.

Chang *et al.* (2017b) avaliaram o uso do ultrassom conjuntamente com a produção de SNP de amido de batata por nanoprecipitação com etanol, utilizando frequência: de 22 kHz, ponteira de chifre cônica de 10 mm, potência: 100 W e tempos de 5, 10, 15, 20, 25 e 30 min. Os autores obtiveram SNP com

tamanhos menores que 75 nm e mais uniformes, com menor índice de polidispersidade, após tratamento com ultrassom.

Agi *et al.* (2019) produziram SNP utilizando ácido acético, (ácido fraco) e álcool. Posteriormente aplicaram ultrassom por 60 min a uma frequência de 40 kHz e potência de 500 W, obtendo SNP com diâmetro médio de 100 nm. Os autores observaram que o ultrassom reduziu o tamanho das partículas.

Hedayati, Niakousari e Mohsenpour (2020) obtiveram SNP de amido de tapioca utilizando acetona e ultrassom. Os parâmetros utilizados foram frequência de 20 kHz, amplitude de 100%, potência de 150 W e 60 min. Os autores observaram perda da cristalinidade e aumento da eficiência de produção de SNP nas amostras que foram modificadas por ultrassom.

2.2. Curcumina

A curcumina é um polifenol extraído dos rizomas de *Curcuma longa* Linn, uma planta pertencente à família *Zingiberaceae*, característica de regiões tropicais e subtropicais da Índia e China (GHOSH; BANERJEE; SIL, 2015; KHARAT *et al.*, 2020). A curcumina é o principal ativo constituinte da cúrcuma, também conhecido como açafrão, e é amplamente utilizado como conservante, aromatizante e corante natural em bebidas e em alimentos (CODEVILLA *et al.*, 2015). Além disso, esse composto apresenta várias propriedades medicinais, como antioxidante, anti-inflamatório, antibacteriano, antifúngico, anti-hipocolestrolêmico, antitumoral e antiproliferativo (RAVIADARAN *et al.*, 2018).

O rizoma da cúrcuma tem como principais constituintes óleo essencial, amido, proteínas e fibras, além dos pigmentos curcuminóides, que são compostos por três substâncias principais: curcumina (77%), desmetoxicurcumina (17%) e bisdesmetoxicurcumina (3%). Esses pigmentos são estáveis a pH ácido e sensíveis a luz, porém altamente estáveis ao calor (PEREIRA; STRINGHETA, 1998).

A curcumina é caracterizada como um antioxidante fenólico de cor amarela natural praticamente insolúvel em água e solúvel em metanol, etanol, acetona, dimetilformoldeído (DMF), dimetilsufóxido (DMSO), clorofórmio,

acetonitrila (ACN). Sua estrutura química é composta por dois anéis metoxifenois (Fig. 3), que são simetricamente ligados em conjugação através da porção β-dicetona (NAKSURIYA, 2014).

Figura 3 – Representação estrutural da molécula de curcumina

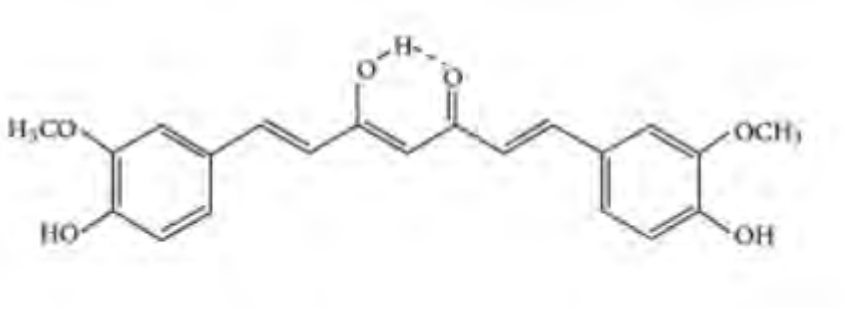

Fonte: Naksuriya (2014).

Porém, a curcumina apresenta uma baixa biodisponibilidade quando ingerida pelo organismo, além de ser uma molécula hidrofóbica, o que dificulta sua inserção em matrizes alimentícias ou farmacêuticas (GÓMEZ-ESTACA; GAVARA; HERNÁNDEZ-MUÑOZ, 2015). O encapsulamento pode ser um meio para facilitar o manuseio e a dosagem de certos ingredientes, aditivos ou compostos bioativos que são voláteis, viscosos, ou pouco solúveis em água, ou para liberar um composto ativo a taxas controladas ou sob condições específicas (CODEVILLA *et al.*, 2015).

Vários estudos relataram biodisponibilidade melhorada de compostos ativos encapsulados em emulsões (RAVIADARAN *et al.*, 2018; FENG *et al.*, 2020; ZHAO *et al.*, 2023). A emulsão é capaz de incorporar drogas hidrofóbicas e anfipáticas e é um dos métodos mais eficaz na liberação de curcumina, melhorando a estabilidade durante o armazenamento e protegendo o bioativo dos processos metabólicos digestivos (NAKSURIYA, 2014; RAVIADARAN *et al.*, 2018).

2.3. Óleo de canola

As emulsões utilizadas em produtos alimentícios frequentemente contêm óleos com propriedades de bioativos, sendo de grande interesse em vários estudos devido às suas propriedades farmacêuticas, cosméticas e nutricionais

(YU *et al.*, 2015; RODRÍGUEZ *et al.*, 2016; MA *et al.*, 2017; CHEN; XV; YUAN, 2022).

A canola (*Brassica napus, Brassica rapa ou Brassica juncea)* é uma das culturas oleaginosas mais comumente cultivadas por causa de seu teor de óleo extremamente alto (~40%) e valor nutricional abundante, rico em ácidos graxos poli-insaturados, vitaminas e minerais (YU *et al.*, 2015). Originalmente produzido em maior escala no Canadá, a canola só foi considerada segura para o consumo humano a partir de meados de 1970, quando, por meio de melhoramentos genéticos da colza, foi desenvolvida uma variedade com teores de glicosinolatos e ácido erúcico reduzidos a níveis considerados seguros para a ingestão (EMBRAPA, 2013).

A canola, variedade da colza geneticamente modificada, é uma semente oleaginosa que contém cerca de 38% de óleo. Este óleo apresenta um baixo percentual de gordura saturada (aproximadamente 6,9%), sendo que os ácidos graxos insaturados representam 93% da sua composição. O ácido oleico é o principal ácido graxo insaturado encontrado no óleo de canola, representando 70% do total (PEDERSSETTI, 2008). O óleo de canola é considerado saudável por apresentar uma composição de ácidos graxos que auxilia na redução do risco de doenças cardiovasculares. Ele é rico em Ômega-3, um ácido graxo essencial que ajuda a reduzir os níveis de triglicerídios no sangue. Também ajuda a reduzir a inflamação, que pode contribuir para o desenvolvimento da arteriosclerose. Além disso, possui vitamina E (que atua como antioxidante e contribui na redução de radicais livres), e baixo teor de gordura saturada, que é um fator de risco para doenças cardiovasculares. Médicos e nutricionistas indicam o óleo de canola como o de melhor composição de ácidos graxos para as pessoas interessadas em dietas saudáveis (EMBRAPA, 2013).

2.4. Emulsões *Pickering*

Emulsões são misturas de duas fases imiscíveis, em que uma fase é dispersa na outra na forma de pequenas gotas. As emulsões podem ser classificadas como óleo em água (O/A), água em óleo (A/O) ou emulsões

múltiplas (RAYNER *et al.*, 2012). A estabilização das gotas de emulsão é frequentemente alcançada pela adição de surfactantes ou emulsificantes que atuam diminuindo a tensão interfacial entre as fases, e aumentam o impedimento estérico e a repulsão eletrostática entre as gotas e, assim, aumentam a estabilidade da emulsão (RAYNER *et al.*, 2012; REMANAN; ZHU, 2023).

No entanto, as emulsões estão sujeitas à processos de desestabilização, que podem ocorrer por quatro fenômenos diferentes: coagulação, floculação, cremeação e coalescência (SHAW, 1975). A coagulação ocorre quando um eletrólito inorgânico é adicionado à emulsão e reduz a espessura da dupla camada elétrica ao redor das gotas, diminuindo as forças repulsivas eletrostáticas entre as partículas, permitindo que elas se aproximem uma das outras. Quando as gotas estão suficientemente próximas, as forças de atração de van der Waals predominam e as gotas coalescem. A floculação é um fenômeno de agregação de partículas mediante adição de polímeros floculantes, que atuam diminuindo a repulsão eletrostática entre as partículas e promove a formação de agregados maiores, chamados de flocos. Na cremeação ocorre um deslocamento das gotas de óleo para a superfície do sistema, devido à diferença de densidade entre as fases. A coalescência ocorre com a redução da dupla camada elétrica, em que as gotas tendem a se aproximar umas das outras e a coalescer irreversivelmente, levando à formação de agregados maiores, até tornar-se novamente uma fase contínua separada do meio dispersante (SHAW, 1975).

As emulsões *Pickering* são estabilizadas por uma camada de partículas sólidas adsorvidas na superfície das gotas da emulsão. Esse tipo de emulsão apresenta alta estabilidade à coalescência, mesmo com tamanhos de gotas grandes e por longos períodos de tempo. Essa alta estabilidade se deve a formação da camada de partículas adsorvidas na interface das gotas, desenvolvendo uma barreira quase irreversível (XIAO; LI; HUANG, 2016; MARTA *et al.*, 2023; WANG *et al.*, 2023).

Considerando a biodegradabilidade e biocompatibilidade do amido, esse polímero natural está se tornando um substituto promissor para partículas sintéticas e inorgânicas usadas como estabilizantes de *Pickering*. A partícula coloidal, com modificação adequada, estabiliza a emulsão *Pickering,* formando

uma barreira mecânica na interface da emulsão, o que resulta em um sistema estável e funcional (XIAO; LI; HUANG, 2016; LI *et al.*, 2020).

As nanopartículas de amido podem ser utilizadas como estabilizante nesse tipo de emulsão (Fig. 4), devido ao seu tamanho reduzido e características físico-químicas. Além disso, a crescente preocupação do consumidor com o consumo de produtos mais saudáveis, reforça a importância do uso de estabilizantes naturais , como as nanopartículas de amido (MURRAY, 2019; MARTA *et al.*, 2023).

Figura 4 – Esquema da aplicação de nanopartículas de amido como estabilizantes de emulsão de Pickering.

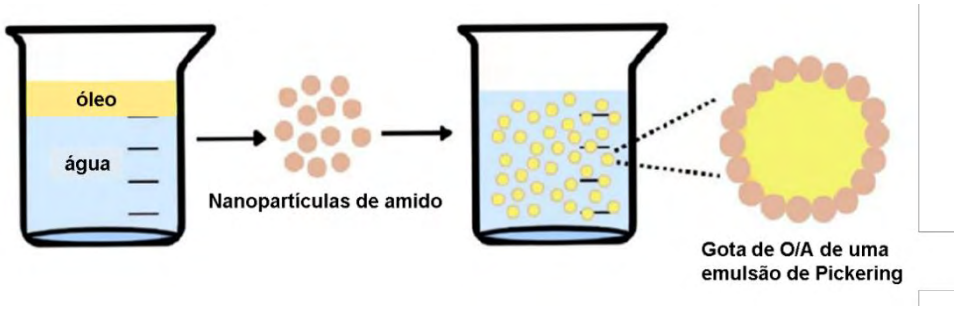

Fonte: Marta *et al.* (2023).

Existem vários estudos sobre a produção de emulsões *Pickering*, utilizando inclusive diferentes tipos de amidos modificados (RAYNER *et al.*, 2012; XIAO; LI; HUANG, 2016; MURRAY, 2019; LI *et al.*, 2020; ZHAI *et al.*, 2020). No entanto, poucos são os relatos desse tipo de emulsão utilizando SNP de amido.

Daniel *et al.* (2020) produziram emulsões *Pickering* com NC de amido de feijão, mandioca e milho, posteriormente oxidados por hipoclorito de sódio, com concentração de nanocristais de 1, 3 e 5% e proporções água:óleo de 1:1 3:1 1:3 (v/v). Os nanocristais foram eficazes na estabilização das emulsões por 21 dias, conforme relatado pelos autores.

Saari *et al.* (2017) produziram emulsões O/A utilizando SNP de amido de milho ceroso modificadas com anidrido octenilsuccínico (OSA) e precipitadas com DMSO e/ou etanol. A concentração de 1 mg de amido/ mL de óleo foi capaz de formar gotas de emulsão com tamanho de 0,5-45 µm, enquanto concentrações menores ou iguais a 0,5 mg/ mL não foram suficientes para

formar a interface gota de óleo/água. As emulsões foram estáveis por até 7 dias, sendo a concentração ótima de amido de 8 mg/ mL.

Guida (2021) produziu emulsões O/A com SNP de amido de mandioca nativo, com proporção óleo:água de 20:80 e concentração de SNP de 1, 2, 3 e 3,5% (m/m) na fase aquosa. O ultrassom foi utilizado durante a produção das emulsões, com potência de 525 W, frequência de 20 kHz, ponteira de titânio e tempo de processamento de 3, 6 e 9 min. A estabilidade cinética das emulsões *Pickering* foi melhorada pelo uso de ultrassom, que reduziu o tamanho das gotas e a polidispersividade. As amostras estabilizadas por amido nativo, que não passaram pelo ultrassom, apresentaram coalescência.

2.5. Géis carregados de emulsão

Recentemente, o uso de emulsão *Pickering* na produção de gel carregado de emulsão e a avaliação do efeito da concentração de agentes gelificantes, fração de volume de óleo e magnitude das forças do sistema têm sido o foco de muitas pesquisas (TORRES *et al.*, 2017; MAO *et al.*, 2018; ZHANG *et al.*, 2022; ZHAO *et al.*, 2023). Vários estudos demonstraram que os sistemas de entrega à base de gel podem melhorar a estabilidade e a biodisponibilidade de muitos ingredientes alimentares com atividade biológica (bioativos) (GEREMIAS-ANDRADE *et al.*, 2017; MAO *et al.*, 2020). No entanto, a investigação sobre os géis carregados de emulsão *Pickering* que utilizam amido para a fase gel e para as SNP na estabilização dessas emulsões ainda é limitada (LI *et al.*, 2020).

Torres *et al.* (2017) produziram géis de amido de trigo na fase gel e amido de milho ceroso modificado com anidrido octenilsuccínico (OSA), como estabilizante da emulsão *Pickering*. Os géis foram preparados com concentrações de 17,2-40% de amido e aquecimento da suspensão (amido + água destilada) a 80 ºC por 40 min, sob agitação manual. Os géis carregados de emulsão foram obtidos com a proporção gel:emulsão de 50-87,5% da fase gel e 12,5-50% de emulsão, em que as duas fases foram misturadas a 80 ºC. Os autores observaram que as gotas de emulsão atuaram como partículas ativas no gel de amido nativo, ficando firmemente ligadas à rede de gel.

Zhang *et al.* (2021) produziram géis de amido de batata na fase gel e amido de milho modificado com anidrido octenilsuccínico (OSA) como estabilizante da emulsão. As formulações variaram de 10 a 30% de emulsão,16% amido batata e 54-71% de água deionizada (m/m). O aquecimento da formulação foi feito a 78 ºC, por 5 min sob agitação mecânica. As gotas de óleo se agregaram nos géis com maiores concentrações de emulsão (25 e 30%). As gotas de óleo atuaram como cargas ativas nos géis. A força do gel dos sistemas pode ser ajustada pelo volume das emulsões. Além disso, os sistemas apresentaram boa estabilidade de cremeação.

Malone e Appelqvist (2003) utilizaram amido de trigo e amido de amaranto para a fase gel e caseinato de sódio e xantana como estabilizantes. As emulsões O/A foram feitas com 10% (m/m) de óleo de girassol, 0,5% de caseinato de sódio e 10% de amido, a 95 ºC por 20 min, utilizando misturador mecânico; e posterior dispersão em goma xantana 1% (m/m). Os autores relataram que foi possível controlar a liberação de voláteis lipofílicos em produtos alimentícios com baixo teor de gordura e os principais fatores que afetaram a taxa de liberação foram o tamanho e o teor de óleo da partícula.

Os géis carregados podem incorporar bioativos lipofílicos, que são benéficos à saúde. As redes de polímeros do gel podem proteger esses bioativos contra estresses ambientais (luz, calor, oxigênio), aumentando a estabilidade do bioativo durante o armazenamento do produto final (DICKINSON, 2012; LU *et al.*, 2019).

A presença de um agente gelificante na fase aquosa converte uma emulsão clássica em um gel carregado (ZHANG *et al.*, 2015). Os géis são sistemas semissólidos formados pela rede tridimensional de um agente gelificante que aprisionam uma fase líquida. Eles são caracterizados por sua rigidez e elasticidade únicas, o que lhes confere propriedades de textura e reológicas favoráveis. Essas propriedades encontram ampla aplicação nas indústrias alimentícia, farmacêutica e cosmética (MAO *et al.*, 2020).

A incorporação de ingredientes bioativos em géis fornece proteção eficaz para melhorar a estabilidade desses ingredientes (PIEVE *et al.*, 2011). Além disso, alguns sistemas de gel também podem melhorar a solubilidade e dispersibilidade de compostos bioativos, inibindo sua cristalização (YU *et al.*, 2012). Assim, as gotas de emulsão são encapsuladas dentro de uma fase sólida

macia, que protege os compostos lipofílicos contra a oxidação (BEAULIEU *et al.*, 2002). Alguns sistemas de gel também podem entregar bioativos lipofílicos e hidrofílicos simultaneamente (Fig. 5) (LU *et al.*, 2019).

Figura 5 – Esquema da formação de um gel de emulsão (O/A) e encapsulação de ingrediente funcional lipofílico e hidrofílico.

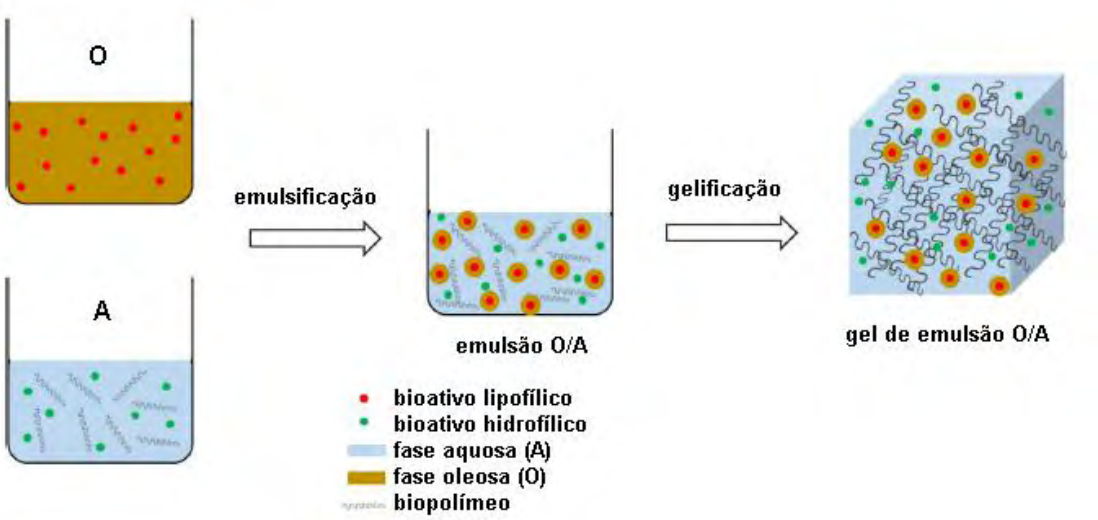

Fonte: Lu *et al.* (2019b).

Os géis carregados podem ser formados por meio de técnicas de gelificação induzida por calor, sal, ácido, pressão, enzima ou cisalhamento em sistemas de emulsão (DICKINSON, 2012). No entanto, a concentração crítica de gelificação dos biopolímeros em géis carregados é geralmente menor do que em hidrogéis, pois as gotas de óleo aprisionadas na rede de gel podem aumentar a força do gel. Neste caso, as gotas de óleo são denominadas cargas ativas, cujas camadas interfaciais interagem com a matriz de gel (DICKINSON, 2012; MAO *et al.*, 2020). Proteínas e/ou amidos com boas propriedades emulsificantes e de gelificação podem formar este tipo de géis carregados. Nestes sistemas novos, o papel das partículas de *Pickering* no desenvolvimento da rede de gel não é totalmente compreendido (MAO *et al.*, 2020).

Além disso, é importante destacar que projetar esses materiais com polímeros biocompatíveis, como o amido, é uma alternativa vantajosa, pois o amido é o segundo biopolímero mais abundante na natureza e é livre de toxicidade (TORRES *et al.*, 2017).

Referências

ACEVEDO, B. A. *et al.* Modification of structural and physicochemical properties of cowpea (Vigna unguiculata) starch by hydrothermal and ultrasound treatments. **Food Hydrocolloids**, v. 124, n. October 2021, 2022.

AGI, A. *et al.* Influence of nanoprecipitation on crystalline starch nanoparticle formed by ultrasonic assisted weak-acid hydrolysis of cassava starch and the rheology of of their solutions. **Chemical Engineering & Processing: Process Intensificatio**, v. 142, 2019.

ARAUJO-FARRO, P. C. **Desenvolvimento de filmes biodegradaveis a partir de derivados do grão de quinoa (Chenopodium quinoa Willdenow) da variedade "Real"**. 2008. 320f.; Tese (Doutorado); Universidade Estadual de Campinas, 2008.

ASCHENBRENNER, E. *et al.* Using the Polymeric Ouzo Effect for the Preparation of Polysaccharide-Based Nanoparticles. **Langmuir**, v. 29, n. 28, p. 8845–8855, 2013.

ATWELL, W. A. *et al.* Characterization of Quinoa Starch. **Cereal Chemistry**, v. 60, n. 1, p. 9–11, 1983.

BEAULIEU, L. *et al.* Elaboration and characterization of whey protein beads by an emulsification/cold gelation process: Application for the protection of retinol. **Biomacromolecules**, v. 3, n. 2, p. 239–248, 2002.

BENINCA, C. **Emprego de técnicas termoanalíticas na análise de amidos nativos e quimicamente modificados de diferentes fontes botânicas**. 2008. 79f.; Dissertação (Mestrado); Universidade Estadual de Ponta Grossa, 2008.

BULÉON, A. *et al.* Mini review starch granules: structure and biosynthesis. **International Journal of Biological Macromolecules**, v. 23, p. 85–112, 1998.

BUZEA, C.; PACHECO, I. I.; ROBBIE, K. Nanomaterials and nanoparticles: Sources and toxicity. **Biointerphases**, v. 2, n. 4, p. MR17, 2007.

CHACON, W. D. C. *et al.* Mathematical Models for Prediction of Water Evaporation and Thermal Degradation Kinetics of Potato Starch Nanoparticles Obtained by Nanoprecipitation. **Starch - Stärke**, v. 71, n. 1–2, p. 1–7, 2019.

CHANG, Y. *et al.* High efficiency and low cost preparation of size controlled starch nanoparticles through ultrasonic treatment and precipitation. **Food Chemistry**, v. 227, p. 369–375, 2017a.

CHANG, Y. *et al.* Influence of ultrasonic treatment on formation of amylose nanoparticles prepared by nanoprecipitation. **Carbohydrate Polymers**, v. 157, p. 1413–1418, 2017b.

CHEN, Y.; XV, J.; YUAN, F. Curcumin-loaded nano-emulsion prepared by high pressure homogenization: impact of emulsifiers on physicochemical stability and in vitro digestion. **Food Science and Technology**, v. 42, 13 jul. 2022.

CHIN, S. F.; PANG, S. C.; TAY, S. H. Size controlled synthesis of starch nanoparticles by a simple nanoprecipitation method. **Carbohydrate Polymers**, v. 86, n. 4, p. 1817–1819, 15 out. 2011.

CODEVILLA, C. F. *et al.* Incorporação da curcumina em sistemas nanoestruturados: Revisão. **Ciência e Natura**, v. 37, p. 152, 2015.

DANIEL, T. H. G. *et al.* Pickering Emulsions Produced with Starch Nanocrystals from Cassava (Manihot esculenta Crantz), Beans (Phaseolus vulgaris L .), and Corn (Zea mays L .). **Starch - Stärke**, v. 1900326, p. 1–8, 2020.

DENARDIN, C. C.; SILVA, L. P. da. Estrutura dos grânulos de amido e sua relação com propriedades físico-químicas. **Ciência Rural**, v. 39, n. 3, p. 945–954, 2009.

DICKINSON, E. Food Hydrocolloids Emulsion gels : The structuring of soft solids with protein-stabilized oil droplets. **Food hydrocolloids**, v. 28, n. 1, p. 224–241, 2012.

DUFRESNE, A. Cellulose-Based Composites and Nanocomposites. **Monomers, Polymers and Composites from Renewable Resources**, p. 401–418, 2008.

EMBRAPA. **Definição e histórico da Canola**. Disponível em: <http://www.cnpt.embrapa.br/culturas/canola/definicao.htm>. Acesso em: 19 maio. 2021.

FARZI, M. *et al.* Original article Effect of ultrasonic treatment on the rheological properties and particle size of gum tragacanth dispersions from different species. **International Journal of Food Science and Technology**, v. 46, p. 849–854, 2011.

FENG, T. *et al.* Emulsion-based delivery systems for curcumin: Encapsulation and interaction mechanism between debranched starch and curcumin. **International Journal of Biological Macromolecules**, v. 161, p. 746–754, 15 out. 2020.

FLEMING, J. E.; GALWEY, N. W. Quinoa (Chenopodium quinoa). In: WILLIAMS, J. T. (Ed.). **Cereals and pseudocereals**. London: Chapman and Hall: Underutilised crop series, 1995. p. 3–83.

GALLANT, D. J.; BOUCHET, B.; BALDWIN, P. M. Microscopy of starch: evidence of a new level of granule organization. **Carbohydrate Polymers**, v. 8617, n. 97, p. 177–191, 1997.

GEREMIAS-ANDRADE, I. M. *et al.* Rheological and mechanical characterization of curcumin-loaded emulsion-filled gels produced with whey protein isolate and xanthan gum. **Lwt**, v. 86, p. 166–173, 2017.

GHOSH, S.; BANERJEE, S.; SIL, P. C. The beneficial role of curcumin on inflammation, diabetes and neurodegenerative disease: A recent update. **Food and Chemical Toxicology**, v. 83, p. 111–124, 2015.

GÓMEZ-ESTACA, J.; GAVARA, R.; HERNÁNDEZ-MUÑOZ, P. Encapsulation of curcumin in electrosprayed gelatin microspheres enhances its bioaccessibility and widens its uses in food applications. **Innovative Food Science and Emerging Technologies**, v. 29, p. 302–307, 2015.

GORDON, R. N. h. langton. **Journal of sound and vibration**, v. 10, p. 22–31, 1969.

GUIDA, C. **Produção e caracterização de emulsões Pickering estabilizadas com nanopartículas de amido de mandioca**. 2021. 108 f. Dissertação (Mestrado). Faculdade de Engenharia de Alimentos. Universidade Estadual de Campinas, Campinas, 2021.

HEDAYATI, S.; NIAKOUSARI, M.; MOHSENPOUR, Z. Production of tapioca starch nanoparticles by nanoprecipitation-sonication treatment. **International Journal of Biological Macromolecules**, v. 143, p. 136–142, 2020.

HOOVER, R. Composition, molecular structure, and physicochemical properties of tuber and root starches: A Review. **Carbohydrate Polymers**, p. 253–267, 2001.

HOOVER, R. The Impact of Heat-Moisture Treatment on Molecular Structures and Properties of Starches Isolated from Different Botanical Sources. **Critical Reviews in Food Science and Nutrition**, v. 50, n. 9, p. 835–847, 2010.

IYER, S. .; MATTINSON, D. S. .; FELLMAN, J. Study of the Early Events Leading to Cassava Root Postharvest Deterioration. **Tropical Plant Biology**, v. 3, n. 3, p. 151–165, 2010.

JI, N. *et al.* Effects of heat moisture treatment on the physicochemical properties of starch nanoparticles. **Carbohydrate Polymers**, v. 117, p. 605–609, 6 mar. 2015.

JOYE, I. J.; MCCLEMENTS, D. J. Production of nanoparticles by anti- solvent precipitation for use in food systems. **Trends in Food Science & Technology**, v. 34, n. 2, p. 109–123, 2013.

JUNA, S. *et al.* Microwave mediated preparation of nanoparticles from wx corn starch employing nanoprecipitation. **Starch - Stärke**, v. 66, n. 3–4, p. 316–325, 1 mar. 2014.

KASEMSUWAN, T. *et al.* Characterization of the Dominant Mutant Amylose-Extender (Ae1-5180) Maize Starch. **Cereal Chemistry**, v. 72, p. 457–464, 1995.

KAUR, J. *et al.* Cereal starch nanoparticles - A prospective food additive: A review. **Critical Reviews in Food Science and Nutrition**, v. 58, n. 7, p. 1097–1107, 2018.

KIM, H.-S.; KIM, B.-Y.; BAIK, M.-Y. Application of Ultra High Pressure (UHP) in Starch Chemistry. **Critical Reviews in Food Science and Nutrition**, v. 52, n. 2, p. 123–141, 2012.

KIM, J. H. *et al.* Starch nanoparticles resulting from combination of dry heating under mildly acidic conditions and homogenization. **Carbohydrate Polymers**, v. 168, p. 70–78, 2017.

KIM, J. H.; PARK, D. H.; KIM, J.-Y. Effect of heat-moisture treatment under mildly acidic condition on fragmentation of waxy maize starch granules into nanoparticles. **Food hydrocolloids**, v. 63, p. 59–66, 2017.

KIM, J. Y.; LIM, S. T. Preparation of nano-sized starch particles by complex formation with n-butanol. **Carbohydrate Polymers**, v. 76, n. 1, p. 110–116, 2 mar. 2009.

KOKSEL, H. *et al.* Improving effect of lyophilization on functional properties of resistant starch preparations formed by acid hydrolysis and heat treatment. **Journal of Cereal Science**, v. 47, n. 2, p. 275–282, 2008.

LAGARRIGUE, S. *et al.* Swelling kinetics of waxy maize and maize starches at high temperatures and heating rates. **Carbohydrate Polymers**, v. 73, n. 1, p. 148–155, 2008.

LEITE, A. L. M. P. **Obtenção e caracterização de nanofibras de celulose a partir de subprodutos da mandioca (Manihot esculenta Crantz)**. 2016. 97f.; Dissertação (mestrado); Universidade Estadual de Campinas, 2016.

LEONEL, M. Analysis of the shape and size of starch grains from different botanical species. **Ciencia e Tecnologia de Alimentos**, v. 27, n. 3, p. 579–588, 2007.

LI, G.; ZHU, F. Quinoa starch: Structure, properties, and applications. **Carbohydrate Polymers**, v. 181, p. 851–861, 2018.

LI, S. *et al.* Pickering emulsion gel stabilized by octenylsuccinate quinoa starch granule as lutein carrier : Role of the gel network. **Food Chemistry**, v. 305, p. 125476, 2020.

LIMA, K. T. dos S. *et al.* Physicochemical Properties of Modified Starches Obtained by Anti-Solvent Precipitation Containing Anthocyanins from Jambolan (Syzygium cumini) Fruit. **Starch/Stärke**, v. 73, n. 3–4, 2021.

LU, Y. *et al.* Development of Emulsion Gels for the Delivery of Functional Food Ingredients: from Structure to Functionality. **Food Engineering Reviews**, v. 11, n. 4, p. 245–258, 2019.

MA, P. *et al.* Preparation of curcumin-loaded emulsion using high pressure homogenization: Impact of oil phase and concentration on physicochemical stability. **LWT**, v. 84, p. 34–46, 1 out. 2017.

MALONE, M. E.; APPELQVIST, I. A. M. Gelled emulsion particles for the controlled release of lipophilic volatiles during eating. **Journal of Controlled Release**, v. 90, p. 227–241, 2003.

MAO, L. *et al.* Emulsion design for the delivery of β-carotene in complex food systems Critical Reviews. **Food Science and Nutrition**, v. 58, n. 5, p. 770–784, 2018.

MAO, L. *et al.* Design of gel structures in water and oil phases for improved delivery of bioactive food ingredients. **Critical Comments on Food Science and Nutrition**, v. 60, p. 1651–1666, 2020.

MARTA, H. *et al.* Starch Nanoparticles: Preparation, Properties and Applications. **Polymers**, v. 15, n. 5, p. 1–31, 2023.

MURRAY, B. S. Pickering emulsions for food and drinks. **Current Opinion in Food Science**, v. 27, p. 57–63, 2019.

NAKSURIYA, O. *et al.* Curcumin nanoformulations: a review of pharmaceutical properties and preclinical studies and clinical data related to cancer treatment. **Biomaterials**, v. 35, n. 10, p. 3365–3383, 2014.

OGUNGBENLE, H. N. Nutritional evaluation and functional properties of quinoa (Chenopodium quinoa) flour. **International journal of food sciences and nutrition**, v. 54, n. 2, p. 153–158, 2003.

OLADEBEYE, A. O. *et al.* Functional, thermal and molecular behaviours of ozone-oxidised cocoyam and yam starches. **Food Chemistry**, v. 141, n. 2, p. 1416–1423, 2013.

OLIVEIRA, N. R. de *et al.* Acetylated Starch-Based Nanoparticles: Synthesis, Characterization, and Studies of Interaction With Antioxidants. **Starch - Stärke**, v. 70, n. 3–4, p. 1700170, 1 mar. 2018.

OLOMO, V.; AJIBOLA, O. Processing factors affecting the yield and physicochemical properties of starch from cassava chips and flour. **Starch - Stärke**, v. 55, n. 10, p. 476–481, 2003.

PARK, E. Y. *et al.* Production of starch nanoparticles using normal maize starch via heat-moisture treatment under mildly acidic conditions and homogenization. **Carbohydrate Polymers**, v. 151, p. 274–282, 2016.

PEDERSSETTI, M. . **Análise dos efeitos da temperatura e pressão na extração supercrítica do óleo essencial de canola com dióxido de carbono supercrítico e n-propano pressurizado**. 2008. 74 f; Dissertação (mestrado); Universidade Estadual do Oeste do Paraná, 2008.

PEREIRA, A. S. .; STRINGHETA, P. C. Considerações sobre a cultura e processamento do açafrão. **Horticultura Brasileira**, v. 16, n. 2, p. 102–105, 1998.

PÉREZ, S.; BALDWIN, P. M.; GALLANT, D. J. Structural Features of Starch Granules I. In: **Starch**. 3. ed. Academic Press, 2009. p. 149–192.

PÉREZ, S.; BERTOFT, E. The molecular structures of starch components and their contribution to the architecture of starch granules: A comprehensive review. **Starch - Stärke**, v. 62, n. 8, p. 389–420, 2010.

PIECYK, M.; DOMIAN, K. Effects of heat–moisture treatment conditions on the physicochemical properties and digestibility of field bean starch (Vicia faba var.

minor). **International Journal of Biological Macromolecules**, v. 182, p. 425–433, 2021.

PIEVE, S. D. *et al.* Effect of monoglyceride organogel structure on cod liver oil stability. **Food Research International**, v. 44, n. 9, p. 2978–2983, 2011.

PINTO, V. Z. *et al.* Effect of Physical Pretreatments on the Hydrolysis Kinetic, Structural, and Thermal Properties of Pinhão Starch Nanocrystals. **Starch - Stärke**, v. 73, n. 7–8, p. 2000008, 1 jul. 2021.

PRICE, G. J.; SMITH, P. F. Ultrasound generator sySadmng piing er Ultrasound. **European Polymer Journal**, v. 29, n. 2, p. 419–424, 1993.

QIU, C. *et al.* A review of green techniques for the synthesis of size-controlled starch-based nanoparticles and their applications as nanodelivery systems. **Trends in Food Science & Technology**, v. 92, n. October 2018, p. 138–151, 2019.

RAVIADARAN, R. *et al.* Optimization of palm oil in water nano-emulsion with curcumin using microfluidizer and response surface methodology. **Lwt**, v. 96, n. March, p. 58–65, 2018.

RAYNER, M. *et al.* Quinoa starch granules as stabilizing particles for production of Pickering emulsions. **Faraday Discussions**, v. 158, p. 139–155, 2012.

REMANAN, M. K.; ZHU, F. Encapsulation of rutin in Pickering emulsions stabilized using octenyl succinic anhydride (OSA) modified quinoa, maize, and potato starch nanoparticles. **Food Chemistry**, v. 405, p. 134790, 30 mar. 2023.

RODRÍGUEZ, J. *et al.* Current encapsulation strategies for bioactive oils : From alimentary to pharmaceutical perspectives. **Food Research International journal**, v. 83, p. 41–59, 2016.

SAARI, H. *et al.* Production of starch nanoparticles by dissolution and non-solvent precipitation for use in food-grade Pickering emulsions. **Carbohydrate Polymers**, v. 157, p. 558–566, 2017.

SHABANA, S. *et al.* Ultrasound assisted acid hydrolyzed structure modi fi cation and loading of antioxidants on potato starch nanoparticles. **Ultrasonics - Sonochemistry**, v. 51, n. July 2018, p. 444–450, 2019.

SHAW, D. J. **Introdução à química dos colóides e de superfícies**. São Paulo: Edgard Blücher Ltda, 1975.

TESTER, R. F. Properties of damaged starch granules: composition and swelling properties of maize, rice, pea and potato starch fractions in water at various temperatures. **Food hydrocolloids**, v. 11, n. 3, p. 293–301, 1997.

TESTER, R. F.; KARKALAS, J.; QI, X. Starch - Composition, fine structure and architecture. **Journal of Cereal Science**, v. 39, n. 2, p. 151–165, 2004.

TORRES, O. *et al.* Novel starch based emulsion gels and emulsion microgel particles : Design , structure and rheology. **Carbohydrate Polymers**, v. 178, n. September, p. 86–94, 2017.

VAN SOEST, J. J. G.; VLIEGENTHART, J. F. G. Crystallinity in starch plastics: consequences for material properties. **Trends in biotechnology**, v. 15, n. 6, p. 208–213, 1997.

VELÁSQUEZ-CASTILLO, L. E. *et al.* Quinoa starch nanocrystals production by acid hydrolysis: Kinetics and properties. **International Journal of Biological Macromolecules**, v. 143, p. 93–101, 2020.

WANG, H. *et al.* Insights into the multi-scale structure and digestibility of heat-moisture treated rice starch. **Food Chemistry**, v. 242, p. 323–329, 1 mar. 2018.

WANG, R. *et al.* Characterization of Pickering emulsion by SCFAs-modified debranched starch and a potent for delivering encapsulated bioactive compound. **International Journal of Biological Macromolecules**, v. 231, p. 123164, 15 mar. 2023.

WIGATI, L. P. *et al.* Application of pregelatinized corn starch and basil essential oil edible coating with cellulose nanofiber as Pickering emulsion agent to prevent quality-quantity loss of mandarin orange. **Food Packaging and Shelf Life**, v. 35, n. September 2022, p. 101010, 2023.

WURZBURG, O. B. Nutritional Aspects and Safety of Modified Food Starches. **Nutrition Reviews**, v. 44, n. 2, p. 74–79, 1986.

XIAO, J. .; LI, Y. .; HUANG, Q. Recent advances on food-grade particles stabilized Pickering emulsions: Fabrication, characterization and research trends. **Trends in Food Science and Technology**, v. 55, p. 48–60, 2016.

XIE, S. X.; LIU, Q.; CUI, S. W. Starch Modifications and Applications. In: CUI, S. W. (Ed.). **Food Carbohydrates: Chemistry, Physical Properties, and Applications**. 1 st ed. London, New York, Singapore: Boca Raton, 2005. p. 357–406.

YU, H. *et al.* Development of a food-grade organogel with high bioaccessibility and loading of curcuminoids. **Food Chemistry**, v. 131, n. 1, p. 48–54, 2012.

YU, X. *et al.* A new way for the oil plant biomass valorization : Polyphenols and proteins extraction from rapeseed stems and leaves assisted by pulsed electric fields. **Industrial Crops & Products**, v. 74, p. 309–318, 2015.

ZHAI, K. *et al.* Synthesis of millimeter-sized hydrogel beads by inverse Pickering polymerization using starch-based nanoparticles as emulsifier. **polymers for advanced technologies**, 2019, p. 1321–1329, 2020.

ZHANG, L. *et al.* Ultrasonics Sonochemistry Ultrasound effects on the degradation kinetics , structure and rheological properties of apple pectin. **Ultrasonics Sonochemistry**, v. 20, n. 1, p. 222–231, 2013

ZHANG, Y. *et al.* Physical properties and salt release of potato starch-based emulsion gels with OSA starch-stabilized oil droplets. **LWT**, v. 141, p. 110929, 2021.

ZHANG, Z. *et al.* Designing hydrogel particles for controlled or targeted release of lipophilic bioactive agents in the gastrointestinal tract. **European Polymer Journal**, v. 72, p. 698–716, 2015.

ZHAO, X. *et al.* Role of gelation temperature in rheological behavior and microstructure of high elastic starch-based emulsion-filled gel. **Food Hydrocolloids**, v. 135, n. July 2022, p. 108208, 2023.

ZHU, F. Composition, structure, physicochemical properties, and modifications of cassava starch. **Carbohydrate Polymers**, v. 122, p. 456–480, 2015.

ZOBEL, W. Potato starch. In: **Methods in carbohydrate chemistry**. New York, USA: Academic Press, 1964.

3. CAPÍTULO 3: COMBINED METHODS FOR CASSAVA STARCH MODIFICATION BY PHYSICAL TREATMENTS FOR PRODUCTION OF *PICKERING* STABILIZERS

Abstract

In current research, cassava starch nanoparticles (SNP) were produced by the nano-precipitation method after modification of starch granules by ultrasound (US) or heat moisture treatment (HMT). The particles produced showed cluster plate formats, which were smooth for particles produced by native starch (NSNP) and rough for particles from modified starch by US (USNP) or HMT (HSNP) with smaller size ranges presented by HSNP (~63-674 nm) compared with USNP (~123-1300 nm) and NSNP (~25 to 1450 nm). SNP had low surface charge values between -1.4 and -3.4 mV, as well as V-type crystalline structure. The reduction of crystallinity was confirmed by FTIR and thermal analyses. The SNP produced after physical pre-treatments (US, HMT) showed an improvement in lipophilicity with oil absorption capacity in decreasing order from HSNP, USNP to NSNP, which was confirmed by the significant increase in contact angles from ~68.4° (NSNP) to ~76° (USNP; HSNP). USNP (in concentrations = 4 g/ 100 g emulsion) were not capable of stabilizing an oil-water emulsion (20%v/v oil), whereas for HSNP at same concentration, this emulsion did not show separation during the monitoring period (7 days at 20 ºC). Emulsions produced with NSNP exhibited phase separation after preparation. Our findings, therefore, demonstrate the potential of physical modifications to obtain starch nanoparticles for applications as Pickering stabilizers in clean-label food grade products.

Keywords: anti-solvent precipitation, starch modification, cassava starch, Pickering emulsions.

3.1. Introduction

Starch is a widely utilized carbohydrate source for food and non-food applications that can be found in plants, tubers and roots (BULATOVIĆ *et al.*, 2021; KHAKPOUR; PIRSA; AMIRI, 2023). This polysaccharide is formed by straight chains of amylose (20%–30%) and branched chains of amylopectin (70%–80%) with an amylose/amylopectin ratio, depending on the source (OTACHE *et al.*, 2021; RAHAMAN *et al.*, 2021). Furthermore, starch granules possess a semi-crystalline structure that is associated with amylopectin chains interactions. These granules are typically classified as A-, B- and C-type polymorphisms, which are typical of cereal, tuber and legume starches, respectively (FROST *et al.*, 2009).

Native starches have low solubility in cold water, easy retrogradation, and low emulsification capacity that limits their food applications (ALI; DASH; ROUTRAY, 2020; OTACHE *et al.*, 2021). An alternative to improve the physicochemical properties of native starches is to modify them through chemical, physical, or enzymatic treatments (LIMA *et al.*, 2021; OTACHE *et al.*, 2021). Additionally, there is a strong concern about using safe and environmentally friendly technologies for starch modification. Physical modification of starch is an alternative since it is a totally green process and free of toxic residues, commonly referred to as clean-label starch. Among these technologies, there are modifications by ultrasound (US), heat moisture treatment (HMT), and nano-precipitation with anti-solvent.

Ultrasound is a non-thermal processing technology that can be used to modify starch by mechanical and cavitation effects. During sonication treatment, the sound waves generate mechanical effects such as agitation and particle dispersion, and the ultrasound energy is transferred through a phenomenon called cavitation. Such phenomenon involves the formation and rapid collapse of bubbles in a liquid, resulting in heat and pressure elevations (MALLAKPOUR; KHODADADZADEH, 2018). This technique is useful for modifying the physicochemical and functional properties of starch granules because it offers the advantage of higher selectivity in a short processing time (AMINI; RAZAVI; MORTAZAVI, 2015).

On the other hand, HMT, starch is processed at low moisture content (< 35%) and high temperatures (T > 90 °C) for a certain period of time (1 – 16 h). This treatment significantly affects the thermal stability of starch and leads to alterations in structural factors such as crystallinity and granule shape (LI; WARD; GAO, 2011; JI *et al.*, 2015). In addition, HMT can increase the linkage of starch chains by disrupting crystalline and helical structures, followed by the re-association of damaged crystals and increased mobility of the amorphous region that causes the ordering of the double helix (PRATIWI; FARIDAH; LIOE, 2018).

Regarding anti-solvent precipitation method or nano-precipitation, this involves gelatinizing starch granules through heating and subsequently precipitating of the biopolymer by adding ethanol dropwise (LIMA *et al.*, 2021). The anti-solvent used in this method is typically a liquid in which the starch is insoluble or has a significantly lower solubility. This process is considered safe and non-toxic. Moreover, the nanoparticles produced are amorphous, which increases their flexibility and could aid in the formation and stabilization of the interfacial layer in Pickering-type emulsions (ZHU, 2019).

To the best of our knowledge, studies have scarcely reported a comprehensive analysis of the microstructural changes and their relationship with the functional properties of cassava starch with dual modification (US + nanoprecipitation or HMT + nanoprecipitation). Therefore, this study focused on the correlation between the structural and techno-functional properties of cassava starch modified by two physical methods, as a contribution to the application of this nanomaterial as a stabilizer of Pickering emulsions. Thus, we were able to propose a simple and environmentally friendly method for the preparation of tailored cassava starch nanoparticles.

3.2. Material and Methods

3.2.1. Material

Cassava starch (Siamar, Neves Paulista, SP, Brazil) was employed as the macromolecule, and canola oil (Liza, Cargil, Mairinque, SP, Brazil), soybean oil (Liza, Cargil, Mairinque, SP, Brazil) and absolute ethanol (99.8%, Êxodo,

Sumaré, SP, Brazil) were used in processing. All reagents were of analytical grade.

3.2.2. Starch physical pretreatments

Native cassava starch 12.5 ± 0.1% moisture content (wb); 0.1 ± 0.0% of ashes; 0.2 ± 0.1% of proteins (db); 0.4 ± 0.1% of fibers (db) and 0.0 ± 0.0% of total lipids (db) contents) were previously modified by two separate physical methods: US and HMT.

Native cassava starch was modified by US using the method described by Sujka and Jamroz (2013). A starch suspension (10% w/v) was placed in an ultrasound bath (Q5.9/25A, Eco-Sonics, Indaiatuba, SP, Brazil), at a frequency of 25 kHz and a power of 154 W, for 30 min. Afterward, the sample was centrifuged, and the precipitate was dried in an air convection oven (TE-394/3, Tecnal, Piracicaba, SP, Brazil), at 30 ºC, until it reached a moisture content ~10% (wb). The dried samples were sieved (100 mesh) and stored in airtight packages.

Starch modification by HMT was conducted following the methodology proposed by Piecyk and Domian (2021), with some modifications. The moisture content of the starch was adjusted to 20%, and the samples were stored in airtight packages under refrigeration (4 ºC) for 24 h. After equilibration, the samples were heated at 130 °C for 4 h in an air convection oven (Tecnal, TE-394/3, Piracicaba, SP, Brazil), cooled, sieved and stored in airtight packages. The starches were named NCS (native cassava starch), UCS (ultrasonic-modified cassava starch) and HCS (HMT-modified cassava starch).

3.2.3. Preparation of starch nanoparticles

The production of SNP was carried out according to the methodology described by Ge *et al.* (2017), with some modifications. Cassava starches (native or modified) were dispersed in distilled water (5% w/v) and gelatinized at 95 ºC for 30 min. After cooling, absolute ethanol was added in a 1:1 (v/v) ratio of water:ethanol, and the mixture agitated for 12 h at 25 ºC. Subsequently, the samples were centrifuged (Eppendorf centrifuge, model 5430R, São Paulo, Brazil) at 3,000xg for 15 min and washed twice with absolute ethanol. The SNP

were freeze-dried in a lyophilizer (LC5500, Terroni, São Carlos, SP, Brazil), crushed, sieved (100 mesh), and stored in hermetically sealed containers. The nanoparticles produced from native starch and starches modified by US or HMT were named as NSNP, USNP, and HSNP, respectively.

3.2.4. Scanning electron microscopy

To analyze the surface of starch samples (native and modified by US or HMT), an electron microscope (SEM HITACHI, TM-3000, Maidenhead, UK) was used. The samples were stored on silica gel and vacuum for 12 hours. A voltage of 15 kV and an increase of approximately magnification of 10,000 × were used.

For the observation of SNP obtained from native or modified starches (US or HMT), a SEM FEG microscope (FEI Magellan 400 L Midland, Canada) with Field Emission Gun and EDS (Energy Dispersive X-Ray Spectroscopy) was utilized. SNP were dispersed in distilled water at concentrations of 0.02% (w/v), deposited directly on carbon tape along with the stub and dried in a desiccator containing with silica gel (25 ºC, 12 h). Afterwards, they were covered with gold and subjected to microscopy (VELÁSQUEZ-CASTILLO *et al.*, 2023).

3.2.5. Particle size analysis and zeta potential measurements

Starch size distribution analysis was performed using a laser diffraction particle size analyzer (Shimadzu, SALD-201V, Kyoto, Japan) and the software Sald Wing, version 1.0 (Sald Wing, Kyoto, Japan). Starch samples were diluted approximately 1000 times in absolute ethanol. The average size of the particles was expressed by the average diameter (Equation 1) and calculated from the size distribution curve of the equipment software itself (MCCLEMENTS, 2004).

$$D_{[4,3]} = \frac{\Sigma n_i d_i^4}{\Sigma n_i d_i^3} \qquad (1)$$

The average particle size and size distribution of SNP (pH ~7.0) was carried out by photon correlation spectroscopy (Malvern, ZetaSizer Ultra, Cambridge, UK), at 25 °C. The samples were diluted in deionized water at a

concentration of 0.1% (w/v) to avoid the phenomenon of multiple scattering of light. Data analyses were performed by software included with the system and are presented as the mean ± standard deviation (JIANG *et al.*, 2016).

The zeta potential of the samples (starches and SNP) (pH ~ 6.0 - 7.0) was determined using Zetaplus equipment (Malvern, Zeta Size Ultra, Cambridge, UK) at 25 °C. Samples were diluted in deionized water at a concentration of 0.1% (w/v) (JIANG *et al.*, 2016). Data analyses were performed by software included with the system and are presented as the mean ± standard deviation.

3.2.6. X-ray diffraction (XRD)

Native or modified starches and SNP were stored in desiccators containing silica gel (25 ºC) for 10 days. Subsequently, the X-ray spectra of the samples was obtained using an X-ray diffractometer (Rigaku brand, model MiniFlex600, Texas, USA), with a 2θ angle ranging from 4º to 36º and a scan rate of $2º.min^{-1}$, 40 kV and 15 mA (VELÁSQUEZ-CASTILLO *et al.*, 2023).

Relative crystallinity (RC, %) was calculated using the ratio between the area of crystalline peaks and the total area under the curve of the XRD spectrum, multiplied by 100. The calculation of the areas was done using Origin Pro software, version 9 (OriginLab, Sumaré, SP, Brazil).

3.2.7. Fourier transform infrared spectroscopy analysis (FTIR)

To evaluate the possible changes in the chemical bonds of the starches and SNP, spectroscopy analysis was performed in the infrared region. The samples were kept in a desiccator containing silica gel (25 ºC) for 10 days. FTIR spectra were obtained in a spectrophotometer (Perkin-Elmer, Massachusetts, USA) with a UATR (Universal Attenuator Total Reflectance) accessory. Analyses were performed in the spectral range from 400 to 4000 cm^{-1}, totaling 16 scans for each sample (VELÁSQUEZ-CASTILLO *et al.*, 2023). FTIR spectra were collected and analyzed with the software Spectrum V 5.3.1 (Perkin-Elmer, Massachusetts, USA). Subsequently, the curves were normalized using Origin Pro software, version 9 (OriginLab, Sumaré, SP, Brazil).

3.2.8. Differential scanning calorimeter (DSC)

Thermal properties of starches and SNP were assessed using a differential scanning calorimeter (DSC TA2010, TA Instrument, New Castle, USA). The samples (2 mg) were weighed in an aluminum sample holder and mixed with deionized water at a starch:water ratio of 1:3. The vials were sealed and allowed to be equilibrated at room temperature for 2 h prior to analysis. Scanning was performed at a rate of 10 °C/min, ranging from 30 to 130 °C (VELÁSQUEZ-CASTILLO *et al.*, 2020). An empty aluminum sample holder was used as a reference. Transition temperatures were determined directly from the thermal curves using the Universal Analysis program, version 1.7F (TA Instruments, New Castle, USA).

3.2.9. Solubility in water (SW) and swelling power (SP)

The solubility in water and swelling power analysis followed the methodology proposed by Ge *et al.* (2022), with some modifications. Starch and SNP (1 wt%) were placed in a bath for 30 min at a temperature of 90 ºC and vortexed every 10 min. Afterwards, the samples were cooled to room temperature and centrifuged at 4,000 rpm for 15 min. The supernatant was separated, dried in an oven at 110 °C for 48 h and weighed. The precipitate was also weighed to calculate the swelling power and solubility in water.

3.2.10. Oil absorbing capacity

To determine the oil absorption capacity, a ratio of 10 mL of soybean oil per 1 g of sample (starch or SNP) was prepared, following the method outlined by Uzomah and Ibe (2011). The mixture was shaken briefly and allowed to stand for 30 min, centrifuged (3,500*x*g, 15 min), and the resulting supernatant was discarded. The residue was weighed, and the excess weight was taken as the oil absorption capacity.

3.2.11. Contact angle measurement

Dispersions containing 4% of gelatinized starch (90°C, 30 min) or 4% SNP dispersion in water were placed on a glass slide and dried in an oven at 30 ºC, until a thin layer of film formed. A drop of milli Q water (5 µL) was placed on top of each film and remained at rest for 45 s. The contact angle was measured with a tensiometer (Theta Tensiometer, Attension, São Paulo, Brazil) and the software of the equipment itself (DEWI *et al.*, 2022).

3.2.12. Production of Pickering emulsions with SNP as stabilizers

Emulsions were prepared with a ratio of 20:80 (canola oil:water), with 2.4, 3 and 4% (w/w) of SNP as stabilizers (added in the water phase). The dispersed phase (O) was added to the continuous phases (W) at room temperature, and homogenized using a rotor-stator homogenizer (Ultra-Turrax IKA, model T25, Labotechnik, Staufen, Germany) at 14,000 rpm for 3 min (RAMOS *et al.*, 2023). Pickering emulsions stabilized with SNP were monitored for 7 days, at 20°C, away from light, to observe stability to phase separation.

3.2.13. Statistical Analyses

All analyses were performed in at least triplicate. The results were submitted to analysis of variance (ANOVA), and the means were compared by the Tukey test ($p < 0.05$) using SAS software, version 9.4 (Statistical Analysis System, São Paulo, Brazil).

3.3. Results and Discussion

3.3.1. Scanning electron microscopy

Figure 1 displays SEM micrographs of native and modified starches (a,b,c), as well as SNP produced with native and modified starches by nano-precipitation (d,e,f). Native cassava starch presented granules with rounded,

oval, or oval-truncated shapes with very heterogeneous sizes and smooth surfaces without cracks (Fig. 1.a). Velásquez-Castillo *et al.* (2023) reported similar results for native cassava starch. Starch granules did not show significant differences in shape or on the surface after modification by US (Fig. 1.b) or HMT (Fig. 1.c), which indicates a softer change that can be explained by the treatment conditions used in this study.

Figure 1 - SEM analysis of native cassava starch (NCS) (a) and modified cassava starch by US (UCS) (b) or HMT (HCS) (c); and starch nanoparticles produced by native starch (NSNP) (d) and modified starch by US (USNP) (e) or HMT (HSNP) (f). Scale bar 50 µm or 500 nm

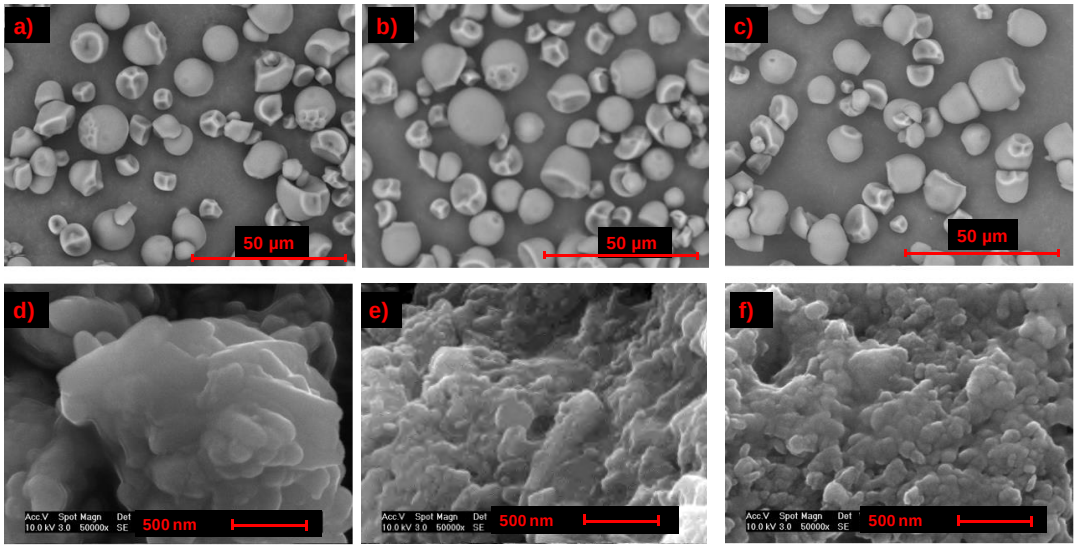

Source: own authorship.

Gunaratne and Hoover (2002) reported similar results for ultrasonically treated cassava starch. Dewi *et al.* (2022) modified sago starch by HMT (20% moisture content 120 ºC/1h) and reported that there was no change in the shape of the granules, but roughness, cracks, and cavities were observed on their surface. These differences could be due to differences in processing or differences in the source of starch used.

SNP showed the existence of laminar aggregates with large particle sizes due to hydrogen bonding interactions, resulting from a high number of hydroxyl groups on the surface of the SNP during nano-precipitation (GE *et al.*, 2017). After nano-precipitation, with the formation of aggregate plaques, the interaction between glycosidic chains increases, which decreases the hydroxyl groups available for hydration, increasing the hydrophobicity of these particles (SNP)

when compared to starches (GE *et al.*, 2017; WANG; LI; ZHENG, 2021). In addition, the SNP produced from starches modified by US and HMT showed higher surface roughness (Fig. 1.e, f) when compared to NSNP (Fig. 1.d), which had a smooth plate shape. Ethanol precipitation generally confers surface roughness and expansion of the starch particle, making the structure more porous after nano-precipitation (FENG *et al.*, 2022).

The surface roughness of the USNP can be explained by the pre-attack US treatment in the granule, which may have weakened its structure, making it more susceptible to greater damage after nano-precipitation. As for HSNP, the rough surface can be explained due to the evaporation of water during the heat treatment, which induces the molecules of the amylopectin helix double chain to reorganize into a denser packing structure by acting as a barrier to penetration water in starch granules (DEWI *et al.*, 2022).

A similar result was reported by Kamwilaisak *et al.* (2022), who obtained rice starch nanocrystals through acid hydrolysis and also obtained laminar aggregates after starch hydrolysis. Ji *et al.* (2015) produced waxy maize starch SNP by modification with hydrogen phosphate and citric acid, followed by gelatinization and enzymatic reaction. These authors applied HMT (20 and 30% and 90 and 100 ºC, 4 h) after particle production and also reported that the shapes of SNP obtained by HMT+NP combination remained without visible changes.

3.3.2. Particle size analysis and zeta potential measurement

Figure 2 shows the particle size distribution of starches and SNP. Native cassava starch (NCS) showed a bimodal distribution with a lower peak at 2.2 µm and a higher peak at 19 µm (Fig. 2.a), values similar to those presented by Lima *et al.* (2021) for native cassava starch (2-30 µm). Ultrasound-modified starch (UCS) showed a unimodal distribution, with a single peak at 17 µm (Fig. 2.a), which can be explained by the breakage of agglomerates during ultrasonic processing. The starch modified by HMT (HCS) showed a polymodal distribution, with peaks at 0.7, 1.9, and 30 µm (Fig. 2.a); this effect may be due to the weakening of the granule during treatment with heat and moisture.

Figure 2 - Size distribution of native cassava starch (NCS) and modified cassava starch by US (UCS) or HMT (HCS) (a); and starch nanoparticles produced by native starch (NSNP) and modified starch by US (USNP) or HMT (HSNP) (b)

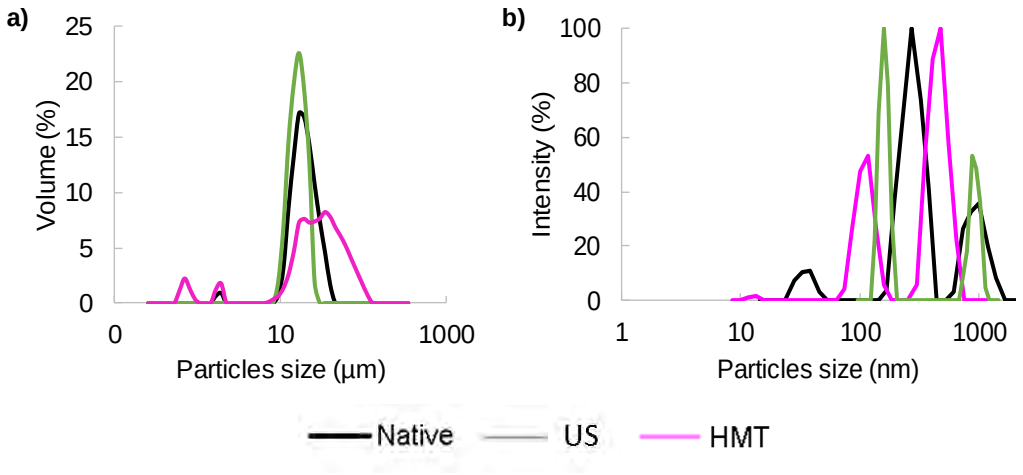

Source: own authorship.

Similar results have been reported in the literature. Amini; Razavi and Mortazavi (2015) sonicated corn starch (25 - 65 ºC, 5 - 15 min) and observed that US treatment did not considerably change granule size at temperatures below 65 °C. Chandla, Saxena and Singh (2017) modified amaranth starch by HMT (28% moisture content, 110 °C for 2.5 h) and reported an increase in mean granule size from 1.4 to 10 µm, which could be attributed to the formation of aggregates or melting during heat treatment.

The SNP also showed different size distributions depending on the treatment each starch was submitted. The NSNP exhibited peaks at 38, 207, and 1030 nm (Fig. 2.b), representing the widest distribution range among the SNP and exhibiting a polymodal distribution. Similar results were found by Lima *et al.* (2021), who reported the size distribution of cassava SNP, produced by nano-precipitation with a slightly acidified ethanol method, ranging from 30 - 100 nm and 200 - 900 nm. Ge *et al.* (2017) produced SNP from maize, tapioca, and sweet potato starches through the ethanol nano-precipitation method and reported mean diameter sizes between 184 - 227 nm. This difference in the sizes obtained by this author, as compared to our study, may be due to different times and speeds of agitation in the preparation of the nanoparticles.

USNP showed peaks at 160 and 950 nm (bimodal) due to the disaggregation effects caused by ultrasound (Fig. 2). HSNP exhibited peaks at 117 and 470 nm (bimodal), being the only sample with sizes smaller than ~700 nm compared to the other SNP. The formation of smaller particles by HSNP can be explained by the pre-weakening of the granule after HMT modification, which facilitated the breakage and formation of smaller structures during nano-precipitation. Ji *et al.* (2015) produced SNP from waxy maize starch with enzymatic reaction and modified these particles by HMT. These authors observed that the SNP sizes were 50–120 nm and, sizes smaller than those found in this study. This difference may be due to the different techniques and order of modifications used in the production of the particles.

Polydispersity index (PDI) ranged from 0.80 to 0.42 (Table 1) with a reduction in particles produced after physical pretreatments (US and HMT) and a significant reduction for HSNP (PDI = 0.42). This indicates that the HSNP produced particles of more homogeneous sizes among the tested treatments.

The Zeta potential values (ZP) of native cassava starch were -50.5 mV (Table 1), a value similar to that reported by Lima *et al.* (2021). Modified starches also showed high zeta potentials, with no significant difference between them (-44 to -45.3 mV). Conversely, SNP presented much lower ZP values (-2.0 mV, an average) (Table 1), which indicates low surface charge, typical of Pickering-type emulsion stabilizers, and did not differ from each other. Other authors reported different results. Lima *et al.* (2021) reported ZP values for cassava SNP of ~ -18 mV. Ge *et al.* (2017) produced SNP from corn, tapioca and sweet potato starches and reported ZP values from ~ -14 to -17 mV. These values are higher than those obtained in this study. This difference can be explained by differences in starch sources or in SNP production methodology.

Table 1 - Polydispersity index (PDI) and zeta potential (ZP) of native cassava starch (NCS) and modified cassava starch by US (UCS) or HMT (HCS), and starch nanoparticles produced by native starch (NSNP) and modified starch by US (USNP) or HMT (HSNP).

Sample	PDI	Zeta Potential (mV)
NCS	-	-50.5 ± 1.3^{c}
UCS	-	-44.0 ± 1.0^{b}
HCS	-	-45.3 ± 2.9^{b}
NSNP	0.80 ± 0.11^{a}	-1.0 ± 0.2^{a}
USNP	0.65 ± 0.12^{a,b}	-1.7 ± 0.5^{a}
HSNP	0.42 ± 0.01^{b}	-3.4 ±0.6^{a}

Different lowercase letters in the same column indicate a significant difference ($p < 0.05$). Source: own authorship.

3.3.3. X-ray diffranction (XRD)

Native and modified starches exhibited A-type crystal diffraction patterns, respectively (Fig. 3.a), with diffraction peaks at 15°, 17°, 18°, 20º and 23° that were similar to those reported in the literature for native cassava starch (LIMA *et al.*, 2021; RAHAMAN *et al.*, 2021). The relative crystallinity (RC) of these samples stayed ~22% for native and modified starches. The process parameters applied in the pre-modification of starch did not alter starch crystallinity when compared to the native starch. Similar results have been reported by Rahaman *et al.* (2021).

Figure 3 - XRD diffraction and relative crystallinity of native cassava starch (NCS) and modified cassava starch by US (UCS) or HMT (HCS) (a); and starch nanoparticles produced by native starch (NSNP) and modified starch by US (USNP) or HMT (HSNP) (b)

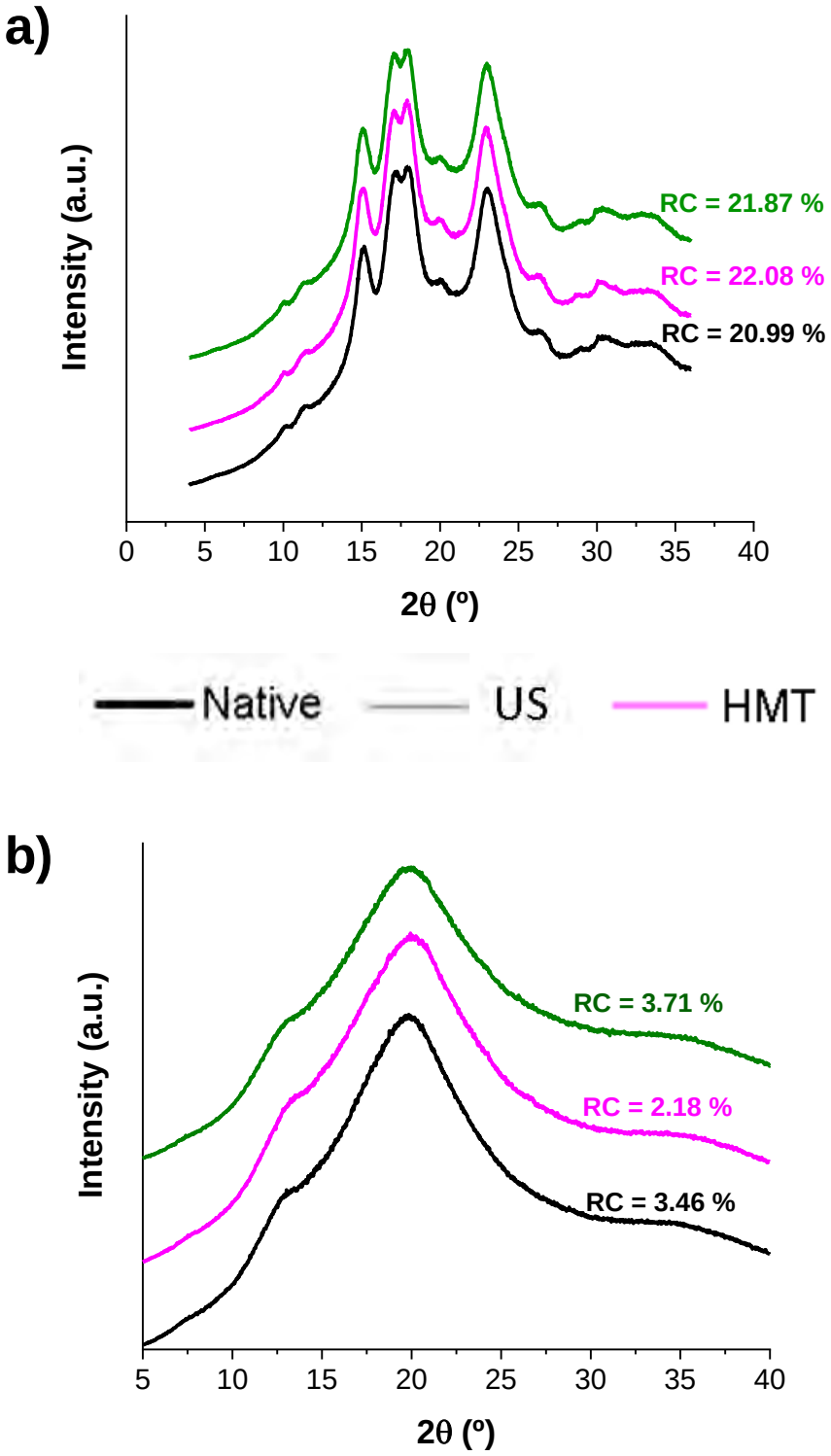

Source: own authorship.

On the other hand, other authors reported a slight reduction in RC for US treated starches (AMINI; RAZAVI; MORTAZAVI, 2015; RAHAMAN *et al.*, 2021), suggesting that the US may have damaged the crystalline structure of the starch granules, which did not happen in this study. Ali, Dash and Routray (2020) reported more drastic changes for HMT-treated lotus seed starch, with an increase in RC from 37.1 to 44.2%, and explained this fact due to the displacement of the double helices towards the interior of the crystallites during the HMT, leading to a more compact and ordered arrangement, a behavior also not observed in this study. This indicates that, in this case, the physical pretreatments (US, HMT) were milder.

SNP showed a V-type crystal structure with a small diffraction peak at 13° and a halo at 20° (Fig. 3.b). This crystalline structure is typical of starches with low crystallinity (LIMA *et al.*, 2021). The SNP presented much lower RC values than the native and modified starches, staying around 3%. This reduction in the RC value is related to the breakdown of the starch crystalline structure after gelatinization and precipitation with anti-solvent. Similar results were reported by Lima *et al.* (2021) (RC = 1.0% - 2.5%). Furthermore, the strong peak intensity of V-type and the low relative crystallinity of the SNP suggest that gelatinization was complete, and there was amylose/amylopectin dispersion of the starch granules after nano-precipitation. In addition, the V-type crystal structure was formed by the rapid formation of amylose-ethanol complexes (FENG *et al.*, 2022).

3.3.4. Fourier transform infrared spectroscopy analysis (FTIR)

The FTIR spectra of native and modified starches, as well as SNP, are depicted in Fig. 4. The absorbance spectra were quite similar for all samples. This observation is likely attributed to the absence of new chemical groups introduced into the starch molecules due to through the modifications induced by the US, HMT or nano-precipitation.

Figure 4 - FTIR spectra of native cassava starch (NCS) and modified cassava starch by US (UCS) or HMT (HCS) (a); and starch nanoparticles produced by native starch (NSNP) and modified starch by US (USNP) or HMT (HSNP) (b)

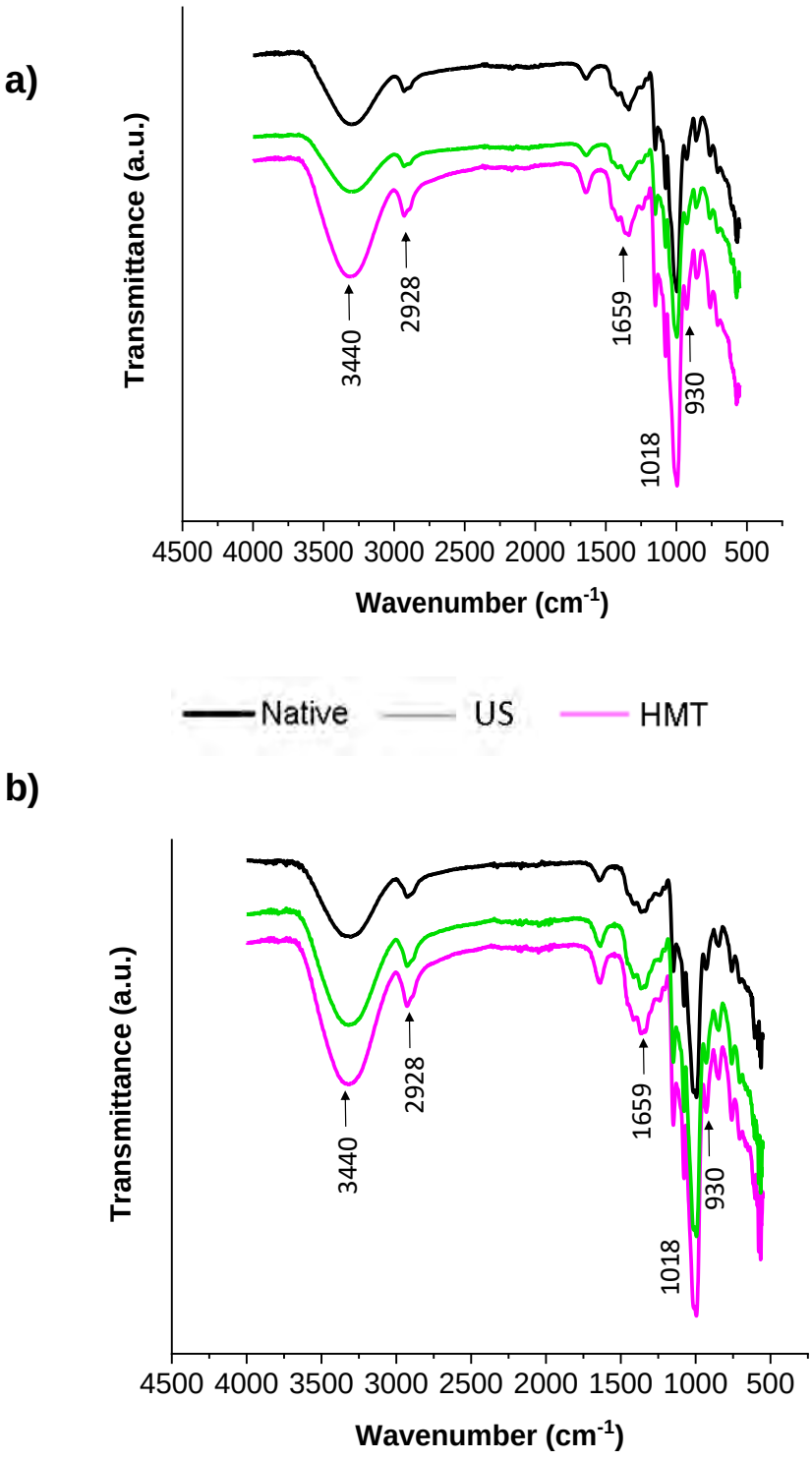

Source: own authorship.

The peak at 3440 cm^{-1} corresponds to the stretching vibration of the -OH groups, related to intra and intermolecular hydrogen bonds. The bands between 2800 and 3000 cm^{-1} are attributed to CH stretching vibrations, which reflect the hydrophobicity and lipophilicity of the starch (NIKOLIC; CAKIC, 2007). The band at ~1640 cm^{-1} is associated with the moisture content of the samples that connect to the vibrations of water molecules adsorbed in the non-crystalline region (SAMMON *et al.*, 2006). The peaks at 1010, 1080, and 1150 cm^{-1} are attributed to the C–O and C–C stretching vibrations of the polysaccharide molecules (PAL; MAL; SINGH, 2005). Furthermore, the absorption bands between 950 and 1150 cm^{-1} are related to the vibrations of the glycosidic bonds C–O, C–O–C and C–O–H (RAZAVI *et al.*, 2014).

After starch pre-modification by US or HMT, there was an increase in peak intensity at 2928 cm^{-1}, which reflects an increase in the lipophilicity of the modified starch. Similar results were reported by Wang *et al.* (2020) for ultrasonic-treated potato starch. Furthermore, after nano-precipitation, the peak at 1659 cm^{-1} showed a reduction, suggesting that fewer water molecules hydrated the SNP, i.e., an indication that the SNP has a higher hydrophobicity in water when compared to starches. Lima *et al.* (2021) reported similar results for cassava and potato SNP; furthermore, bands 1022 and 1047 cm^{-1} are indicative of amorphous and crystalline structures, respectively. All SNP showed an increase in the 1018 cm^{-1} band when compared to starches, indicating an increase in the amorphous content of this material, which corroborates the XRD results.

3.3.5. Differential scanning calorimeter (DSC)

The differential scanning calorimetry (DSC) curves of the NCS (Fig. 5.a) showed a peak temperature (Tp) of 69.3 ºC (Table 2) with no significant difference for the UCS. These values are similar to those reported by Lima *et al.* (2021) for native cassava starch. HCS, on the other hand, showed significantly lower values for Tp (67.8 ºC), which can be explained by the weakening of the granule after heat treatment.

Figure 5 - Heat flow curves of native cassava starch (NCS) and modified cassava starch by US (UCS) or HMT (HCS) (a); and starch nanoparticles produced by native starch (NSNP) and modified starch by US (USNP) or HMT (HSNP) (b)

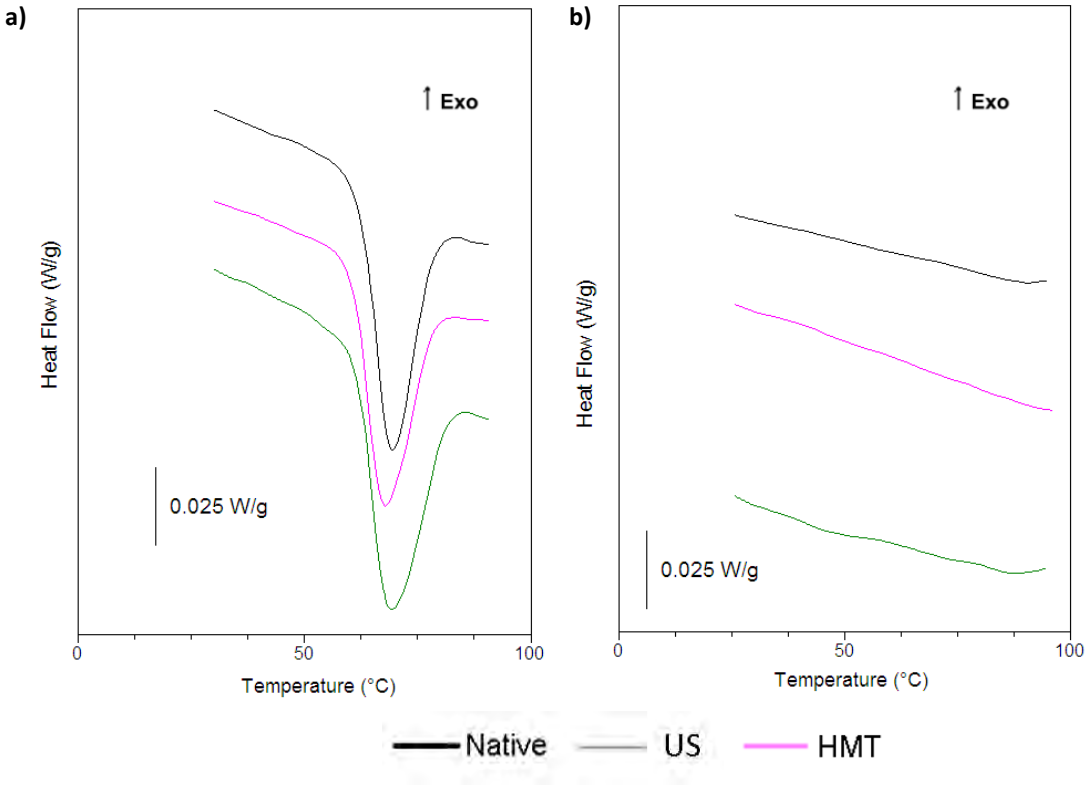

Source: own authorship.

All SNP showed DSC curves related to amorphous materials, with no gelatinization transition (Fig. 5.b). These results are in agreement with the X-ray diffractograms, confirming that the nano-precipitation of the starches promoted the breaking of the crystalline structure.

Table 2 - Thermal parameters of native (NCS) and modified cassava starches by US (UCS) or HMT (HCS)

Sample	T_o (ºC)	T_p (ºC)	T_c (ºC)	ΔH (J/g)
NCS	62.8 ± 0.2[a]	69.3 ± 0.1[a]	83.5 ± 0.9[a]	14.4 ± 0.8[a]
UCS	62.2 ± 0.3[a]	69.3 ± 0.1[a]	84.8 ± 1.0[a]	13.9 ± 0.3[a]
HCS	61.0 ± 0.1[b]	67.8 ± 0.2[b]	83.1 ± 0.9[a]	13.6 ± 0.1[a]

T_o: initial gelatinization temperature; T_p: peak gelatinization temperature; T_c conclusion gelatinization temperature of peak; ΔH: gelatinization enthalpy. Different lowercase letters in the same column indicate a significant difference ($p < 0.05$). Source: own authorship.

Similar results were reported by Lima *et al.* (2021), which produced cassava and potato SNP by nano-precipitation and did not observe peaks in the DSC curves of these samples, related to amorphous materials.

3.3.6. Solubility in water, Swelling Power and Oil absorbing capacity

The solubility in water (SW) and swelling power (SP) values at 90 ºC of native and modified starches and SNP are shown in Fig. 6.a,b. The SW of native cassava starch was ~84%, a result that was a little higher than that reported by Agyemang *et al.* (2020) (SW~74%). Differences in these values may be due to particle size, amylose/amylopectin ratio, gelatinization temperature, different periods of plant maturation or different types of cultivars or methods of extraction.

Figure 6 - Solubility in water (a); swelling power (b) and oil absorbing capacity (c) of native (NCS) and modified by US (UCS), HMT (HCS) cassava starches – blue; and starch nanoparticles produced by native (NSNP) and modified by US (USNP) and HMT (HSNP) starches - orange

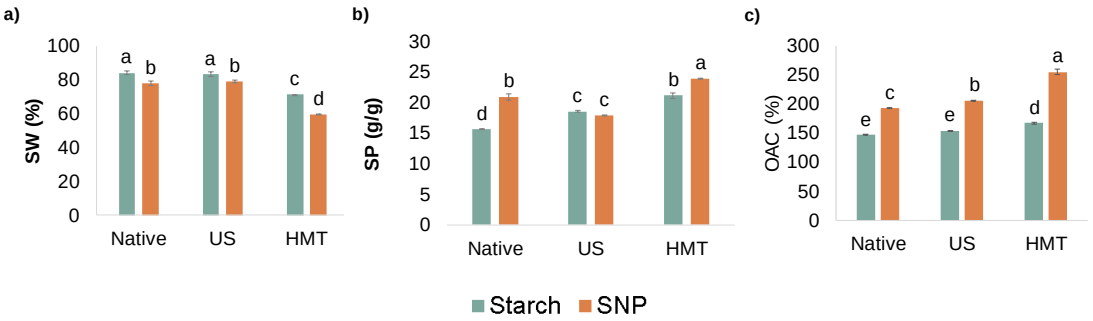

Source: own authorship.

After US pretreatment, the samples did not show differences in SW values when compared to native starch. Different results were reported by Sujka and Jamroz (2013), who modified potato, wheat, and rice starches by US and reported an increase in SW in all cases, indicating that the increase would be due to damage to the crystalline molecular structure of starch and to the binding of water molecules to the free hydroxyl groups of amylose and amylopectin by hydrogen bonds. In our study, crystallinity remained the same after US (Fig. 3.b), which corroborates with the SW value for UCS.

HMT pretreatment significantly decreased the SW of both starch (84-71%) and SNP (78-60%). During the HMT process, the mobility of molecules increases, resulting from the interaction of amylose-amylose and amylose-amylopectin chains, which decreases the hydroxyl groups available for hydration and diffusion of amylose-amylopectin molecules (DEWI *et al.*, 2022). These results corroborate with Dewi *et al.* (2022), who modified the sago starch using HMT at 20% moisture content and 120 °C/ 1 h and also reported a reduction in SW from 38.5 to 25% after modification.

Overall, the SW of starches (84, 83 and 71%) was always higher than their SNP counterparts (78, 79 and 60%), which could indicate that starch is more soluble in water. This result agrees with the FTIR results, which indicated that SNP have more lipophilic characteristics when compared to starches. The smooth and highly hydrophilic surface of starch can promote its higher solubility in water.

The swelling power (SP) of the native cassava starch was ~16 g/g, which corroborates what was reported by Dudu *et al.* (2019) as (~17 g/g). HMT pretreatment increased the SP of both starch (16-21 g/g) and SNP (21-24 g/g) when compared to their native counterparts. This may occur due to amylose/amylopectin chain rearrangement during HMT, allowing greater starch swelling. Contrary to the results found in this study, Dewi *et al.* (2022) reported a reduction of SP from 20.4 to 15 g/g.

US pretreatment increased the SP of cassava starch due to the depolymerization of the chains during this physical treatment, which would allow greater swelling of the granule. Contrary to the SP values presented in this study, Li *et al.* (2019) modified millet starch by US (10% w/w, 30 min) and also did not observe significant changes in SP values. In general, SP values showed an increase after nano-precipitation, from 16-21 g/g for NSNP and 21-24 g/g for HSNP, with the exception of USNP, which did not show a significant difference in relation to UCS starch (value average of ~18 g/g).

Regarding oil absorption capacity (OAC) of NCS, it was similar to that reported by Agnes; Felix and Ugochukwu (2017) (Fig. 6.c). The modification by HMT increased the ability of starch to absorb oil (169 %) compared to NCS or UCS (~150%). This indicates that the HCS became much more lipophilic. This behavior may be associated with a granular expansion and the release of helical structures from the starch granules after treatment. These results agree with those presented in the FTIR spectrum (Fig. 4), where there was an increase in the intensity of the band related to the lipophilic of cassava starch after physical modifications.

Other authors have observed similar results. Wang *et al.* (2020) reported a little increase in OAC of 60 - 60.7% for potato starch after US treatment with different times (0 - 10 min) and amplitudes (0 - 40%). Dewi *et al.* (2022) also reported an increase in the lipophilic affinity (OAC) of 25% HMT-modified sago starch from 65 to 78%.

The nano-precipitation method increased the OAC values of all samples when compared to their starch counterparts, from 147-193% for native, 154-205% for US and 167-255% for HMT, indicating greater lipophilicity of SNP. This behavior can be explained due to the formation of aggregates in the form of plates after starch nano-precipitation, which increases the lipophilicity of the particle. In

addition, ethanol precipitation imparts surface roughness and expansion of the starch particle, further strengthening internal capillary strength and oil affinity (WANG; LI; ZHENG, 2021).

Furthermore, the formation of the V-type structure allows the amylose helix, with a hydrophilic outer surface and an inner hydrophobic helical cavity (WANG *et al.*, 2015), to assemble into a crystalline structure and further accommodate hydrophobic compounds, such as oil molecules, which are mainly driven by hydrophobic interactions, hydrogen bonding, and diffusion concentration (FENG *et al.*, 2022). Similar results were reported by Feng *et al.* (2022), who produced corn starch SNP by nano-precipitation and reported a 75 to 160% increase in OAC after nano-precipitation. These results corroborate the results of the FTIR, which indicated greater hydrophilicity of the SNP in relation to starches.

3.3.7. Water contact angle measurement

Measuring the water contact angle enables a qualitative estimation of changes in the hydrophobicity of native and modified starches and SNP (Fig. 7). Among all analyzed samples, NCS had the smallest contact angle (26.3º). The pretreatment with US and HMT led to an increase in the contact angle of the starch (~38 and 49º, Fig. 7), suggesting enhanced hydrophobicity. This finding is in line with the results obtained from OAC and FTIR results.

Figure 7 - Images of contact angles of native cassava starch (NCS) and modified cassava starch by US (UCS) or HMT (HCS), and starch nanoparticles produced by native starch (NSNP) and modified starch by US (USNP) or HMT (HSNP), as a function of time

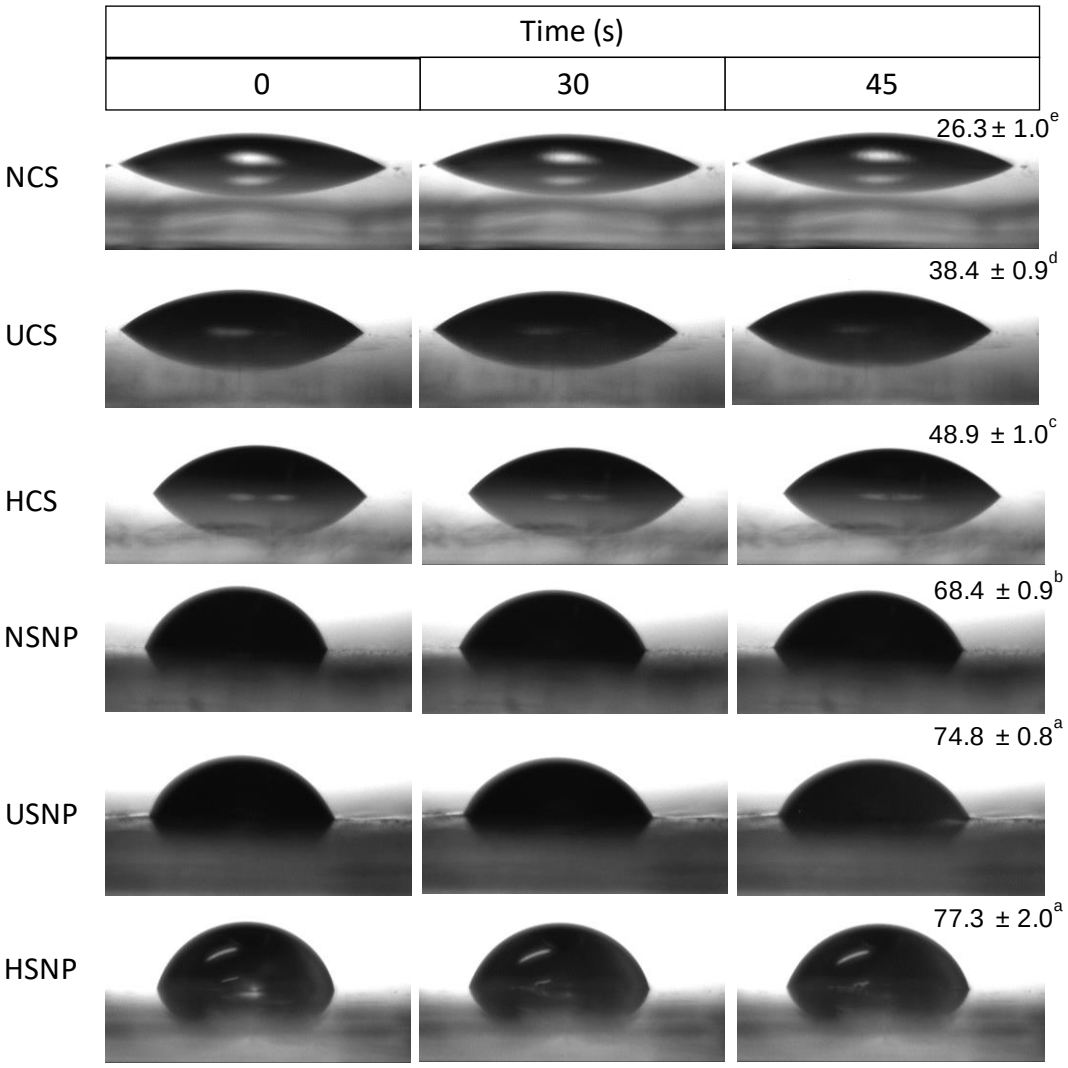

Source: own authorship.

After nano-precipitation, the SNP presented drastically higher values (~68 to 77º) than the starches (~26 to 49°), and the HSNP presented the highest value of contact angle. This behavior can be explained by the V-type polymorphism exhibited by SNP, where hydroxyl glycosyl groups are located on the outer surface of the helix of V-amylose complexes, and the inner surface is coated with methylene groups and glycosidic oxygen, resulting in a more hydrophobic cavity similar to that of cyclodextrins (WANG *et al.*, 2015). Furthermore, the surface roughness of the modified SNP (Fig. 1.e, f) increased lipophilic affinity, allowing the formation of a more resistant barrier to water droplets on the surface through

the development of aggregate plaques after nano-precipitation. These results are in agreement with the OAC analysis (Fig. 6.c).

In addition, for all samples the water contact angle values remained relatively stable with time (0 to 45 s) (Fig. 7). Similar results were found in the literature. Ge *et al.* (2017) produced SNP from tapioca, sweet potato, and corn starches by the nano-precipitation method and reported contact angles of ~84 to 94°. Dewi *et al.* (2022) modified sago starch by HMT and OSA and reported higher contact angles after double modification, indicating that HMT helped to make the starch more hydrophobic. In addition, these authors observed that for the native starch, the angle decreased during the observation time of the analysis from 0 to 90 s, which did not occur so visibly for the modified starches.

Additionally, the water contact angle measurement allows for the assessment of the interfacial wettability (water-oil) of the particles. For Pickering-type emulsions, this is a fundamental factor to understand its behavior as a stabilizer, as any hydrophobic variation of the particles would affect its wetting properties (WANG *et al.*, 2015). In general, SNP with an almost neutral contact angle (~90º) has a greater potential to stabilize this type of emulsion (GE *et al.*, 2017).

3.3.8. SNP as Pickering emulsion stabilizers

The SNP produced were applied as a stabilizer of oil-in-water Pickering emulsions, in various concentrations (2.4 – 4 g SNP / 100 g emulsion) (Fig. 8). The emulsions were monitored through phase separation on day 0 and 7th of production.

Figure 8 - Pictures of O/W emulsions (20% canola oil) stabilized with NSNP, USNP and HSNP, respectively, at concentrations of 2.4. 3 and 4% (w/w), in freshly emulsions and after 7 days of storage. Red arrows indicate phase separation

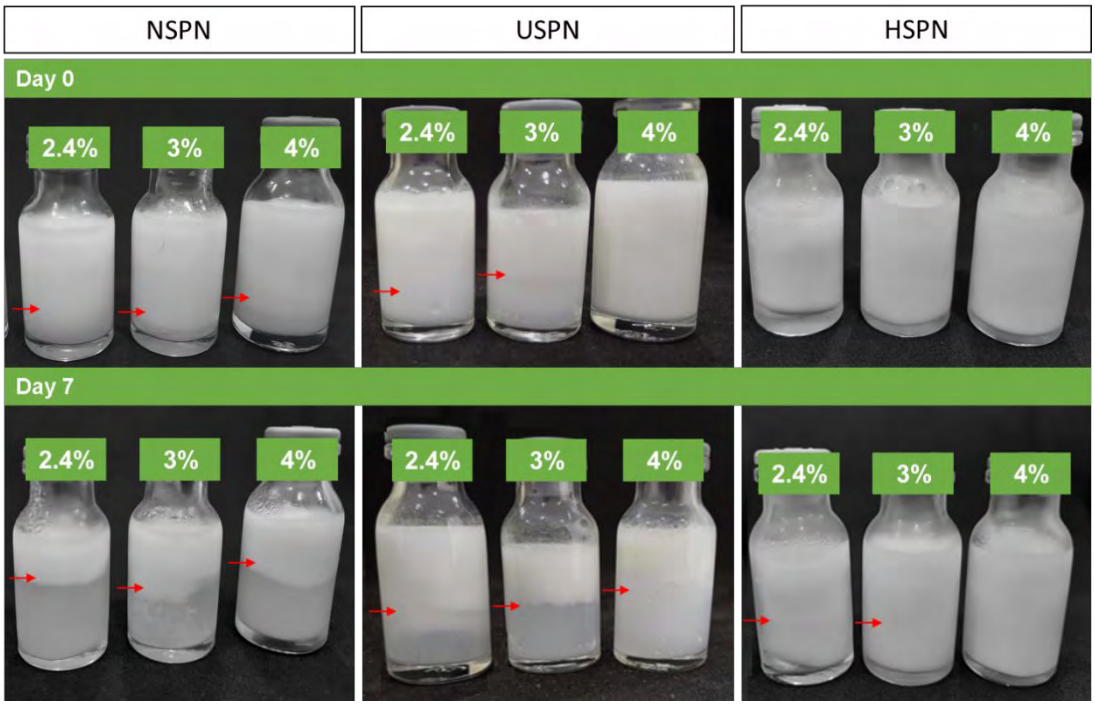

Source: own authorship.

Oil-water emulsions with NSNP or USNP exhibited phase separation at all tested concentrations; however, the emulsion prepared with NSNP showed more pronounced separation after preparation. USNP promoted stability for up to 24 h in the highest concentration (4%). The emulsion stabilized with HSNP showed stability at higher concentrations (4%), and phase separation did not occur over the storage period. Higher concentrations of SNP allow for more efficient coating at the droplet interface (GE *et al.*, 2017). These results supported the data obtained for the water contact angle measurements, which had the highest values (HSNP), and exhibited more effective stabilization. In addition, the smaller particle size of HSNP and the surface roughness contribute to a more hydrophobic behavior of the SNP, further enhancing its stabilization properties.

Ge *et al.* (2017) also produced SNP from corn, tapioca, and sweet potato starches and applied these particles in Pickering-type emulsions with different concentrations of SNP (0.25–2 wt%) and oil fractions (0.25 – 0.75); however, these authors reported phase separation of the emulsion as early as the first day of monitoring for all SNP produced. This difference may be due to the different

sources of starch used for SNP production, the water-oil ratio used in the formulation, and most likely, the fact that in this study there was no pretreatment of the starches for the production of SNP. This hypothesis is strong because in our study the native cassava SNP also failed to efficiently stabilize the emulsion, i.e., the effect of physical pre-treatment (HMT) clearly improved this property of the SNP.

Conclusion

By changing the properties of starch nanoparticles through surface modifications, particle size control, and the production of effective changes in the lipophilicity of the material, it was feasible to produce stabilizers for o/w Pickering emulsions. All SNP produced were amorphous and the dual modification promoted increases in roughness, lipophilicity, and a significant reduction in average sizes. In addition, HSNP stands out for its smallest size and largest OAC. These properties yielded the formation of a robust and stable interfacial layer that prevented droplet coalescence and provided emulsion stability. The US + nano-precipitation combination was not able to stabilize the Pickering emulsion, whereas the HMT + nano-precipitation combination produced nanoparticles with synergistic properties which stabilized the emulsion for 7 days, at 20ºC. In addition, this biomaterial is classified as a clean label and safe for the consumer.

Acknowledgements

The authors thank:

- This study was financed in part by the Coordenação de Aperfeiçoamento de Pessoal de Nível Superior - Brasil (CAPES) - Finance Code 001.
- The Laboratory of Structural Characterization (LCE/DEMa/UFSCar) for the general facilities.

References

AGNES, A. C.; FELIX, E. C.; UGOCHUKWU, N. T. Morphology, Rheology and Functional Properties of Starch from Cassava, Sweet Potato and Cocoyam. **Asian Journal of Biology**, v. 3, n. 3, p. 1–13, 2017.

AGYEMANG, P. N. *et al.* Effect of the use of starches of three new Ghanaian cassava varieties as a thickener on the physicochemical, rheological and sensory properties of yoghurt. **Scientific African**, v. 9, 2020.

ALI, N. A.; DASH, K. K.; ROUTRAY, W. Physicochemical characterization of modified lotus seed starch obtained through acid and heat moisture treatment. **Food Chemistry**, v. 319, p. 126513, 2020.

AMINI, A. M.; RAZAVI, S. M. A.; MORTAZAVI, S. A. Morphological, physicochemical, and viscoelastic properties of sonicated corn starch. **Carbohydrate Polymers**, v. 122, p. 282–292, 2015.

BULATOVIĆ, V. O. *et al.* Biodegradable Polymer Blends Based on Thermoplastic Starch. **Journal of Polymers and the Environment**, v. 29, n. 2, p. 492–508, 2021.

CHANDLA, N. K.; SAXENA, D. C.; SINGH, S. Processing and evaluation of heat moisture treated (HMT) amaranth starch noodles; An inclusive comparison with corn starch noodles. **Journal of Cereal Science**, v. 75, p. 306–313, 2017.

DEWI, A. M. P. *et al.* Dual Modification of Sago Starch via Heat Moisture Treatment and Octenyl Succinylation to Improve Starch Hydrophobicity. **Polymers**, v. 14, n. 6, p. 1–17, 2022.

DUDU, O. E. *et al.* Structural and functional characteristics of optimised dry-heat-moisture treated cassava flour and starch. **International Journal of Biological Macromolecules**, v. 133, p. 1219–1227, 2019.

FENG, Y. *et al.* Effect of V-type crystallinity and starch particle structure on the oil loading capacity and anti-oxidation. **Carbohydrate Polymers**, v. 297, 2022.

FROST, K. *et al.* Crystallinity and structure of starch using wide angle X-ray scattering. **Carbohydrate Polymers**, v. 78, n. 3, p. 543–548, 2009.

GE, S. *et al.* Characterizations of Pickering emulsions stabilized by starch nanoparticles: Influence of starch variety and particle size. **Food Chemistry**, v. 234, p. 339–347, 2017.

GE, X. *et al.* Insight into the improving effect on multi-scale structure, physicochemical and rheology properties of granular cold water soluble rice starch by dielectric barrier discharge cold plasma processing. **Food Hydrocolloids**, v. 130, 2022.

GUNARATNE, A.; HOOVER, R. Effect of heat-moisture treatment on the structure and physicochemical properties of tuber and root starches. **Carbohydrate Polymers**, v. 49, n. 4, p. 425–437, 2002.

JI, N. *et al.* Effects of heat moisture treatment on the physicochemical properties of starch nanoparticles. **Carbohydrate Polymers**, v. 117, p. 605–609, 2015.

JIANG, S. *et al.* Evaluation of rheological behavior of starch nanocrystals by acid hydrolysis and starch nanoparticles by self-assembly: A comparative study. **Food Hydrocolloids**, v. 52, p. 914–922, 2016.

KAMWILAISAK, K. *et al.* Rheology, stability, antioxidant properties, and curcumin release of oil-in-water Pickering emulsions stabilized by rice starch nanoparticles. **International Journal of Biological Macromolecules**, v. 214, p. 370–380, 2022.

KHAKPOUR, F.; PIRSA, S.; AMIRI, S. Modified Starch/CrO/Lycopene/Gum Arabic Nanocomposite Film: Preparation, Investigation of Physicochemical Properties and Ability to Use as Nitrite Kit. **Journal of Polymers and the Environment**, v. 31, n. 9, p. 3875–3893, 2023.

LI, S.; WARD, R.; GAO, Q. Effect of heat-moisture treatment on the formation and physicochemical properties of resistant starch from mung bean (Phaseolus radiatus) starch. **Food hydrocolloids**, v. 25, n. 7, p. 1702–1709, 2011.

LI, Y. *et al.* Comparative studies on structure and physiochemical changes of millet starch under microwave and ultrasound at the same power. **International Journal of Biological Macromolecules**, v. 141, p. 76–84, 2019.

LIMA, K. T. dos S. *et al.* Physicochemical Properties of Modified Starches

Obtained by Anti-Solvent Precipitation Containing Anthocyanins from Jambolan (Syzygium cumini) Fruit. **Starch/Stärke**, v. 73, n. 3–4, 2021.

MALLAKPOUR, S.; KHODADADZADEH, L. Ultrasonic-assisted fabrication of starch/MWCNT-glucose nanocomposites for drug delivery. **Ultrasonics Sonochemistry**, v. 40, p. 402–409, 2018.

MCCLEMENTS, D. J. **Food Emulsions: Principles, Practices and Techniques**. 2. ed. University of Massachusetts, Amherst: Boca Raton: CRC Press, 2004.

NIKOLIC, G. S.; CAKIC, M. D. Physical investigation of the colloidal iron-inulin complex. **Colloid Journal**, v. 69, n. 4, p. 464–473, 2007.

OTACHE, M. A. *et al.* Advances in the Modification of Starch via Esterification for Enhanced Properties. **Journal of Polymers and the Environment**, v. 29, n. 5, p. 1365–1379, 2021.

PAL, S.; MAL, D.; SINGH, R. P. Cationic starch: An effective flocculating agent. **Carbohydrate Polymers**, v. 59, n. 4, p. 417–423, 2005.

PIECYK, M.; DOMIAN, K. Effects of heat–moisture treatment conditions on the physicochemical properties and digestibility of field bean starch (Vicia faba var. minor). **International Journal of Biological Macromolecules**, v. 182, p. 425–433, 2021.

PRATIWI, M.; FARIDAH, D. N.; LIOE, H. N. Structural changes to starch after acid hydrolysis, debranching, autoclaving-cooling cycles, and heat moisture treatment (HMT): A review. **Starch - Stärke**, v. 70, n. 1–2, p. 1700028, 2018.

RAHAMAN, A. *et al.* Ultrasound based modification and structural-functional analysis of corn and cassava starch. **Ultrasonics Sonochemistry**, v. 80, p. 105795, 2021.

RAMOS, G. V. C. *et al.* Impact of emulsification time and concentration of modified starch nanoparticles on Pickering stability. **Chemical Engineering Transactions**, n. (accepted article), 2023.

RAZAVI, S. M. A. *et al.* Some physicochemical properties of sage (Salvia macrosiphon) seedgum. **Food Hydrocolloids**, v. 35, p. 453–462, 2014.

SAMMON, C. *et al.* The application of attenuated total reflectance Fourier transform infrared spectroscopy to monitor the concentration and state of water in solutions of a thermally responsive cellulose ether during gelation. **Polymer**, v. 47, n. 2, p. 577–584, 2006.

SUJKA, M.; JAMROZ, J. Ultrasound-treated starch: SEM and TEM imaging, and functional behaviour. **Food Hydrocolloids**, v. 31, n. 2, p. 413–419, 2013.

UZOMAH, A.; IBE, C. The functional properties, pasting and baking behaviour of chemically modified sour cassava starches. **African Journal of Food Science**, v. 5, n. 12, p. 686–694, 2011.

VELÁSQUEZ-CASTILLO, L. E. *et al.* Quinoa starch nanocrystals production by acid hydrolysis: Kinetics and properties. **International Journal of Biological Macromolecules**, v. 143, p. 93–101, 2020.

VELÁSQUEZ-CASTILLO, L. E. *et al.* Cassava Starch Films Containing Quinoa Starch Nanocrystals: Physical and Surface Properties. **Foods**, v. 12, n. 3, p. 1–18, 2023.

WANG, L. J. *et al.* Fabrication and characterization of antioxidant pickering emulsions stabilized by zein/chitosan complex particles (ZCPs). **Journal of Agricultural and Food Chemistry**, v. 63, n. 9, p. 2514–2524, 2015.

WANG, Q.; LI, L.; ZHENG, X. Recent advances in heat-moisture modified cereal starch: Structure, functionality and its applications in starchy food systems. **Food Chemistry**, v. 344, p. 128700, 2021.

WANG, S. *et al.* Preparation and characterization of highly lipophilic modified potato starch by ultrasound and freeze-thaw treatments. **Ultrasonics Sonochemistry**, v. 64, 2020.

ZHU, F. Starch based Pickering emulsions: Fabrication, properties, and applications. **Trends in Food Science & Technology**, v. 85, p. 129–137, 2019.

4. CAPÍTULO 4: ENCAPSULATION OF CURCUMIN IN PICKERING EMULSIONS STABILIZED WITH MODIFIED STARCH NANOPARTICLES

Abstract

Curcumin is a hydrophobic bioactive, with limited potential applications, however, incorporating it into lipid-based carriers can significantly enhance its bioaccessibility. The Pickering emulsion serves as a structured system for encapsulation, protection, and delivery of curcumin. The study aimed to produce Pickering O/W emulsions stabilized by starch nanoparticles (SNP) and to encapsulate the bioactive curcumin. Native starch nanoparticles (NSNP) were not effective stabilizing the emulsions within the evaluated concentration range (0.25 – 4wt%), on the other hand, modified starch nanoparticles (HSNP) in concentrations greater than 3% demonstrated efficient stabilization. Emulsions stabilized with 4% HSNP remained stable for more than 14 days, and were employed to encapsulate curcumin. CLSM showed that the SNP was located at the droplet interfaces. The interfacial tension for HSNP exhibited initial values of 40~33 mN/m, quickly reaching equilibrium. The zeta potential was low (-5.39 mV), indicating low surface activity. Stable emulsions displayed shear thinning behavior, and the Power Law model demonstrated an excellent fit to the experimental data ($R^2 \geq 0.998$). Curcumin encapsulation in the system lowered interfacial tension, droplet size, apparent viscosity, and consistency index. After 60 days, curcumin retention remained at 100%. Our findings indicate that HSNP-stabilized Pickering emulsion hold promise for enhanced functionalities in food products, like long-term stability, and effective protection of hydrophilic bioactive.

Keywords: modified starch, HMT, encapsulation, interfacial tension, rheology

4.1. Introduction

Curcumin, a low molecular weight polyphenolic compound, is a powerful natural antioxidant found in the rhizomes of *Curcuma longa* L. (GHOSH; BANERJEE; SIL, 2015; GEREMIAS-ANDRADE *et al.*, 2017) and is widely used as a preservative, flavoring and natural coloring in beverages and foods (BORRIN *et al.*, 2016). In addition, this compound has been very studied for its several medicinal properties, such as anti-inflammatory, antibacterial, antifungal, antitumor, anti-hypocholesterolemic, and antiproliferative properties (RAVIADARAN *et al.*, 2018). However, this bioactive is hydrophobic, photosensitive, and degrades faster when exposed to light and oxygen, which limits its use in many foods (DAMMAK; SOBRAL, 2018).

In recent years, much research has explored the ability of different systems to protect bioactive compounds (LEE; TARTÉ; ACEVEDO, 2021; WANG *et al.*, 2023). Due to high stabilization and high food safety, in terms of toxicity, Pickering emulsions have been considered ideal options to protect and release curcumin (LEE; TARTÉ; ACEVEDO, 2021). Thus, this type of emulsion can be used to encapsulate hydrophobic nutraceuticals and enhance encapsulation efficiencies (MWANGI *et al.*, 2020). Furthermore, many studies investigate the encapsulation efficiency of these bioactive in several systems (DAMMAK; SOBRAL, 2018; KHARAT; ZHANG; MCCLEMENTS, 2018).

The Pickering stabilization system forms through a rearrangement of solid particles at the droplet interface to form a dense and thick interfacial layer, generally irreversible due to the high energy of desorption (WANG *et al.*, 2023). In addition, studies have shown that Pickering-type emulsion-based polyphenol delivery systems provide greater physical and chemical stability and greater encapsulation efficiency compared to emulsion stabilized with surfactants (DAMMAK; SOBRAL, 2018; KHARAT; ZHANG; MCCLEMENTS, 2018; MWANGI *et al.*, 2020).

Solid particles, such as starch, can be used as emulsifiers to produce Pickering emulsions. Starch is GRAS (Generally Recognized as Safe), non-allergenic, abundant, and low-cost (ZHU, 2019). However, native starch has high hydrophilicity, making it difficult to use as a stabilizer at the oil-water interface.

So, modified starches are evaluated for this type of application and the most common methods include octenyl succinic anhydride (OSA) modification (REMANAN; ZHU, 2023), hydrolysis (LIANG *et al.*, 2016), milling (LU; XIAO; HUANG, 2018), solvent-less precipitation (GE *et al.*, 2017), modification with acid and nanoprecipitation (LIMA *et al.*, 2021), ultrasound (HAAJ; MAGNIN; BOUFI, 2014), and high-pressure treatments (VILLAMONTE; JURY; DE LAMBALLERIE, 2016).

Physical modification of starch by heat-moisture treatment (HMT), treatment with low moisture content (< 35%) and high temperatures (T > 90 °C) for a time (1 – 16 h) (LI; WARD; GAO, 2011), or nanoprecipitation (gelatinization followed by precipitation with ethanol) is a safe process, free of toxicity and, therefore, it presents itself as an interesting option to produce particles capable of stabilizing emulsion (GE *et al.*, 2017; LIMA *et al.*, 2021). Furthermore, several factors affect the stability of starch-based Pickering emulsions, such as type of starch particles, degree of modification, starch source and concentration, type of oils, emulsion composition, pH, and ionic strength (ZHU, 2019).

These methods are interesting, because HMT makes the granule more rigid and resistant to heating, producing more hydrophobic granules (FONSECA *et al.*, 2021), and in the nanoprecipitation method, the nanoparticles are amorphous, which improves their degree of flexibility and could help in the formation and stabilization of the interfacial layer (GE *et al.*, 2017; ZHU, 2019).

Therefore, in this context, the aim of this study was to encapsulate curcumin in a Pickering emulsion stabilized by nanoparticles of modified cassava starch, by HMT and nanoprecipitation, and to evaluate the stability of the bioactive for 60 days. Pickering emulsion without curcumin was used as a control.

4.2. Material and Methods

4.2.1. *Material*

Canola oil (Liza, Cargil, Mairinque, SP, Brazil) and cassava starch (Siamar, Neves Paulista, SP, Brazil), starch type I, were used. Nile Red and Nile Blue A were purchased from Sigma Aldrich (St Louis, MO, USA). All reagents used in the analyzes were of analytical standard.

4.2.2. *Preparation of SNP*

Native cassava starch was modified by HMT (heat-moisture treatment) according to Piecyk and Domian (2021), with some modifications. Briefly, the starch moisture content was corrected to 20wt% and after equilibration (at 4 ºC/ 24 h), the samples were heated to 130 °C for 4 h in an air convection oven (Tecnal, TE-394/3, Piracicaba, SP, Brazil).

The production of SNP was carried out according to the methodology proposed by Ge *et al.* (2017), with some modifications. In short, native and modified cassava starches were dispersed in distilled water (5wt%) and gelatinized at 95 ºC, for 30 min. After cooling, absolute ethanol was added in the ratio (v/v) of 1:1 water:ethanol, which remained under mechanical stirring for 12 h at room temperature. Then, the samples were centrifuged (Eppendorf centrifuge, model 5430R, São Paulo, Brazil) at 3000 x g for 15 min and washed twice with absolute ethanol. The SNP were lyophilized (LC5500, Terroni, São Carlos, SP, Brazil) and stored in hermetically sealed containers. The particles were named NSNP or HSNP when produced from native or HMT starches, respectively.

4.2.3. Production of Pickering emulsions and encapsulation of curcumin

The oil-water (O/W) emulsions were prepared with 20% of canola oil as the oil phase. The starch nanoparticles were added to the aqueous phase and the emulsification process was carried out using a rotor-stator homogenizer (Ultra-Turrax IKA, model T25, Labotechnik, Staufen, Germany) at 14,000 rpm for 3 min. In addition, sodium benzoate at 0.02wt% was used as a preservative. The effect of the SNP type and concentration (0.8, 2.4, 3, or 4%) (g of SNP/100 g of emulsion) on the properties of the emulsions were evaluated (WANG *et al.*, 2023).

The formulation with a lower instability index (lumisizer method, section 2.4.1) was selected for the addition of 0.07 g of the curcumin/100 g emulsion (MA *et al.*, 2017).

Emulsions containing NSNP and HSNP were named EN and EH, respectively, following the number 1, 2, 3, or 4 according to particles concentrations (EN1 and EH1 = 0.8%; EN2 and EH2 = 2.4% EN3 and EH3 = 3% EN4 and EH4 = 4%). The EHC4 sample has curcumin in the formulation.

4.2.4. Characterization of Pickering emulsions

4.2.4.1. Physical stability

The emulsion was stored in a glass bottle at 20 °C in a BOD incubator (MA 415, Marconi, Piracicaba, SP, Brazil) for 14 days. The physical stability was assessed by visual analysis, creaming index (CI), and instability index (II) measurements. The CI was calculated by Equation 1 (OWENS *et al.*, 2018).

$$CI\ (\%) = \frac{Hs}{Ht}100 \qquad (1)$$

where *Hs* and *Ht* are the height of the serum layer (if destabilization occurred) and of fresh emulsion, respectively.

Moreover, a photo centrifuge LUMiSizer (LS 610, LUM GmbH, Berlin, Germany) was used to evaluate emulsion stability under accelerated conditions at 25 °C. Aliquots of 0.4 mL of sample were placed in polycarbonate cells (r = 130 mm) and immediately centrifuged at 4,000 rpm. This measurement registered the intensity of the transmitted light (at 865 nm) as a function of time and position over the sample at every 10 s for 60 min. Instability index values (II) were obtained directly from the SepView software version 4.1 (L.U.M., Berlin, Germany) (LERCHE; SOBISCH, 2011).

4.2.4.2. Confocal laser scanning microscopy (CLSM)

The interfacial structure of the Pickering emulsion droplets was observed using a confocal laser scanning microscope (Upright, LSM780-NLO, Madrid, Spain). Nile red solution (0.1% w/v, in ethanol) was prepared and 10 µL of this solution/g of lipid was used in the oil phase. To stain the SNP, Nile Blue dye was used at 0.05 mg/mL SNP suspension. A small droplet was placed on a glass

slide, covered with a coverslip, and observed. The Nile red and Nile blue fluorescent dyes were excited at 488 nm and at 633 nm, respectively (KO; KIM, 2021).

4.2.4.3. Morphology and droplet size distribution

Pickering O/W emulsions were analyzed by optical microscopy (Leica DM. 500 / ICC 50W, São Paulo, Brazil). A small droplet was placed on a glass slide, covered with a coverslip, and observed with a 100 x objective lens. Images were processed using the software Leica Laz Ez, version 3.4.0 (Leica, São Paulo, Brazil). This analysis was performed on days zero, 7, and 14.

For each sample, at least 30 microscopic images were taken, and then the droplet size of the emulsion was analyzed by observing at least 40 droplets for each micrography. The droplet size distribution was analyzed using ImageJ v.1.53 (National Institutes of Health and the Laboratory for Optical and Computational Instrumentation, Maryland, USA) and Mathematica version 13.1 (Wolfram Mathematica, Oxfordshire, Reino Unido) software. The droplet size was expressed as volume-weighted mean diameter ($D[_{4,3}]$) calculated by Equation (2), where n_i is the number of particles of diameter d_i (KO; KIM, 2021).

$$D[4.3] = \frac{\sum n_i d_i^4}{\sum n_i d_i^3} \qquad (2)$$

Span was calculated using Equation (3), in which D_i is the diameter, below which i% of the sample is contained (i= 10, 50, 90) (BENETTI; SILVA; NICOLETTI, 2019).

$$Span = \frac{D_{90} - D_{10}}{D_{50}} \qquad (3)$$

4.2.4.4. Dynamic interfacial tension

Interfacial tension measurements of the water/oil interface phases were performed using a tensiometer (Teclis, Tracker-S, Tokyo, Japan) by the pendant droplet method, at 25 °C during 3,600 s (GOMES; COSTA; CUNHA, 2018).

4.2.4.5. Zeta potential

The Zeta potential of the samples (pH ~7.0) was determined using Zetaplus equipment (Brookhaven Instruments Company, Holtsville-NY, USA) at 25 °C. The samples (1%, w/v) were diluted in deionized water. The data were obtained by the equipment software (JIANG *et al.*, 2016).

4.2.4.6. Rheological behavior

The rheological behavior of the emulsions was determined at 25 ºC using a AR 2000 rotational rheometer (TA Instruments, New Castle, USA) with cone-plate geometry (4º, 60 mm). Flow curves of the samples (shear stress or viscosity as a function of the shear rate) were measured by up-down continuous ramp mode in the shear rate range from 0.01 to 100 s^{-1} (DAUDT *et al.*, 2015). The Power Law model (Equation 4) fitted the down curve experimental data by using the Rheology Advantage Data Analysis version 5.3.1 software (AR 2000, TA Instruments, New Castle, USA).

$$\tau = k.\dot{\gamma}^{n} \qquad (4)$$

Where τ is the shear stress; *k* is the consistency index, $\dot{\gamma}$ is the shear rate and *n* is the flow behavior index.

4.2.4.7. Quantification of encapsulated curcumin

The quantification of curcumin encapsulated in Pickering emulsions followed the methodology of Chignell *et al.* (1994). A 1:10 dilution of the sample was made in deionized water and 1 mL of this first dilution was diluted again in 9 mL of DMSO. The curcumin concentration was determined by reading the absorbance in a spectrophotometer (FEMTO, CIRRUS 805T, São Paulo, Brazil) at 430 nm. The absorbance (Abs) was converted into curcumin concentration (c) using a standard curve (Abs = 0.1493*c + 0.0262, R^2 = 0.9983) at a concentration range from 0.5 to 6.0 µg/mL.

4.2.5. Statistical Analysis

Experiments were performed in at least triplicate. The results were submitted to analysis of variance (ANOVA) and the means were compared by the Tukey test ($p < 0.05$), using SAS software version 9.4 (Statistical Analysis System, São Paulo, Brazil).

4.3. Results and Discussion

4.3.1. Effect of SNP type and concentration on emulsion stability

4.3.1.1 Visual appearance and physical stability

Figure 1(a) shows the visual appearance of Pickering emulsions, monitored for up to 14 days of storage. All emulsions produced with NSNP, regardless of the nanoparticle concentration, were destabilized before 14 days of storage, in fact, the phases separated after a few hours of preparation (< 24 h). On the other hand, the sample with the highest HSNP concentration (3 and 4%), remained stable after 14 days of storage. The Pickering emulsions were monitored by observing the phase separation during storage, through the creaming index (CI%) (Figure 1.b). Samples stabilized with NSNP showed higher CI (70 - 40%) than emulsions stabilized with HSNP (CI = 70 - 0%). The instability index (II) values (Figure 1.c), determined using Lumisizer equipment, corroborate with the CI results, in which all samples with NSNP had higher instability index (0.40 – 0.89) than samples with HSNP (0.20 – 0.62), at the same concentration range. The lower the instability index values (closer to zero) the higher the stability of the emulsion.

Figure 1 - Visual aspect of emulsions (a), creaming index (b), and instability index (c) of Pickering emulsions. EN and EH named emulsions prepared by NSNPN and HSNPN, respectively. The numbers 1, 2, 3, and 4 specify the SNP concentrations of 0.8; 2.4; 3, and 4%, respectively. Values followed by the same lowercase letters do not differ significantly ($p<0.05$).

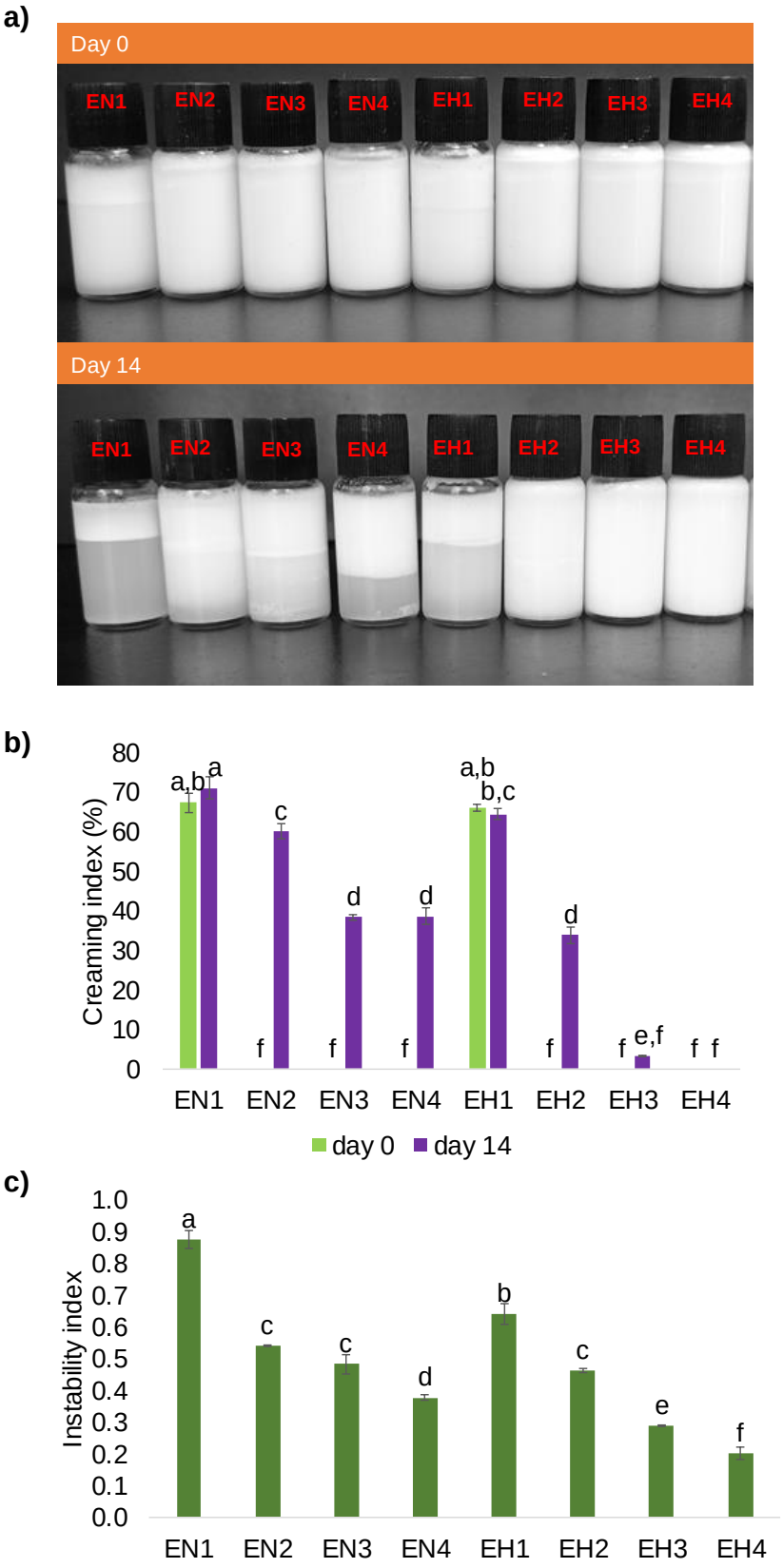

Source: own authorship.

Formulations with SNP concentration ≤ 3% showed phase separation, regardless of the type of particle used. This occurs because lower stabilizer concentrations may have been insufficient to fully cover the droplet area, which explains the greater instability of these formulations. On the other hand, higher concentrations of HSNP (>3%) are able to cover the interfacial area, resulting in a high number of small droplets. Kamwilaisak *et al.* (2022) produced Pickering O/W emulsion (30:70 sunflower oil: water) stabilized with rice starch nanoparticles crosslinked by citric acid and also observed that the increase of SNP concentration from 0.5 to 4.0% improved the stability of emulsions.

Furthermore, some reasons may explain the difference between SNP types and the way they stabilize oil droplets at the system interface. Studies show that HMT-modified starch can present a weaker granule, with roughness and cracks on its surface, due to the aggressions of heat and moisture treatment, in addition to a reduction in the crystalline area of the granule (ANDRADE *et al.*, 2014; DEWI *et al.*, 2022). Dewi *et al.* (2022) modified cassava starch by HMT and observed roughness, cracks, and hollows in the center of the granules, which was not observed for native cassava starch, in addition to a reduction in relative crystallinity from ~36.5 to 28.7% after thermal modification.

The reduction in relative crystallinity and the formation of cavities and holes after modification by HMT is caused by the recombination of the amylose and amylopectin chains, forming a more compact amorphous region (DEWI *et al.*, 2022). These authors observed that HMT-modified starch had a rough surface and justified the results by the evaporation of water molecules, inducing the double helix chain of amylopectin to reorganize itself into a denser packing structure, which acts as a barrier to the penetration of water into the starch granules. This weakening of the HMT starch granule, as well as the rearrangements of the amylose/amylopectin chains, can lead to the production of nanoparticles with smaller sizes. Smaller particles can more easily adhere to the O/W interface, promoting more efficient physical barrier formation.

Furthermore, after nanoprecipitation, HSNP particles have a higher surface roughness when compared to the NSNP surface (RAMOS *et al.*, 2023). This is due to the rearrangement of laminar aggregates formed by strong hydrogen bonding interactions during nanoprecipitation, resulting from the high

number of hydroxyl groups on the particle surface. The rough surface leads to an increase in the hydrophobic property. The higher hydrophobicity of the particle allows platelets to be more strongly organized by hydrophobic peaks to form a dense interfacial monolayer or multilayer film on the surface of their emulsified droplet units.

In fact, it is widely known in the literature that Pickering emulsions use solid particles with intermediate hydrophobicity strongly adsorbed at the interface between two immiscible liquids to provide a steric hindrance against aggregation of emulsion droplets (DICKINSON, 2012). Ge *et al.* (2017) studied the effect of the type of SNP (corn, tapioca, sweet potato), obtained by nanoprecipitation, on stabilization of Pickering emulsions. These authors reported that starches with intermediate hydrophobicity, i.e., almost neutral wettability (θ ~ 90°) were suitable for Pickering stabilization. When highly hydrophilic particles were used, the droplet size becomes large due to the high number of hydrogen bonds formed with water, and such particles are unlikely to be efficient Pickering stabilizers (GE *et al.*, 2017).

Thus, in this study, the most stable emulsion, that is, the one with the lowest instability index and creaming index (EH4), was selected to encapsulate the bioactive curcumin (EHC4). The microstructure of the EH4 emulsion was investigated (CLSM) to better understand the stabilization system. Furthermore, these two formulations (with and without curcumin) were characterized in terms of size distribution, interfacial tension, zeta potential, and flow behavior, and the quantification of encapsulated curcumin was monitored for up to 60 days.

4.3.2. Characterization of stable Pickering emulsions

Regarding stability, the Pickering emulsion with encapsulated curcumin (EHC4) did not present creaming indexes (CI) during storage (14 days). The instability index (II) showed that curcumin reduced the instability of the emulsion with HSNP from 0.20 ± 0.02 (EH4, Figure 1.c) to 0.08 ± 0.02 (EHC4).

This fact indicates that curcumin interfered with HSNP adhesions at the droplet interface, resulting in a more compact formation of the system. Curcumin has 2 aromatic rings linked by a carbon chain in its composition and, therefore, it is a molecule with hydrophilic parts (hydroxyl/ketone) and hydrophobic parts

(aromatic) and, despite being a molecule typically insoluble in water, it can be easily allocated in the O/W interface (ZEMBYLA *et al.*, 2019).

In fact, some studies show that curcumin molecules can even stabilize Pickering emulsions. Zembyla, Murray, and Sarkar (2018) produced W/O (5:95 water: soybean oil) emulsions, with curcumin crystals as a stabilizer, varying the concentration of this particle from 0.06 -1.5wt% and in the average particle concentration ~0.14%, they observed stability and keep off the size of droplets of emulsions for up to 7 days of storage. These authors also showed that the water droplets were surrounded by a dense layer of curcumin particles, through CLSM, confirming the preferential location of the polyphenol crystals at the W/O interface.

4.3.2.1. Microstructure of Pickering emulsion

Pickering emulsion stabilized with 4wt% HSNP proved to be highly stable and its microstructure was investigated using CLSM microscopy (Figure 2). The technique allows coloring the SNP (Figure 2.a, blue) and the oil (Figure 2.b, red) with dyes of different colors (Nile Blue A and Nile Red, respectively), allowing to visualize the interaction of the materials at the interface and stabilization of the emulsion. The images clearly show blue halos around a red oil droplet. The micrograph showed that HSNP were adsorbed at the O/W interface (Figure 2.a), with no significant number of particles in the continuous phase. The layer of HSNP on the surface of the emulsion droplets works as a strong physical barrier (Figure 2.c), providing high storage stability.

Figure 2 - CLSM images of Pickering emulsion stabilized by HSNP (4wt%). In this image, (a) SNP stained with Nile blue, (b) oil stained with Nile Red, and (c) HSNP + oil. Scale bar = 5 µm.

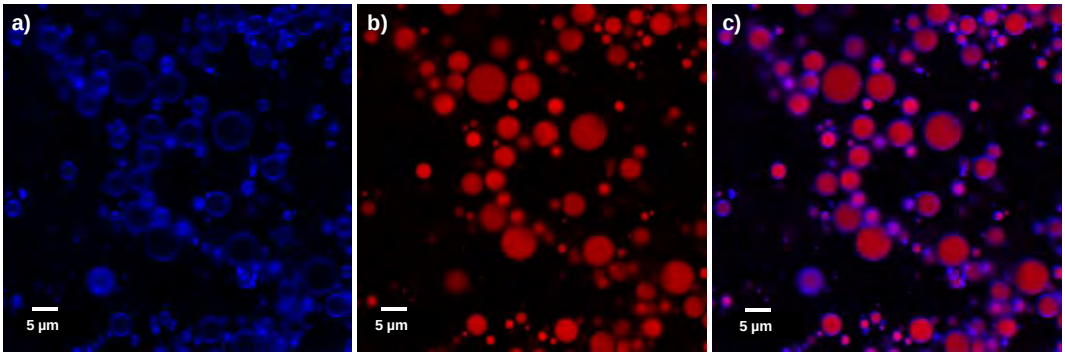

Source: own authorship.

Ren et al (2023) observed, through CLSM, different droplet sizes and starch/xanthan SNP present in the droplet interface and in the continuous phase of the emulsion, indicating that some particles did not adsorb at the interface. These authors also reported that the excess particles, which were in the continuous phase, formed three-dimensional networks that could effectively capture oil droplets and prevent their movement and aggregation. This behavior was not observed in our study, since the particles remained essentially at the droplet interface.

4.3.2.2. Optical microscopy and droplet size distribution

Optical microscopy of stable emulsions produced on days 0 and 14 (Figure 3) was evaluated. The micrograph of the emulsions stabilized by 4% HSNP, without (EH4) and with curcumin (EHC4) showed small and homogeneous droplets. The storage time seems not to have influenced the morphology of the emulsions analyzed in optical microscopy, during the monitored period (up to 14 days, data not shown), which confirms the stability of these emulsions.

Figure 3 - Visual aspect of emulsions, optical microscopy, and droplet size as a function of the accumulated mass fraction, of Pickering emulsions stabilized by HSNP (4wt%), without (a,c,e) and with curcumin (b,d,f) on days 0 (a,b,e,f) and 14 (c,d) of production. Scale bar = 20 µm.

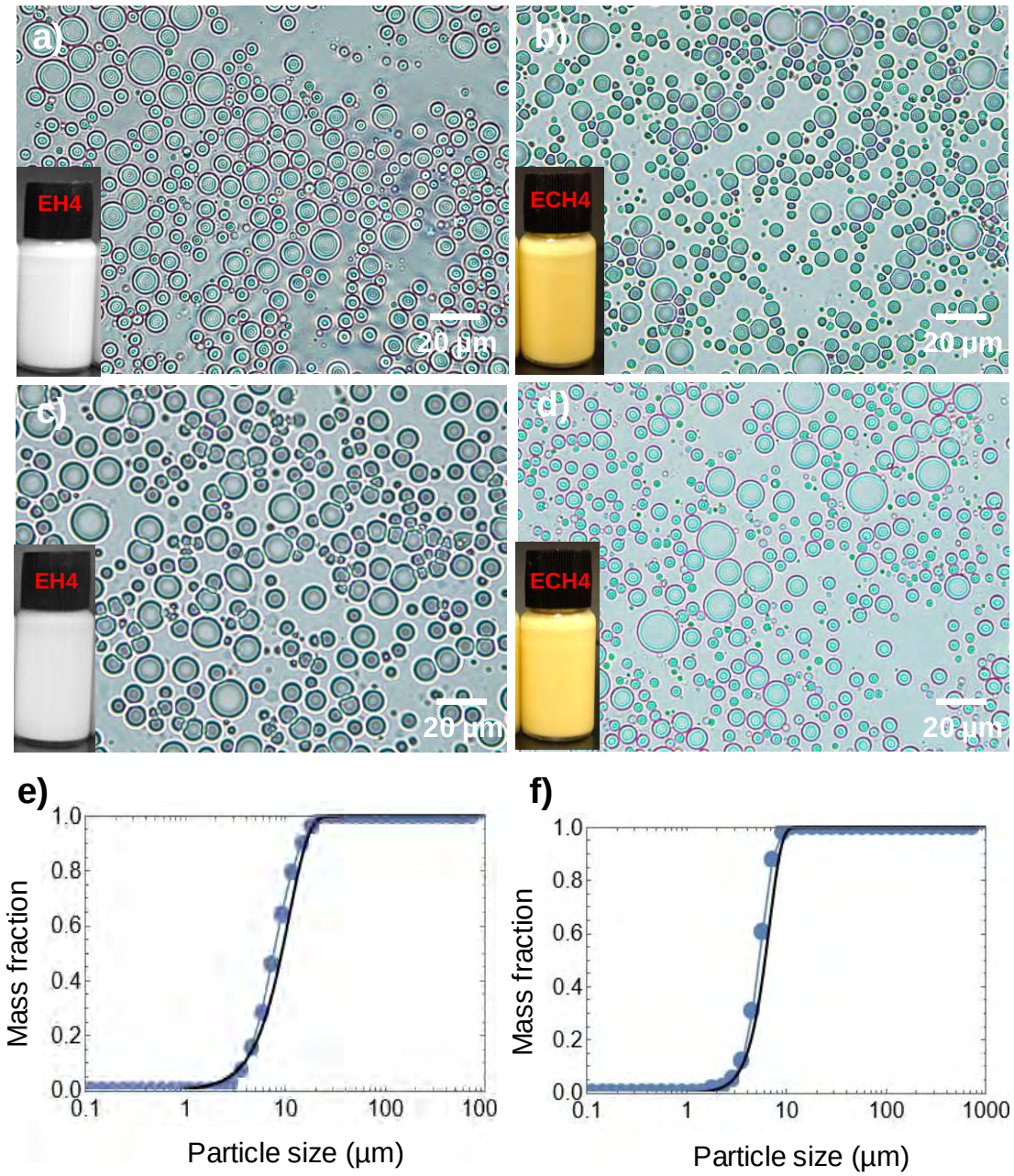

Source: own authorship.

The accumulated mass fraction of the droplets (Figure 3 e,f), volume-weighted mean diameter values ($D[_{4,3}]$), as well as the accumulated diameters (D_{10}, D_{50}, and D_{90}), and the Span (Table 1) of freshly Pickering emulsions, were made with the help of Mathematica. The provided Mathematica Wolfram code snippet applies a sequence of image processing methods to an imported image (Figure 4). Firstly, the image is subjected to edge detection, highlighting the

edges using a specified radius and threshold. Border components are then removed to eliminate noise near the image's edges. The highlighted edges are dilated to connect any disjointed segments, and the resulting regions are filled. Finally, components with a circularity greater than 0.9 are selected, effectively filtering out non-circular objects. These operations collectively serve to preprocess the image, enhance edges, remove unwanted particles, and isolate circular emulsion droplets of interest (DACANAL; HIRATA; MENEGALLI, 2013).

Figure 4 - Image processing of raw emulsion droplets using Wolfram Mathematica software.

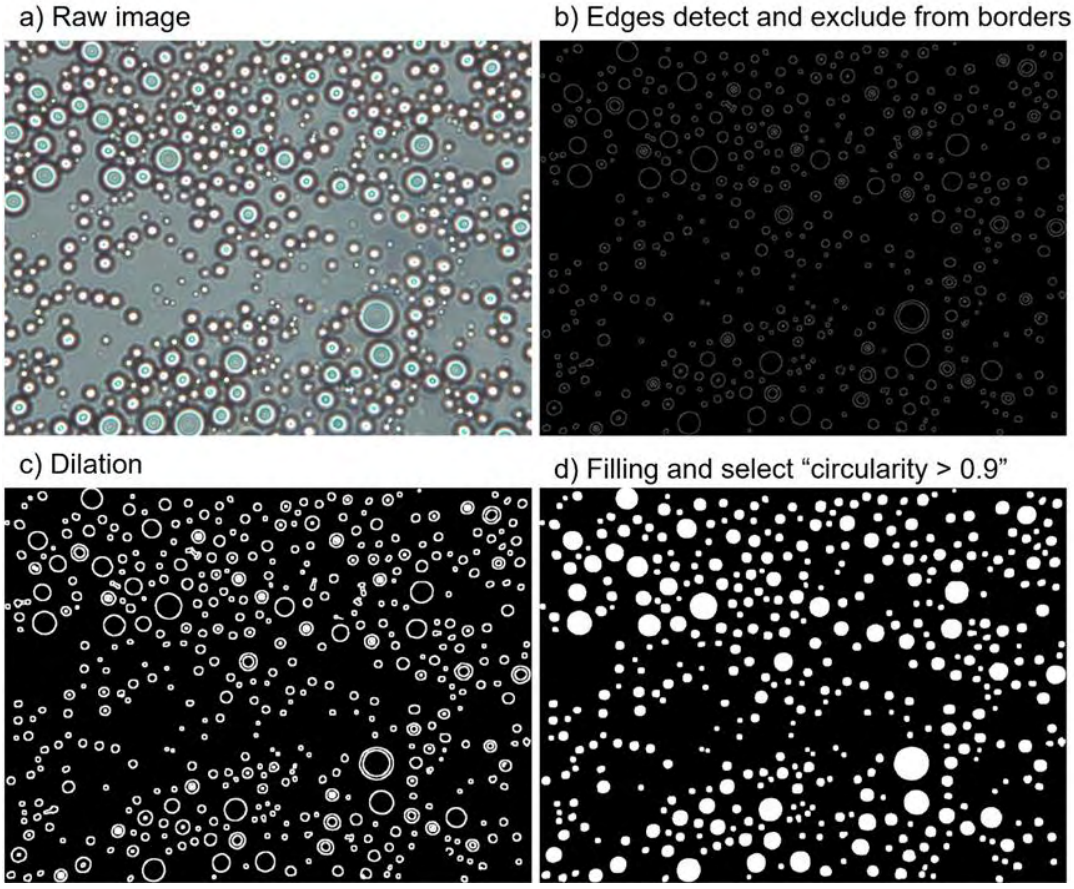

Source: own authorship.

Table 1 - Mean droplet size ($D_{[4,3]}$) and Span of emulsions produced by HSNP (4wt%) without (EH4) and with curcumin (EHC4). Values followed by the same lowercase letters in the same column do not differ significantly ($p<0.05$).

Sample	$D_{[4,3]}$ (µm)	D_{10} (µm)	D_{50} (µm)	D_{90} (µm)	Span
EH4	9.54 ± 0.18^{a}	3.82 ± 0.23^{a}	9.13 ± 0.23^{a}	15.91 ± 0.04^{a}	1.32 ± 0.06^{a}
EHC4	6.07 ± 0.03^{b}	3.56 ± 0.28^{a}	6.07 ± 0.08^{b}	8.54 ± 0.28^{b}	0.82 ± 0.10^{b}

Source: own authorship.

The mean diameter $D_{[4,3]}$ and Span of the EH4 emulsion droplets was 9.54 µm and 1.32 (Table 1), respectively. The $D_{[4,3]}$ value was lower than those obtained by Wang *et al.* (2023), who produced Pickering emulsion stabilized with debranched and/or esterified starch, reporting $D_{[4,3]}$ droplet sizes ranging from 31 - 105 µm. It was also lower than the result from Kamwilaisak *et al.* (2022), who determined a mean diameter of 50 µm for droplet size of Pickering emulsion (30:70 O:W) stabilized with 4wt% rice starch nanoparticles crosslinked by citric acid. The EHC4 emulsion showed appearance and droplet shapes similar to the sample without curcumin (EH4), with no changes in storage time.

However, the $D_{[4,3]}$ of the samples with the bioactive was significantly smaller (6.07 µm) (Table 1) than the emulsion without curcumin. Feng *et al.* (2020) also reported droplet size reduction, from 219 nm to 171 nm when curcumin was incorporated into the O/W emulsion formulation using debranched starch and Tween 80. Additionally, according of these authors, the addition of curcumin maintained the droplet size unchanged even after 7 days of storage, a phenomenon that did not occur for the same formulation without the bioactive compound.

The term span, which refers to the range of droplet sizes within the emulsion, can influence its stability. For Pickering emulsions, this parameter is linked to the arrangement of solid particles at the oil-water interface. This rearrangement can be optimized with a narrower span, leading to improved coverage of droplet surfaces, and resulting in enhanced stability (ARKOUMANIS; NORTON; SPYROPOULOS, 2019). The curcumin-loaded Pickering emulsion displayed a significantly lower span value (0.82) than the emulsion without the bioactive (Table 1). This finding is justified by the fact that smaller particles can lead to a narrower span and more uniform sizes, which could contribute to better stability and this result is according to the instability index.

4.3.2.3. Dynamic interfacial tension

The interfacial tension (Figure 5) between the water-oil phase with the addition of 4 g HSNP/100 g was evaluated to understand the role of the components in the stability of the emulsion and formation of the interfacial film.

Figure 5 - Interfacial tension curves of systems composed of two phases, as follows: water-oil (blue); water-curcumin loaded oil (red); HSNP water-oil (green), HSNP water- curcumin loaded oil (purple). HSNP was added, when applicable, at a concentration of 4wt%.

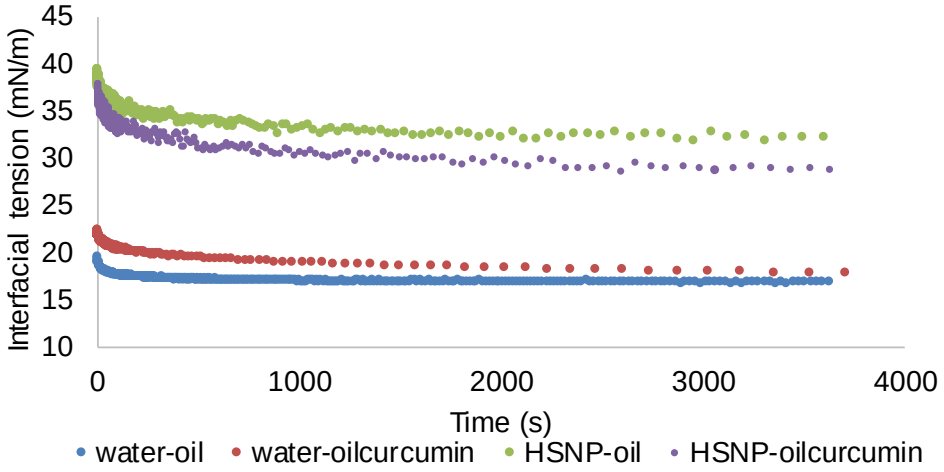

Source: own authorship.

The water-oil curves showed initial interfacial tension values of ~20 mN/m. These values increased to ~40 mN/m after the addition of HSNP particles in the aqueous phase. The initial interfacial tension of the HSNP water-curcumin loaded oil system (Figure 5) was 36 Nm/m, a lower value than the HSNP water–oil system (~40 mN/m). However, the opposite phenomenon occurs with the curves without stabilizer particles in the system (water- curcumin loaded oil), where the addition of curcumin increased the initial interfacial tension in relation to the water-oil curve, from ~20 to 22 mN/m. The bioactive molecule, as mentioned earlier, can also interact at the droplet interface and interfere with the stabilization mechanism. Moreover, research has demonstrated that curcumin can engage with the amylose chains, forming complexes. This interaction could explain the decreased tension observed in the curve when both molecules are present (FENG *et al.*, 2020).

Feng *et al.* (2020) demonstrated, using the molecular dynamics simulations, that in the interactions among debranched starch (DBS), curcumin, and water, hydrogen bonds were formed between DBS residues and curcumin molecules and, in systems without curcumin, only unstable hydrogen bonds were formed. Furthermore, these authors reported that the rearrangement of the two molecules over time showed a final structure where curcumin was located within the lumen of the DBS helix.

Typically, the addition of a stabilizer in a formulation tends to decrease the overall interfacial tension of the system. However, this behavior was not observed our study. Han *et al.* (2011) evaluated the interfacial tension of wheat starch in a soybean oil and water system, and reported an initial reduction in the interfacial tension from 50 to 43 Nm/m. Nevertheless, it can be stated that the reduction in interfacial tension is not the mechanism responsible for stabilizing the interface of Pickering emulsions, that is, the particles do not act as surfactants. Therefore, unlike traditional surfactants (such as low molecular weight synthetic surfactants), this decrease in tension is not necessarily expected for this type of system.

Furthermore, this behavior can also be explained by the fact that polysaccharides are less effective in reducing interfacial tension compared to other molecules, such as proteins or low molecular weight surfactants, because they are less able to track thermodynamically unfavorable contacts between nonpolar groups and water (MCCLEMENTS, 2005). In addition, due to the low lipophilic properties of some polysaccharides, adsorption at the oil-water interface is a challenge. However, they can envelop the droplet surface and stabilize the emulsion through steric hindrance (SHAO *et al.*, 2018).

The increase in interfacial tension with the addition of HSNP in the systems may also be associated with the phenomenon of competition between SNP and minor components of canola oil. Canola oil is mainly composed of triacylglycerols (94 - 99%) with a high concentration of oleic acid (61.6%), followed by linoleic acid (21.7%), which are monounsaturated and polyunsaturated fatty acids, respectively. This oil also has minor components such as phospholipids, free fatty acids, tocopherol, sulfur, and iron (PRZYBYLSKI *et al.*, 2005). Thus, these minor components can compete with the SNP for allocation at the droplet interface, causing an increase in the interfacial tension in relation to the system without particles.

The systems without stabilizer (HSPN) reached the equilibrium interfacial tension quickly, ~120 s, and for samples containing HSNP, this time was ~ 300 s of analysis (Figure 5), a similar behavior when comparing the systems with or without curcumin, resulting in a minor reduction in interfacial tension value (~ 5 mN/m). This observation suggests that the mechanism behind emulsion stabilization exhibits low surface activity between the phases. Furthermore, the similar kinetic behavior indicates that the HSNP particles could migrate to the

droplet interface at the same rate, regardless of the presence of the bioactive in the emulsion formulation. Liu *et al.* (2023) also reported in their study that interfacial tensions between chitosan and mineral oil decreased over time and reached equilibrium, indicating their spontaneous adsorption at the oil-water interface (~ 300 s, resulting in about a 2 mN/m reduction in initial interfacial tension).

The adsorption of colloidal particles at the oil-water interface involves at least three steps, (1) bulk diffusion to the interface, (2) penetration at the interface, and (3) structural rearrangement and formation of viscoelastic films at the interface (LIU; TANG, 2016). The kinetics of the initial interfacial tension decrease is related to the degree of diffusion of the emulsifier to the droplet interface. An effective emulsifier must rapidly adsorb onto the surface of newly formed droplets to reduce interfacial tension and therefore prevent the coalescence of the droplets (DICKINSON, 2009). In this study, the HSNP particles were able to quickly adhere to the drop interface, however, there was no reduction in interfacial tension, but an increase in this parameter, which may have occurred due to mechanisms already explained earlier.

4.3.2.4. Zeta Potential

The zeta potential (ZP) of the emulsions was determined to enable the understanding of the interactions at the droplet interface. All samples showed low zeta potential values (~4.7 mV, Table 2), with no significant difference ($p<0.05$) among the samples (Table 2). These low absolute ZP values indicate a characteristic behavior of Pickering emulsions since this type of emulsion has low surface activity and discards its stabilization by electrostatic repulsion (VASILE *et al.*, 2016). This aligns with our previous study (RAMOS *et al.*, 2023), where the starch particles demonstrated a ZP of -3.4 ± 0.6 mV.

Table 2 - Zeta Potential and Power Law model coefficients obtained for flow curves of fresh emulsions stabilized by HSNP (4wt%), without (EH4) and with (EHC4) curcumin. Values followed by the same lower-case letters in the same column do not differ significantly ($p<0.05$).

Sample	Zeta Potential (mV)	n (flow index)	K (Pa.s)	R^2
EH4	-5.05 ± 0.46[a]	0.75 ± 0.01[a]	0.43 ± 0.02[a]	0.999
EHC4	-4.20 ± 0.11[a]	0.76 ± 0.01[a]	0.29 ± 0.00[b]	0.997

Source: own authorship.

In other words, the addition of curcumin in the formulation also did not significantly influence the ZP values (Table 2). These results show that HSNP remains in the composition of the interfacial layer, as a physical barrier-type emulsifier, not showing changes in the intensities of interactions measured by the ZP of the emulsion. Feng *et al.* (2020) produced emulsions with debranched starch (500 mg) and tween80 (aqueous phase) and curcumin (10 mg), lecithin, and ethanol (oil phase) and reported zeta potential values that varied from -15 mV to -17 mV, with the addition of curcumin in the formulation, indicating an improvement in the stability of the emulsion with the bioactive, since for this type of emulsion (with emulsifiers in the formulation, such as Tween80), values of ZP closer to -20 mv indicate more stable emulsions.

Shao *et al.* (2018) produced Pickering O/W emulsions with medium-chain triglyceride oil (50:50 oil:water) and taro SNP (3 - 5wt%) and reported an ZP of the emulsions from -18 to -20 mV in fresh emulsions. Remanan and Zhu (2023) produced emulsions with proportions of SNP to oil at 0.25% w/v using quinoa, corn, and potato starch nanoparticles and reported a range of zeta potential from -27 to -31 mV in these emulsions.

4.3.2.5. Rheological behavior

Rheological properties are used to understand emulsion flow behavior and find a suitable application. Figure 6 (a) can be observed that the emulsions presented a non-linear relationship between shear stress and shear rate, which characterizes non-Newtonian fluid behavior. The Power Law model was fitted to the experimental data of shear stress vs shear rate with good coefficients of determination ($R^2 > 0.997$). All samples showed thinning shear behavior ($n<1$) (Table 2), that is, the apparent viscosity always decreased with increasing shear

rate (Figure 6.b). This behavior may be due to deformation and rupture of the oil-water interfacial film or droplet deformation with increasing the shear rate (SONG *et al.*, 2015).

Figure 6 - (a) Downward flow curves and (b) Apparent viscosity as a function of shear rate of Pickering emulsions stabilized by HSNP (4wt%) without (purple, EH4) and with curcumin (blue, EHC4).

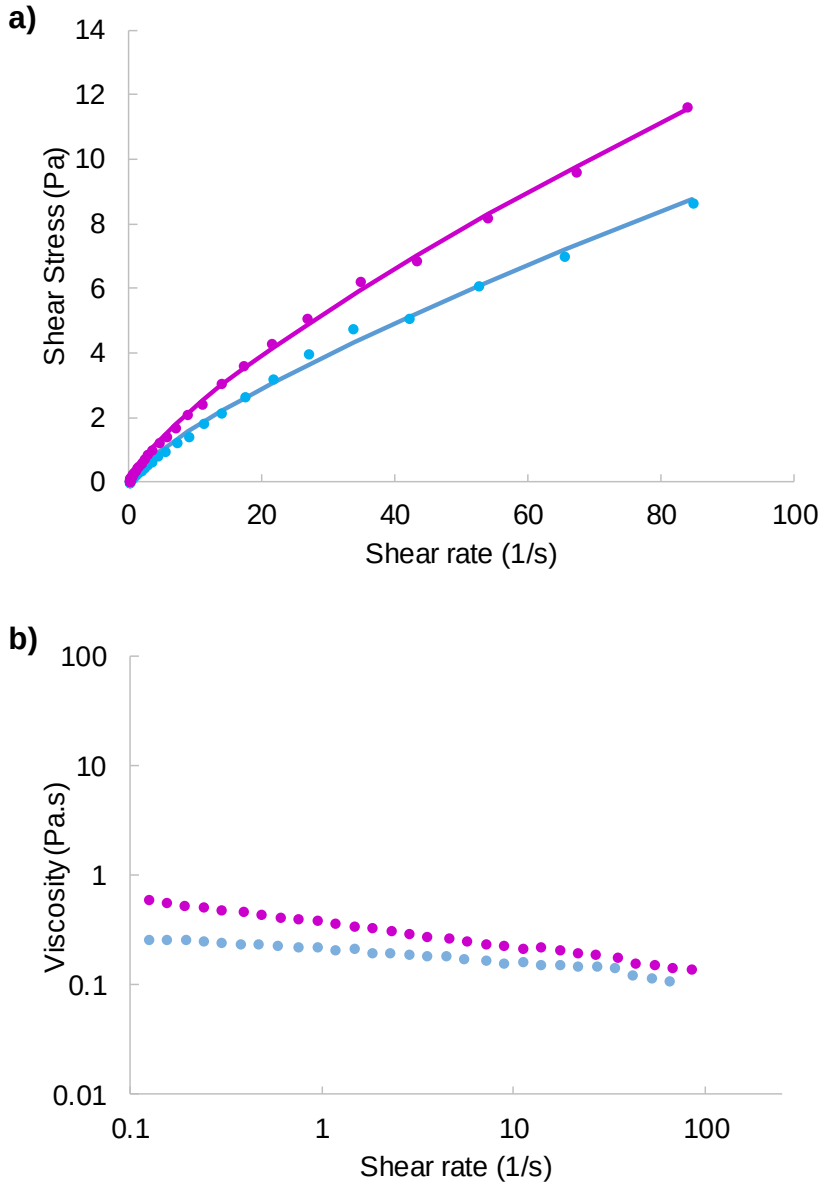

Source: own authorship.

The EHC4 emulsion showed a shear thinning fluid behavior, similar to samples without curcumin (Figure 6.a) with a good fit to the Power Law model (Table 2). However, the addition of curcumin in the formulation promoted a reduction in apparent viscosity values (Figure 6.b) and the consistency index (k)

value from 0.43 to 0.29 Pa.s^n (Table 2), which can be explained by the smaller droplet sizes (Table 1) in this formulation. Kamwilaisak *et al.* (2022) produced Pickering O/W emulsions (30:70) with rice SNP (0.49wt%) and curcumin (1.6 ppm/ mL oil) encapsulated in the sunflower oil phase and also reported a pseudoplastic fluid behavior (n = 0.80), however with yield stress from 0.39 Pa.

Similar results were obtained by Ren *et al.* (2023) when evaluating Pickering emulsions stabilized with xanthan gum/starch nanoparticles and also by Wang *et al.* (2023), who used debranched and/or esterified starch. These authors reported a good fit to the Power Law model, in which the apparent viscosity of all emulsions decreased with increasing shear rate n <1. Qian *et al.* (2020) also observed that there was a decrease in the apparent viscosity of Pickering emulsions stabilized with acetylated starch nanocrystals with the reduction of particles in the formulation.

4.3.3. Quantification of encapsulated curcumin

The quantification of encapsulated curcumin in the emulsions stabilized with 4% HSNP was performed up to 60 days of storage, to evaluate the chemical stability of this bioactive during storage (Figure 7). The amount of curcumin initially determined in the fresh emulsion was approximately 427.3 ± 18.7 µg/mL and this value was maintained, without significant difference ($p<0.05$), up to day 60. This demonstrates the effectiveness of the Pickering-type emulsion in protecting the encapsulated bioactive during storage.

Figure 7 - Quantification of encapsulated curcumin in stabilized Pickering emulsion with 4wt% of HSNP as function storage time.

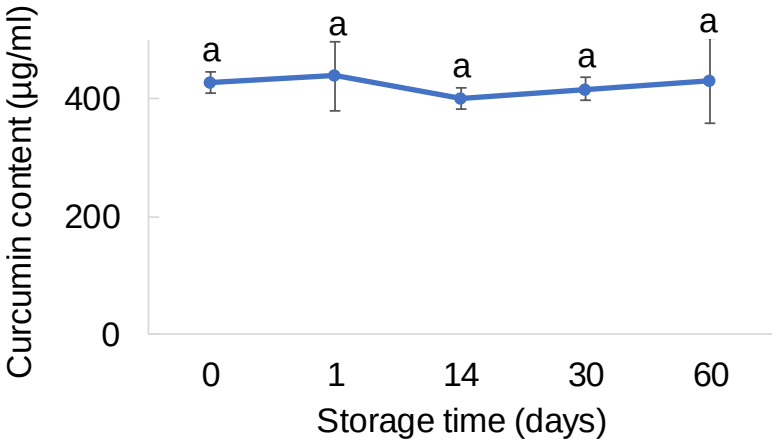

Source: own authorship.

Different results were found in the literature. Lee *et al.*(2021) produced Pickering emulsions stabilized with waxy maize nanoparticles (1%) and chitin nanofibers (0.2%), 10% oil phase with 335 mg/ml curcumin/ g of oil and reported that residual curcumin quantified after 16 days of storage (20 ºC, environment without light) was approximately 50% of that quantified on day zero. Shah *et al.* (2016) produced Pickering emulsions with chitosan-tripolyphosphate nanoparticles, with 5 and 20% medium-chain triglyceride (MCT) in the formulation and the curcumin was added to the oil phase at 0.1wt%. These authors reported that, for both prepared formulations, curcumin was degraded by 50% after 5 days of storage.

Already Kharat *et al.* (2018) produced emulsions with encapsulated curcumin, with different types of emulsifiers: caseinate, Tween 80, gum arabic or saponin, in critical stabilizer concentrations (1.0, 1.2, and 1.6wt%) or in excess 15wt% and evaluated the effect of stabilizer type and concentration on curcumin quantification (retention) during storage. These authors reported that the caseinate, Tween 80, and gum Arabic stabilizers had similar behavior, with a retention of ~75% after 15 days of storage, whereas saponin presented a retention of only 15%. Therefore, it can be inferred that the degradation of encapsulated curcumin depends a lot on the type of emulsifier used to coat the

oil droplets loaded with the bioactive, the formulation used, as well as the stabilization system produced.

Conclusion

A stable Pickering emulsion was produced using 4% HSNP, and curcumin was effectively encapsulated within this formulation. CLSM confirmed that the starch particles were located at the interface of the oil droplets. Curcumin improved the stability of the emulsions, interfering with the adhesion of the drop interface and forming a more compact system, with smaller average diameters. Furthermore, the incorporation of curcumin reduced the interfacial tension of the system, which can be explained by the interaction of the bioactive with the amylose chains. The apparent viscosity was reduced with the addition of curcumin, which can be explained by the formation of smaller droplets. The quantification of curcumin demonstrated its stability within Pickering emulsion for a period up to 60 days. These findings show the potential application of the systems developed in this study in pharmaceutical and food products.

Acknowledgments

The authors thank:

- This study was financed in part by the Coordenação de Aperfeiçoamento de Pessoal de Nível Superior - Brasil (CAPES) - Finance Code 001.
- The access to equipment and assistance provided by the National Institute of Science and Technology on Photonics Applied to Cell Biology (INFABIC) at the State University of Campinas; INFABIC is co-funded by Research Support Foundation of the State of São Paulo (FAPESP) (2014/50938-8) and National Council for Scientific and Technological Development (CNPq) (465699/2014-6).
- To Laboratory of Process Engineering (LEP) Department of Food Engineering (DEA), Faculty of Food Engineering (FEA), University of Campinas (UNICAMP), by the use of dynamic tensiometer.

References

ANDRADE, M. M. P. *et al.* Effects of heat-moisture treatment on organic cassava starch: Thermal, rheological and structural study. **Journal of Thermal Analysis and Calorimetry**, v. 115, n. 3, p. 2115–2122, 23 mar. 2014.

ARKOUMANIS, P. G.; NORTON, I. T.; SPYROPOULOS, F. Pickering particle and emulsifier co-stabilised emulsions produced via rotating membrane emulsification. **Colloids and Surfaces A**, v. 568, n. February, p. 481–492, 2019.

BENETTI, J. V. M.; SILVA, J. T. P.; NICOLETTI, V. R. SPI microgels applied to Pickering stabilization of O/W emulsions by ultrasound and high-pressure homogenization: rheology and spray drying. **Food Research International**, v. 122, p. 383–391, 1 ago. 2019.

BORRIN, T. R. *et al.* Curcumin-loaded nanoemulsions produced by the emulsion inversion point (EIP) method: An evaluation of process parameters and physico-chemical stability. **Journal of Food Engineering**, v. 169, p. 1–9, 2016.

CHIGNELL, C. F. *et al.* Spectral and Photochemical Properties of Curcumin. **Photochemistry and Photobiology**, v. 59, n. 3, p. 295–302, 1994.

DACANAL, G. C.; HIRATA, T. A. M.; MENEGALLI, F. C. Fluid dynamics and Morphological Characterization of Soy Protein Isolate Particles Obtained by Agglomeration in Pulsed-Fluid Bed. **Powder Technology**, v. 247, p. 222–230, 2013.

DAMMAK, I.; SOBRAL, P. D. A. Investigation into the physicochemical stability and rheological properties of rutin emulsions stabilized by chitosan and lecithin. **Journal of Food Engineering**, v. 229, p. 12–20, 2018.

DAUDT, R. M. *et al.* Pinhão starch and coat extract as new natural cosmetic ingredients : Topical formulation stability and sensory analysis. **Carbohydrate Polymers**, v. 134, p. 573–580, 2015.

DEWI, A. M. P. *et al.* Dual Modification of Sago Starch via Heat Moisture Treatment and Octenyl Succinylation to Improve Starch Hydrophobicity. **Polymers**, v. 14, n. 6, p. 1–17, 2022.

DICKINSON, E. Hydrocolloids as emulsifiers and emulsion stabilizers. **Food Hydrocolloids**, v. 23, n. 6, p. 1473–1482, ago. 2009.

DICKINSON, E. Use of nanoparticles and microparticles in the formation and stabilization of food emulsions. **Trends in Food Science and Technology**, v. 24, n. 1, p. 4–12, mar. 2012.

FENG, T. *et al.* Emulsion-based delivery systems for curcumin: Encapsulation and interaction mechanism between debranched starch and curcumin. **International Journal of Biological Macromolecules**, v. 161, p. 746–754, 15 out. 2020.

FONSECA, L. M. *et al.* Physical modification of starch by heat-moisture treatment and annealing and their applications: A review. **Carbohydrate Polymers**, v. 274, p. 118665, 15 nov. 2021.

GE, S. *et al.* Characterizations of Pickering emulsions stabilized by starch nanoparticles: Influence of starch variety and particle size. **Food Chemistry**, v. 234, p. 339–347, 1 nov. 2017.

GEREMIAS-ANDRADE, I. M. *et al.* Rheological and mechanical characterization of curcumin-loaded emulsion-filled gels produced with whey protein isolate and xanthan gum. **Lwt**, v. 86, p. 166–173, 2017.

GHOSH, S.; BANERJEE, S.; SIL, P. C. The beneficial role of curcumin on inflammation, diabetes and neurodegenerative disease: A recent update. **Food and Chemical Toxicology**, v. 83, p. 111–124, 2015.

GOMES, A.; COSTA, A. L. R.; CUNHA, R. L. Impact of oil type and WPI/Tween 80 ratio at the oil-water interface: Adsorption, interfacial rheology and emulsion features. **Colloids and Surfaces B: Biointerfaces**, v. 164, p. 272–280, 1 abr. 2018.

HAAJ, S. B.; MAGNIN, A.; BOUFI, S. Starch nanoparticles produced via ultrasonication as a sustainable stabilizer in Pickering emulsion polymerization. **RSC Advances**, v. 4, n. 80, p. 42638–42646, 2014.

HAN, L. *et al.* Starch stearate as a novel encapsulation wall material and its effect on oil–water interfacial tension. **Journal of Controlled Release**, v. 152, p. e226–

e227, 30 nov. 2011.

JIANG, S. *et al.* Evaluation of rheological behavior of starch nanocrystals by acid hydrolysis and starch nanoparticles by self-assembly: A comparative study. **Food Hydrocolloids**, v. 52, p. 914–922, 2016.

KAMWILAISAK, K. *et al.* Rheology, stability, antioxidant properties, and curcumin release of oil-in-water Pickering emulsions stabilized by rice starch nanoparticles. **International Journal of Biological Macromolecules**, v. 214, n. March, p. 370–380, 2022.

KHARAT, M.; ZHANG, G.; MCCLEMENTS, D. J. Stability of curcumin in oil-in-water emulsions: Impact of emulsifier type and concentration on chemical degradation. **Food Research International**, v. 111, p. 178–186, 1 set. 2018.

KO, E. B.; KIM, J. Application of starch nanoparticles as a stabilizer for Pickering emulsions : Effect of environmental factors and approach for enhancing its storage stability. **Food Hydrocolloids**, v. 120, n. June, p. 106984, 2021.

LEE, Y. S.; TARTÉ, R.; ACEVEDO, N. C. Curcumin encapsulation in Pickering emulsions co-stabilized by starch nanoparticles and chitin nanofibers. **RSC Advances**, v. 11, n. 27, p. 16275–16284, 2021.

LERCHE, D.; SOBISCH, T. Direct and accelerated characterization of formulation stability. **Journal of Dispersion Science and Technology**, v. 32, n. 12, p. 1799–1811, 2011.

LI, S.; WARD, R.; GAO, Q. Effect of heat-moisture treatment on the formation and physicochemical properties of resistant starch from mung bean (Phaseolus radiatus) starch. **Food hydrocolloids**, v. 25, n. 7, p. 1702–1709, 2011.

LIANG, R. *et al.* Preparation of Pickering emulsions with short, medium and long chain triacylglycerols stabilized by starch nanocrystals and their in vitro digestion properties. **RSC Advances**, v. 6, p. 99496–99508, 2016.

LIMA, K. T. dos S. *et al.* Physicochemical Properties of Modified Starches Obtained by Anti-Solvent Precipitation Containing Anthocyanins from Jambolan (Syzygium cumini) Fruit. **Starch/Stärke**, v. 73, n. 3–4, 2021.

LIU, F.; TANG, C. H. Soy glycinin as food-grade Pickering stabilizers: Part. I.

Structural characteristics, emulsifying properties and adsorption/arrangement at interface. **Food Hydrocolloids**, v. 60, p. 606–619, 1 out. 2016.

LIU, Y. W. *et al.* Interfacial adsorption behavior of the Aspergillus oryzae lipase-chitosan complex and stability evaluation of the resultant Pickering emulsion. **International Journal of Biological Macromolecules**, v. 233, p. 123599, 1 abr. 2023.

LU, X.; XIAO, J.; HUANG, Q. Pickering emulsions stabilized by media-milled starch particles. **Food Research International**, v. 105, n. November 2017, p. 140–149, 2018.

MA, P. *et al.* Preparation of curcumin-loaded emulsion using high pressure homogenization: Impact of oil phase and concentration on physicochemical stability. **LWT**, v. 84, p. 34–46, 1 out. 2017.

MCCLEMENTS, D. J. **Food Emulsions: Principles, Practices, and Techniques**. 3. ed., 2005.

MWANGI, W. W. *et al.* Food-grade Pickering emulsions for encapsulation and delivery of bioactives. **Trends in Food Science and Technology**, v. 100, p. 320–332, 1 jun. 2020.

OWENS, C. *et al.* Creaming and oxidative stability of fish oil-in-water emulsions stabilized by whey protein-xanthan-locust bean complexes: Impact of pH. **Food Chemistry**, v. 239, p. 314–322, 15 jan. 2018.

PIECYK, M.; DOMIAN, K. Effects of heat–moisture treatment conditions on the physicochemical properties and digestibility of field bean starch (Vicia faba var. minor). **International Journal of Biological Macromolecules**, v. 182, p. 425–433, 2021.

PRZYBYLSKI, R., MAG, T., ESKIN, N. A. M., MCDONALD, B. E. **Bailey's Industrial Oil and Fat Products** (6 th; F. Shahidi, ed.). Hoboken, NJ: John Wiley & Sons Inc., 2005.

QIAN, X. *et al.* Viscoelasticity of olive oil/water Pickering emulsions stabilized with starch nanocrystals. **Carbohydrate Polymers**, v. 230, p. 115575, 15 fev. 2020.

RAMOS, G. V. C. *et al.* Dual modification of cassava starch by physical

treatments for production of Pickering stabilizers. **Journal of Polymers and the Environment**, p. (submitted article), 2023.

RAVIADARAN, R. *et al.* Optimization of palm oil in water nano-emulsion with curcumin using microfluidizer and response surface methodology. **Lwt**, v. 96, n. March, p. 58–65, 2018.

REMANAN, M. K.; ZHU, F. Encapsulation of rutin in Pickering emulsions stabilized using octenyl succinic anhydride (OSA) modified quinoa, maize, and potato starch nanoparticles. **Food Chemistry**, v. 405, p. 134790, 30 mar. 2023.

REN, X. *et al.* Pickering emulsion: A multi-scale stabilization mechanism based on modified lotus root starch/xanthan gum nanoparticles. **International Journal of Biological Macromolecules**, v. 233, p. 123459, 1 abr. 2023.

SHAH, B. R. *et al.* Preparation and optimization of Pickering emulsion stabilized by chitosan-tripolyphosphate nanoparticles for curcumin encapsulation. **Food Hydrocolloids**, v. 52, p. 369–377, 2016.

SHAO, P. *et al.* Physical stabilities of taro starch nanoparticles stabilized Pickering emulsions and the potential application of encapsulated tea polyphenols. **International journal of biological macromolecules**, v. 118, n. Pt B, p. 2032–2039, 15 out. 2018.

SONG, X. *et al.* Preparation and characterizations of Pickering emulsions stabilized by hydrophobic starch particles. **Food Hydrocolloids**, v. 45, p. 256–263, 1 mar. 2015.

VASILE, F. E. *et al.* Physicochemical, interfacial and emulsifying properties of a non-conventional exudate gum (Prosopis alba) in comparison with gum arabic. **Food Hydrocolloids**, v. 56, p. 245–253, 1 maio 2016.

VILLAMONTE, G.; JURY, V.; DE LAMBALLERIE, M. Stabilizing emulsions using high-pressure-treated corn starch. **Food Hydrocolloids**, v. 52, p. 581–589, 2016.

WANG, R. *et al.* Characterization of Pickering emulsion by SCFAs-modified debranched starch and a potent for delivering encapsulated bioactive compound. **International Journal of Biological Macromolecules**, v. 231, p. 123164, 15

mar. 2023.

ZEMBYLA, M. *et al.* Water-in-oil Pickering emulsions stabilized by an interfacial complex of water-insoluble polyphenol crystals and protein. **Journal of Colloid and Interface Science**, v. 548, p. 88–99, 2019.

ZEMBYLA, M.; MURRAY, B. S.; SARKAR, A. Water-In-Oil Pickering Emulsions Stabilized by Water-Insoluble Polyphenol Crystals. **Langmuir**, v. 34, n. 34, p. 10001–10011, 2018.

ZHU, F. Starch based Pickering emulsions: Fabrication, properties, and applications. **Trends in Food Science and Technology**, v. 85, p. 129–137, 1 mar. 2019.

5. CAPÍTULO 5: RHEOLOGICAL CHARACTERIZATION AND MICROSTRUCTURE OF CURCUMIN-LOADED PICKERING EMULSION-FILLED GELS PRODUCED WITH QUINOA STARCH

Abstract

Curcumin is a bioactive with powerful functional properties but with limitations in terms of solubility. The hydrophobicity of curcumin can be overcome by encapsulating it in matrices with oil phases. The emulsion-filled gel (EFG) is a structured emulsion system involving a dispersed oil phase trapped in the polymeric gel matrix that combines beneficial characteristics of both the hydrophobic material and the hydrogel. In this study, a Pickering emulsion stabilized by cassava starch nanoparticles and loaded with curcumin was used to produce EFG, with different proportions of emulsion. The emulsion was characterized in terms of instability index (II) and curcumin encapsulation efficiency (EE) and the EFG were characterized in relation to color, microstructure, water retention capacity (WRC), mechanical and rheological properties. The II of emulsion was 0.19 at 55 ºC, suggesting high stability and the curcumin EE was 78.5%. The gels exhibited a predominantly yellow color. The confocal laser scanning microscopy showed that the EFG containing a smaller amount of emulsion had smaller and more uniform droplets. Also scanning electron microscopy demonstrated smaller pores and more compact structures as the concentration of emulsion in the gels increased, indicating that spaces within the gel network were filled by emulsion and interactions within the system increased. This result was corroborated by the WRC, which had higher values in EFG with a higher proportion of emulsion. Furthermore, the EFG with higher emulsion content showed greater hardness. The rheological parameters indicated a weak gel behavior (G' > G"), and an elastic character (tan(δ) < 0.12) for all samples. Moreover, the greater incorporation of the emulsion into the EFG increased the viscoelastic moduli (G', G”) and tan(δ), indicating an increase in the resistance of these gels. The creep-recovery analysis confirmed that the EFG exhibited predominantly elastic behavior, whereas the non-filled gel demonstrated a more viscous character. Our findings demonstrate that

incorporating the emulsion in different proportions imparts distinct characteristics and broadens the potential applications of EFG.

Keywords: creep-recovery, rheology, curcumin, CLSM, EFG, starch nanoparticles.

5.1. Introduction

Curcumin is a natural, environmentally sensitive, fat-soluble polyphenol with anti-inflammatory, antibacterial, antifungal, anti-hypocholesterolemic, antitumor, and antiproliferative properties (RAVIADARAN *et al.*, 2018). In addition, curcumin is used as a natural, flavoring and coloring agent in beverages and foods (BORRIN *et al.*, 2016). However, the use of curcumin is limited due to its low water solubility and storage stability (DAMAK; SOBRAL, 2021; ZHANG *et al.*, 2022).

Emulsion systems can be used in the development functional foods, as they can protect bioactive components and enhance their bioaccessibility (KAMWILAISAK *et al.*, 2022; ZHANG *et al.*, 2022). Low molecular weight surfactant emulsifiers can increase the solubility of liposoluble bioactive components in water since it has amphiphilic property allowing the production of oil-in-water (O/W) emulsions (ADITYA *et al.*, 2013). However, most of these emulsifiers do not have a clean label (a clean label requires reducing the use of chemosynthetic additives and using more natural and safer food ingredients), being that the use of plant-based emulsifiers is a trend (DAMAK; SOBRAL, 2021).

Furthermore, their protection in the emulsion system for the bioactive components under different conditions of storage is generally lower when compared to Pickering emulsions for example, which are stabilized with solid particles, which gives them a high desorption energy at the interface. Therefore, the Pickering emulsions present themselves as a solution both to produce GRAS (Generally Recognized as Safe) products and to increase the stability of the system and the target bioactive (LI *et al.*, 2020).

Additionally, the emulsions can be incorporated into gel matrices, resulting in emulsion-filled gel (EFG). The EFG are characterized by their elasticity, offering favorable textural and rheological properties and expanding their application in the food, pharmaceutical, and cosmetic industries (MAO *et al.*, 2020). Emulsion-filled gels, therefore, have the advantages of emulsions and can deliver fat-soluble functional ingredients while also maintaining the advantages of hydrogels, including good mechanical properties and the ability to protect water-soluble functional ingredients against adverse conditions (BU *et al.*, 2023). EFG are complex colloidal materials that contain emulsion droplets and a gel

structure, with the emulsified lipid droplets enclosed in the gel matrix (DICKINSON, 2012). Thus, emulsion-filled gels have attracted great interest in recent years as a type of active ingredient carrier (MAO *et al.*, 2020).

It is widely known that starch is an attractive option for application in systems as a Pickering emulsion stabilizer, as well as for the production of hydrogels, due to its natural abundance, lack of toxicity, and biodegradability. However, the emulsifying property of native starch is limited due to its large particles and hydrophilic properties (ZHU, 2019). One way to overcome this limitation is to modify the starch with the heat-moisture treatment (HMT) followed by anti-solvent precipitation method, as evidenced by the outcomes of our research group (RAMOS *et al.*, 2023b). Furthermore, the loaded curcumin improved the stability and reduced the interfacial tension of an O/W emulsion through the formation of complexes between the starch nanoparticles (SNP) and the bioactive compound, producing smaller and more homogeneous droplets and a more stable system (RAMOS *et al.*, 2023a).

Furthermore, there are still few studies with EFG that use starch both as a stabilizer and to produce the gel phase of these systems. Therefore, in this study, quinoa starch will be used to compose the gel phase of the matrix. Quinoa starch granules are irregular polygons, with sizes from 1 to 3 μm, with an A-type crystalline structure and relative crystallinity from 21.5 to 43.0% (VELÁSQUEZ-CASTILLO *et al.*, 2020). A unique feature of quinoa starch is its low amylose content (3-20%), and its amylopectin with a large number of short and very long chains, which influence various starch properties, such as: low temperature of gelatinization, low peak viscosity , high solubility in water and high swelling power (LI, ZHU, 2018b; ZHU, 2023). These functional properties of quinoa starch are superior to those of other cereal starches, such as rice, wheat, and corn (LIU *et al.*, 2023), and the choice of quinoa starch to compose the gel phase of this study is mainly due to these characteristics.

Thus, emulsion-filled gels offer the flexibility to design formulations with specific rheological properties, improved the texture, viscosity, and consistency of the product, in addition to being able to carry a hydrophobic bioactive due to the presence of the emulsion in the composition of the gels. With that in mind, we proposed the production of starch-based gels filled with curcumin-loaded

Pickering emulsion and evaluated the effect of different emulsion ratios on the rheological properties and microstructure of EFG.

5.2. Material and Methods

5.2.1. *Material*

Canola oil (Liza, Cargil, Mairinque, SP, Brazil), cassava starch (Siamar, Neves Paulista, SP, Brazil), quinoa grains (variety Real, 2020 crop) and absolute ethanol (99.8%, Êxodo, Sumaré, SP, Brazil) were used. Nile Red and Nile Blue A were purchased from Sigma Aldrich (St Louis, MO, USA). All reagents used in the analyses were of analytical standard.

5.2.2. Quinoa starch extraction and chemical composition

Quinoa starch was extracted according to Velásquez-Castillo *et al.* (2020). The main characteristics of the quinoa starch were determined using classical methods (ISO, 1987; AACC, 1995): 12.4 ± 0.2% of moisture content, 0.0 ± 0.0% of ash, 1.2 ± 0.0% of proteins, 0.0 ± 0.0% of total lipids and ~23% of apparent amylose.

5.2.3. *Preparation of starch nanoparticles (SNP)*

Primarily, native cassava starch was modified by HMT (heat-moisture treatment) according to Ramos *et al.* (2023b). Briefly, the starch moisture content was corrected to 20% and after equilibration (at 4 ºC/ 24 h), the samples were heated to 130 °C for 4 h in an air convection oven (Tecnal, TE-394/3, Piracicaba, SP, Brazil).

The production of SNP was carried out according to the methodology proposed by Ramos *et al.* (2023b). In short, HMT-modified cassava starch was dispersed in distilled water (5wt%) and gelatinized at 95 ºC, for 30 min. After cooling, absolute ethanol was added in the ratio (v/v) of 1:1 water:ethanol, which

remained under mechanical stirring for 12 h at room temperature. Then, the samples were centrifuged (KASVI, K14-5000M, São José dos Pinhas, PR, Brazil) at 3,000 x g for 15 min and washed twice with absolute ethanol. The SNP were lyophilized (Heto-Holten, FD 1.0–60, A/S, Allerod, Denmark) and stored in hermetically sealed containers.

5.2.4. Production of curcumin-loaded Pickering emulsions

The curcumin-loaded oil-water (O/W) emulsions were prepared with 20% canola oil as the oil phase and 0.053 g curcumin/100 g emulsion (based on previous tests of curcumin solubility in canola oil, Ma et al. (2017) methodology). The starch nanoparticles 4% (g of SNP/100 g of emulsion) were added to the aqueous phase and the emulsification process was carried out using a rotor-stator homogenizer (Ultra-Turrax IKA, T25, Labotechnik, Staufen, Germany) at 14,000 rpm for 3 min. In addition, sodium benzoate at 0.02 wt% was used as a preservative (RAMOS *et al.*, 2023a).

5.2.5. Characterization of Pickering emulsion

5.2.5.1. Physical stability

A photo centrifuge LUMiSizer (LUM GmbH, LS 610, Berlin, Germany) was used to evaluate emulsion stability under accelerated conditions. LUMiSizer is based on the measurement of transmitted near infrared light (865 nm) as a function of time and position over the entire emulsion sample length simultaneously (DAMMAK; SOBRAL, 2018a). The applied operating parameters were as follows: volume, 1.8 mL of emulsion sample; centrifugal force, 4000 rpm; time interval, 10 s; temperature, 55 °C. Instability index values (II) were obtained directly from the SepView software version 4.1 (L.U.M., Berlin, Germany) (RAMOS *et al.*, 2023a).

5.2.5.2. Efficiency of encapsulation of curcumin

In order to assess the encapsulation efficiency (EE) of curcumin in the emulsion, both the contents of free curcumin and of the total curcumin were determined, following the method by Feng *et al.* (2020). For free curcumin content analysis, 1 mL of the emulsion was mixed vigorously with dichloromethane (5 mL) by vortexing for 2 min. The mixture was separated into an aqueous supernatant and an organic subnatant. The subnatant was collected and dried in a solution concentrator (Tecnal, TE-019, Piracicaba, SP, Brazil) with constant nitrogen flow, at 30 ºC. Afterward, ethanol was added to the container with the dry organic phase, and the solution was transferred to a volumetric flask, and the volume was adjusted to 25 mL. The absorbance of this solution was measured at 422 nm using a UV spectrophotometer (Femto, Cirrus 80 ST, São Paulo, SP, Brazil).

The total curcumin content in the emulsion was determined by destabilizing the emulsions with ethanol. Emulsion (1 mL) was added in ethanol (25 mL), vortexed for 2 min, and centrifuged at 15,000 x g for 20 min (KASVI, K14-5000M, São José dos Pinhais, PR, Brazil). The supernatant was collected for absorbance determination at 422 nm using a UV spectrophotometer (Femto, Cirrus 80 ST, São Paulo, SP, Brazil).

The total curcumin content (tc) was calculated using a standard curve build by diluting different aliquots of curcumin in ethanol within the range of 1-16 µg/mL. The equation for calibration curve was CC = 0.1126Abs + 0.1576 (R^2 = 0.989) where CC stands for the curcumin concentration and “Abs” refers to the recorded absorbance value. The encapsulation efficiency (EE) of curcumin was calculated using Equation 1:

$$\%EE = \frac{tc-fc}{tc}.100 \qquad (1)$$

Where: tc = total curcumin content; fc = free curcumin content.

5.2.6. Production of emulsion-filled gel

Quinoa starch emulsion-filled gels (EFG) were produced according to the methodology proposed by Torres *et al.* (2017), with some modifications. First, quinoa starch gels (non-filled gel) were made, at concentrations of 5, 7, 9, and

11wt%, to determine the minimum starch concentration to produce a self-sustaining gel. The starch non-filled gel was prepared by heating of the suspension with different concentrations of starch under stirring at 500 rpm at 70 ºC for 30 min. The gels were stored in cylinder tubes (25 mm diameter x 27 mm height) for 24 h at 4 ºC. Afterward, the gels were removed, and the minimum concentration of quinoa starch needed for preparation of EFG was determined through visual observation (minimum concentration of self-sustaining gel was 9wt%).

Thus, the EFG were produced with 9% quinoa starch with different proportions of emulsion (0, 25, 50, 75, and 100%) replacing water in the gels (Table 1). In other words, the oil fractions were 18.2, 13.7, 9.1, 4.6, and 0.0% (w/w), named from G1-G5, respectively. The EFG were prepared by directly mixing quinoa starch (9 wt%) with emulsion and/or water. This mixture was gelled at 70 °C for 30 min under stirring at 500 rpm.

Table 1 - Formulation of emulsion filled starch gels.

Sample	Quinoa starch (%)	Emulsion:Water	Total oil fraction (%)
G1	9	0:100	0
G2	9	25:75	4.6
G3	9	50:50	9.1
G4	9	75:25	13.7
G5	9	100:0	18.2

Source: own authorship.

5.2.7. Characterization of emulsion-filled gel

5.2.7.1 Evaluation of color and curcumin stability

The stability evaluation of curcumin encapsulated in the EFG was monitored using instrumental colorimetry at storage times of 0, 7, and 14 days (the sample was maintained at 4 ºC, sheltered from light). The L*, a*, and b* parameters were determined using a colorimeter (Hunterlab, Miniscan XE Plus, Reston, VA, USA). The color changes during storage are expressed as ΔL*, Δa*, Δb*, and ΔE* (total color difference), compared with the color of the fresh gels. The chroma (C^*_{ab}), the hue angle (h^*_{ab}), and the ΔE* were calculated using Equations 2, 3, and 4, respectively (SANT'ANNA *et al.*, 2013).

$$C_{ab}^{*} = \sqrt{(a^{*})^{2} + (b^{*})^{2}} \quad (2)$$

$$h_{ab} = tan^{-1}\left(\frac{b^{*}}{a^{*}}\right) \quad (3)$$

$$\Delta E^{*} = \sqrt{\Delta a^{*2} + \Delta b^{*2} + \Delta L^{*2}} \quad (4)$$

Where: b*: chromaticity on the axis ranging from yellow to blue; a*: chromaticity on the axis ranging from red to green; L*: lightness ranging from black to white. Δa*: a - a_0; Δb*: b - b_0; ΔL*: L - L_0; being L_0*, a_0* and b_0*: parameters obtained on day zero of storage.

5.2.7.2 Confocal laser scanning microscopy (CLSM)

To observe the internal structure of the gels, a confocal laser scanning microscope was used (Upright, LSM780-NLO, Madrid, Spain) (ONG *et al.*, 2012). The quinoa starch was marked with Nile Blue (0.05 mg/mL water and/or emulsion) and the oil with Nile Red (0.1% w/v, in ethanol; and 10 µL of solution Nile Red/g of lipid) and excited at 488 nm and 633 nm, respectively. The sample was placed on a glass slide, drawn, and covered with a coverslip.

5.2.7.3. Scanning electron microscopy (SEM)

To observe the pore structure and internal fractures of the emulsion-filled gels, a scanning electron microscope (SEM) (HITACHI, TM-3000, Maidenhead, UK) was used. The gels were placed in molds (25 mm diameter and 2 mm height) to facilitate posterior fracture, and left to rest for 24 h at 4 ºC, to balance the structure. After that, they were immersed in liquid nitrogen and lyophilized at -55 °C for 48 h on freeze-dried (Heto-Holten, FD 1.0–60, A/S, Allerod, Denmark). The gel was placed on carbon tapes, fractured, and taken for observation under a microscope (CIEŚLA; SARTOWSKA; KRÓLAK, 2015). A voltage of 15 kV and an increase of approximately magnification of 10,000 × were used.

5.2.7.4. Water holding capacity and syneresis

The water holding capacity (WHC) of the emulsion-filled gels followed the methodology proposed by Dun *et al.* (2021). EFG samples (1 g) were weighed on filter paper (Qualy, 14 µm, 80 g/m^2, Φ=15 cm), placed in Falcon tubes, and centrifuged at 2,500 rpm for 10 min (KASVI, K14-5000M, São José dos Pinhais, PR, Brazil). The water holding capacity (WHC) was calculated using Equation 5:

$$\%WHC = \frac{gela}{gelb}.100\% \qquad (5)$$

where: gel_b = weight of the gel before centrifugation; and gel_a = weight of the gel after centrifugation.

For syneresis analysis, the gels were prepared and put into cylinder molds (25 x 27 mm) in 4 ºC for 14 days. The water separated from the gels reflects the retrogradation properties, which was calculated as ratio between excess water weight and the total mass (% syneresis) (WANG *et al.*, 2016):

5.2.7.5. Uniaxial compression tests

The uniaxial compression experiments were conducted with a Texture Analyzer (Stable Micro Systems, TA.XT plus, Surrey, UK) at 25 °C, according to Bu *et al.* (2023) with some modifications. . A P/25 probe was used, and the samples were tested at 25% compression. The testing rate was set to 1 mm/s. The gels were prepared and placed in cylinder molds (25 mm diameter x 27 mm height) and stored at 4°C for 24 h before analysis. Gel hardness was calculated as the position of the peak observed in the mechanical curve. The values of Hencky stress (σH), Hencky strain (εH) and apparent Young's modulus (Eg) were obtained from the force-deformation data according to Equations (6) and (7), respectively:

$$\sigma_H = F_{(t)}.\frac{H_{(t)}}{H_0 A_0} \qquad (6)$$

$$\varepsilon_H = \ln\frac{H_{(t)}}{H_0} \qquad (7)$$

Where $F_{(t)}$ is the force at time t, A_0 is the initial area, H_0 is the initial height, and $H_{(t)}$ is the height at time t. The values of the apparent Young's modulus (Eg)

of the systems were determined by the slope of the first linear interval in the Hencky stress (σ_H) versus Hencky strain (ε_H) curves.

5.2.7.6. Rheological analysis

Small amplitude oscillatory shear testing (SAOS)

The rheological behavior of the gels was assessed at 25 ºC using a compact modular rheometer (Anton Paar, MCR 92, Vila Clementino, SP, Brazil) with rough plate geometry (25 mm, gap 1 mm). The gels were prepared and stored at 4 °C for 24 h. Afterward, the sample was loaded onto the rheometer geometry and allowed to equilibrate for 2 min for structural recovery. Rheological properties were obtained by small-amplitude oscillatory shear.

Strain sweep tests were conducted in the strain range from 0.1 to 100 Hz at a constant frequency of 1 Hz to determine the linear viscoelastic region (LVR) of the samples.

Oscillation frequency sweep tests were carried using a strain amplitude of 0.5% (within the LVR) over an angular frequency range from 0.1 to 100 Hz. The dependence of the viscoelastic moduli (G’ and G”) (Equations 8 and 9) and of the phase angle (δ) (Equation 10) with angular frequency was investigated using the Power Law model (Anton Paar Rheo Compass Software v 1.31) (CHANG *et al.*, 2014).

$$G' = k'\omega^{n'} \quad (8)$$

$$G'' = k''\omega^{n''} \quad (9)$$

$$tan\delta = \frac{G''}{G'} \quad (10)$$

Where ω is an angular frequency (Hz), K′ and K" are model constants (Pa/s^n), and n' and n'' refer to the frequency exponents (dimensionless).

Creep-recovery measurement

The creep-recovery test was performed after allowing the sample to rest for 10 min. Then, the sample was subjected to a sudden constant shear stress value (12 Pa, within the LVR, this value was determined in a preliminary stress sweep test) for 5 min. After this the stress was removed suddenly and the recovery in structure was measured, also for 5 min. Anton Paar Rheo Compass Software v 1.31 was utilized to obtain curves of shear strain (%) versus the time. (CHANG *et al.*, 2014; BRITO-OLIVEIRA *et al.* 2022)

Creep-recovery data were analyzed using the fractional derivative modeling approach, which has been used in polymer studies and the characterization of food materials (SPOTTI *et al.*, 2017). Equation (11) describes the creep-recovery curves in terms of the parameter α, which indicates the degree of viscoelasticity of the sample, where lower values of α indicate elastic gels and higher values indicate more viscous samples. J(t) is the compliance of the material (%/Pa), ε(t) is the instantaneous strain (%), σ(t) is the applied stress (Pa). The rheological parameters α, λ_1, and λ_2 were determined by adjusting the experimental data of creep (fluency) and recovery of the formed gel using the algorithm solver of Excel 2019 version (SPOTTI *et al.*, 2017).

$$J(t) = \frac{\varepsilon(t)}{\sigma_0} = \frac{1}{\gamma(\alpha+1)}(\lambda_1 t^{\alpha} H(t) - \lambda_2 (t - t_m)^{\alpha} H(t - tm)) \qquad (11)$$

Where: γ = gamma function; α = indicates the degree of elasticity, ranging from 0 to 1; λ_1 and λ_2 = inverse of the moduli of elasticity of the gel during creep-recovery, respectively; t = time during the analysis; tm = time the stress is removed (recovery); H(t) is the Heaviside or step function defined as:

$$H(t) = \begin{cases} 0 \; if \; t < 0 \\ 1 \; if \; t > 0 \end{cases} \qquad (12)$$

5.2.8. Statistical Analysis

Experiments were performed in at least triplicate. The results were submitted to analysis of variance (ANOVA) and the means were compared by the Tukey test ($p < 0.05$), using SAS software version 9.4 (Statistical Analysis System, São Paulo, Brazil).

5.3. Results and Discussion

5.3.1. Characterization of Pickering emulsions

The Pickering emulsion formulation chosen to encapsulate curcumin and producing emulsion-filled gels (EFG) was based on our previous study (RAMOS *et al.*, 2023a). In summary, the emulsion did not show phase separation for up to 14 days (cream index = 0%). It displayed an instability index (II) of 0.08 ± 0.02 at 25 ºC, an average droplet size of 6.07 ± 0.03, a zeta potential of -4.20 ± 0.11, and rheological parameters with values of 0.76 ± 0.01 and 0.29 ± 0.00 for n and k (constant of the Power Law model, R^2=0.999) respectively.

5.3.1.1. Physical stability

To evaluate the physical stability (resistance to phase separation) of curcumin-loaded Pickering emulsions, the analysis of the instability index (II) was performed, at 55 ºC (the maximum temperature allowed by the equipment) (Figure 1). It is important to highlight that this temperature was chosen to evaluate the behavior of the system during the heating of the Pickering emulsions, a process that had been carried out in preparing the emulsion-filled gels. The emulsion transmittance range was between ~116 to 130 mm, and the transmittance peak was 50 (%), values similar to those reported by Xu et al. (2023), who presented transmittance values of ~115 to 130 mm and peaks of 60% for Pickering emulsions stabilized by OSA starch/chitosan complexes.

Figure 1 - Visual aspect (day 0) and evolution of transmission profiles of the curcumin loaded Pickering emulsion stabilized with 4wt% of starch nanoparticles (SNP).

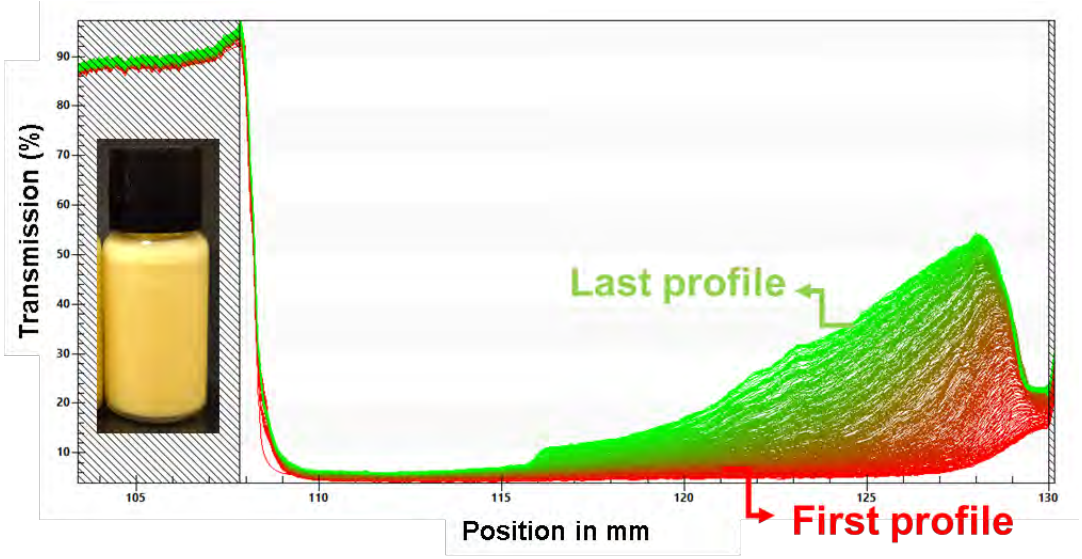

Source: own authorship.

In the transmission profile, the emulsions were gradually stratified using continuous centrifuge separation, while the profiles were being recorded. As indicated in Figure 1, the bottom red line represents the first transmission profile and the top green line represents the last transmission profile (WANYI *et al.*, 2020). At the beginning of the analysis, the emulsions were uniform and opaque dispersion systems, and therefore the transmission of the first red profile was close to zero since the sample was not translucent and did not allow the passage of light. As the centrifugation time increased, the emulsion became unstable, the lighter oil droplets migrated upwards, while the heavier aqueous phase remained at the bottom of the tube (NIU *et al.*, 2022).

The aqueous phase (more translucent) began to allow light to pass through, and the transmission at the bottom of the sample tube gradually increased. Thus, the newly registered red profile moved upwards until the last green profile at the top was registered. Therefore, the smaller the phase separation of the sample, the smaller the transmission area and the more stable the emulsion (DAMMAK; SOBRAL, 2018a).

The instability index (II) was 0.19 ± 0.01, which indicates excellent stability of the emulsion, despite the higher test temperature. Zhang *et al*. (2023) produced Pickering emulsions (W/O), stabilized by ethylcellulose nanoparticles and oleogels, and reported II ranging from ~0.27 to 0.32, at 25 ºC. Dammak and

Sobral (2018b) determined II varying between 0.22 and 0.42 for Pickering emulsion stabilized by chitosan nanoparticles, at 40 ºC. In both studies, II values were higher than those found in this study, indicating less stable emulsions.

5.3.1.2. Efficiency of encapsulation of curcumin

The encapsulation efficiency (EE) of curcumin in the Pickering emulsions was 78.5% ± 3.0. This value can be considered good, implying its potential as an excellent curcumin-loaded vehicle. This result may be a result from the strong structure formed by the layer of starch nanoparticles at the interface of the oil droplet, avoiding the release of curcumin into the system.

Feng *et al.* (2020) produced emulsions stabilized with debranched waxy maize starch, Tween 80, and lecthin, with curcumin in the oil phase, and reported EE values of ~71% for the formulations with the 3 stabilizers (starch, Tween, and lectin) and ~34% for the formulation stabilized only with debranched starch. Wang *et al.* (2023) produced a Pickering emulsion stabilized by gelatinized, debranched, and butyrylated rice starch particles and reported EE~51% for encapsulated curcumin. The result of these authors was lower than that reported by our study. These differences are probably due to the type of starch and production of the particle used in stabilization, and the type and fraction of oil used.

5.3.2. Characterization of emulsion-filled gels

5.3.2.1. Evaluation of color and curcumin stability

The visual appearance of quinoa starch non-filled gel (5 – 11 wt%) is shown in Figure 2a. As expected, it was visible that as the starch concentration increases, the gels become more self-supported, exhibiting a transition from the fluid-like behavior to the gel state. This transition is likely due to increasing intermolecular interactions and entanglements between starch molecules as their concentration rises. The minimum starch concentration of gelation that produced a self-supported gel was 9 wt%, and therefore, this was the concentration selected to produce emulsion-filled gels (EFG).

The water in the non-filled gel was replaced partially by an emulsion with different proportions of curcumin-loaded Pickering emulsion (Figure 2b) and the EFG (G2 – G5) exhibited a yellow color and similar appearance, regardless of varying emulsion amount, while the non-filled gel (0% of oil) remained white. No free surface oil was observed after gelatinization nor after storage of the gels.

Figure 2 - Visual appearance of non-filled gels produced with different starch concentrations of quinoa starch (5-11 wt%) (a); and filled gels of quinoa starch (9 wt%) filled with different emulsion ratio (0, G1, 25%, G2, 50%, G3, 75%, G4 and 100%, G5) (b).

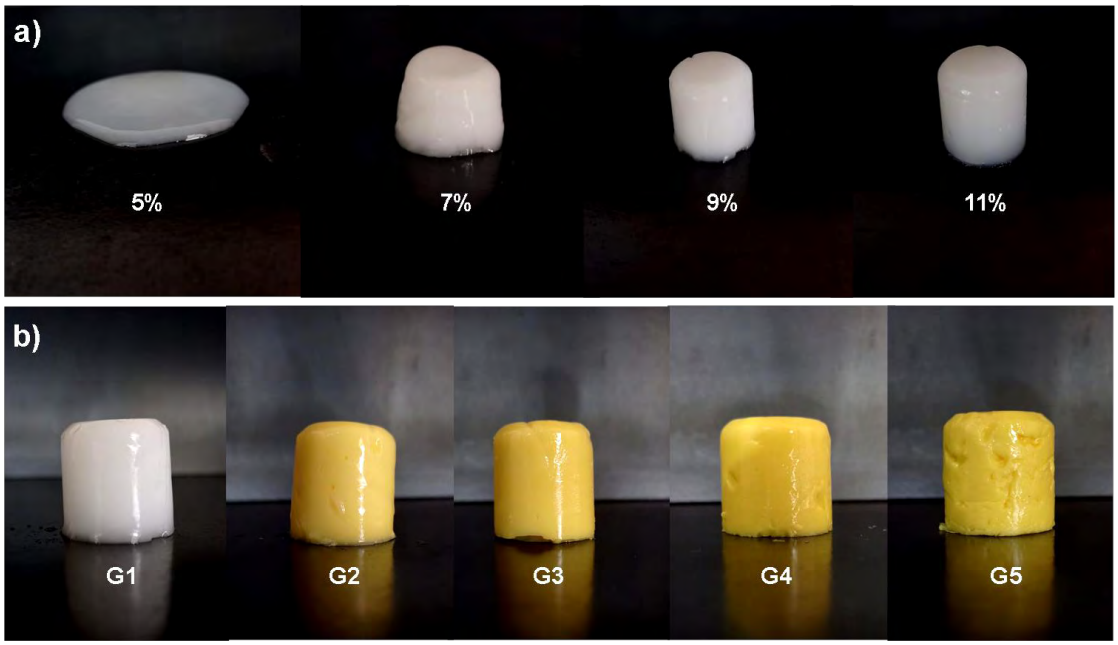

Source: own authorship.

The EFG were stored for 14 days and the colorimetric parameters were analyzed to assess the stability of the curcumin in the samples (Table 2). On the first day, the L* (representing lightness), b* (indicating the variation from yellow (+b*) to blue (-b*)) and a* (indicating the shift from red (+a*) to green (-a*)) parameters shifted from 80 to 55, from 67 to -3, and from -11 to -1, respectively, as the proportion of emulsion in the EFG decreased. These outcomes suggested that the samples became lighter, less yellow, and exhibited a reduction in green coloration, as the curcumin content decreased in the gels.

Table 2 - Color parameters of EFG with different emulsion ratio (0, G1, 25%, G2, 50%, G3, 75%, G4 and 100%, G5). Values followed by the same lowercase letters in the same column and the same uppercase letters in the same line (same parameter) do not differ significantly ($p<0.05$).

Oil fractions (%)	Day 1						Day 7						Day 14					
	L*	a*	b*	C^*_{ab}	h_{ab}	ΔE*	L*	a*	b*	C^*_{ab}	h_{ab}	ΔE*	L*	a*	b*	C^*_{ab}	h_{ab}	ΔE*
18.2	80.4 ± 0.1^{a,A}	-11.6 ± 0.2^{c,B}	67.1 ± 2.1^{a,A}	68.1 ± 0.1^{a,A}	80.2 ± 0.2^{b,A}	-	81.3 ± 0.3^{a,A}	-10.8 ± 0.1^{b,A}	62.4 ± 0.2^{a,B}	63.4 ± 0.2^{a,B}	80.2 ± 0.0^{b,A}	4.8 ± 1.1^{a,B}	81.4 ± 0.8^{a,A}	-10.4 ± 0.4^{b,A}	55.0 ± 0.7^{b,C}	56.0 ±0.8^{b,C}	79.3 ± 0.2^{a,B}	12.2 ± 1.3^{a,A}
13.7	76.9 ± 0.3^{b,B}	-10.2 ± 0.1^{b,B}	66.5 ± 1.1^{a,A}	67.3 ± 1.1^{a,A}	81.3 ± 0.1^{a,B}	-	77.4 ± 0.3^{c,B}	-9.1 ± 0.1^{b,A}	61.4 ± 0.2^{b,B}	62.1 ± 0.2^{b,B}	81.6 ± 0.1^{a,A}	5.3 ± 1.1^{a,A}	79.6 ± 0.2^{a,A}	-10.8 ± 0.0^{b,C}	60.3 ± 0.0^{a,B}	61.2 ± 0.0^{a,B}	79.9 ± 0.0^{a,C}	6.8 ± 1.1^{c,A}
9.1	78.0 ± 0.7^{b,A}	-12.6 ± 0.1^{d,B}	60.7 ± 1.1^{b,A}	62.0 ± 1.0^{b,A}	78.3 ± 0.3^{c,A}	-	79.1 ± 0.3^{b,A}	-11.5 ± 0.2^{d,A}	54.3 ± 0.2^{c,B}	55.5 ± 0.3^{c,B}	78.1 ± 0.2^{c,A}	6.7 ± 0.9^{a,A}	79.6 ± 1.3^{aA}	-12.8 ± 0.3^{d,B}	53.0 ± 0.9^{b,B}	54.6 ± 1.0^{c,B}	76.4 ± 0.1^{b,B}	7.9 ± 1.0^{b,c,A}
4.6	70.1 ± 0.0^{c,C}	-11.8 ± 0.1^{c,A}	48.5 ± 0.6^{c,A}	49.9 ± 0.6^{c,A}	76.3 ± 0.0^{d,A}	-	72.8 ± 0.9^{d,B}	-11.2 ± 0.1^{c,A}	43.4 ± 0.4^{d,B}	44.8 ± 0.4^{d,B}	75.5 ± 0.1^{d,B}	5.9 ± 0.5^{a,B}	75.7 ± 0.4^{bA}	-11.8 ± 0.4^{c,A}	38.8 ± 1.4^{c,C}	40.6 ± 1.4^{c,C}	73.0 ± 0.4^{d,C}	11.2 ± 0.8^{a,b,A}
0.0	55.5 ± 1.2^{d,C}	-1.1 ± 0.0^{a,B,A}	-3.6 ± 0.1^{d,A}	3.8 ± 0.0^{d,A}	72.7 ± 0.6^{e,A}	-	63.2 ± 0.8^{e,B}	-1.2 ± 0.1^{a,B}	-3.7 ± 0.1^{e,A}	3.8 ± 0.0^{e,A}	72.2 ± 1.1^{e,A}	7.7 ± 0.4^{a,B}	66.1 ± 0.4^{cA}	-1.1 ± 0.0^{a,A}	-3.6 ± 0.1^{d,A}	3.8 ± 0.1^{d,A}	73.8 ± 0.3^{c,A}	10.6 ± 1.1^{a,b,A}

Source: own authorship.

Overall, curcumin acted as the most important color-changing factor in the entire system. In general, the a* parameter have a tendency to decrease significantly over the storage time (up to 14 days), with exception of non-filled gel which remained unchanged and the G5, which showed an increase in this parameter. The variation in the L* values was significant for G2 and G1, while the other samples remained without significant differences along the storage time. The b* parameter had a downward trend as the storage time increased from 1 to 14 days, for the samples containing curcumin, mainly for the G5, while it did not show a significant difference for the gel without curcumin (Table 2).

This result corroborates the values of the Chroma parameter (C^*_{ab}), which indicated a slight reduction when comparing day 1 to day 14 of storage, with the exception of the non-filled gel, which remained unchanged. The Hue angle (h^*_{ab}) is expressed in degrees, where 0° corresponds to "+a" (red), 90° corresponds to "+b" (yellow), 180° corresponds to "–a" (green), and 270° corresponds to a "–b" (blue). In this study, the Hue angle values confirm the predominant color as yellow for all samples (~72-80°), with increasing intensity of yellow as the proportion of emulsion in the formulation increased (SANT'ANNA *et al.*, 2013). This parameter showed a downward trend for all EFG with storage time, with the exception of the non-filled gel, which had an increase in h^*_{ab}.

The values of ΔE*, which represents the total color difference, was calculated for days 7 and 14 of gel storage to assess the extent of color change compared to the initial day of analysis. The G5, G2 and G1 showed a significant difference in ΔE* during storage time, with a tendency for this parameter to increase with increasing time, while the G4 and G3 remained without significant difference in this period. For the EFG with less emulsion (G2 and G1), the phenomenon of syneresis occurs with greater intensity (behavior better explained in topic 5.3.2.4). This may explain the greater difference in color of these samples during the monitoring period. The sample with the highest emulsion ratio (G5), despite suffering little syneresis, had greater aggregation of emulsion droplets during the production of EFG (CLSM analysis, topic 5.3.2.2), which may explain its lower stability of color. This demonstrates that EFG with an intermediate emulsion ratio managed to preserve curcumin better than the other formulations.

5.3.2.2. Confocal laser scanning microscopy (CLSM)

The microstructure of the EFG was investigated by confocal laser scanning microscopy (CLSM), with starch marked in blue and oil droplets in red (Figure 3). For the quinoa starch non-filled gel (G1), it was possible to observe only the network matrix formed, with starch marked in blue, as expected. As for the EFG (G2 – G5), the oil droplets (in red) appeared trapped in a starch gel matrix. No free surface oil was observed by CLSM (Figure 3). The black region in these images indicated the presence of pores in the EFG. The size of the black region gradually increased with decreasing oil content in the samples. This indicated that the porosity of the gel network reduced with the incorporation of higher concentrations of emulsion.

Figure 3 - Confocal laser scanning microscopy (CLSM) of EFG with different emulsion ratio (0, G1, 25%, G2, 50%, G3, 75%, G4 and 100%, G5). Coloring in red indicates the oil and coloring in blue the starch.

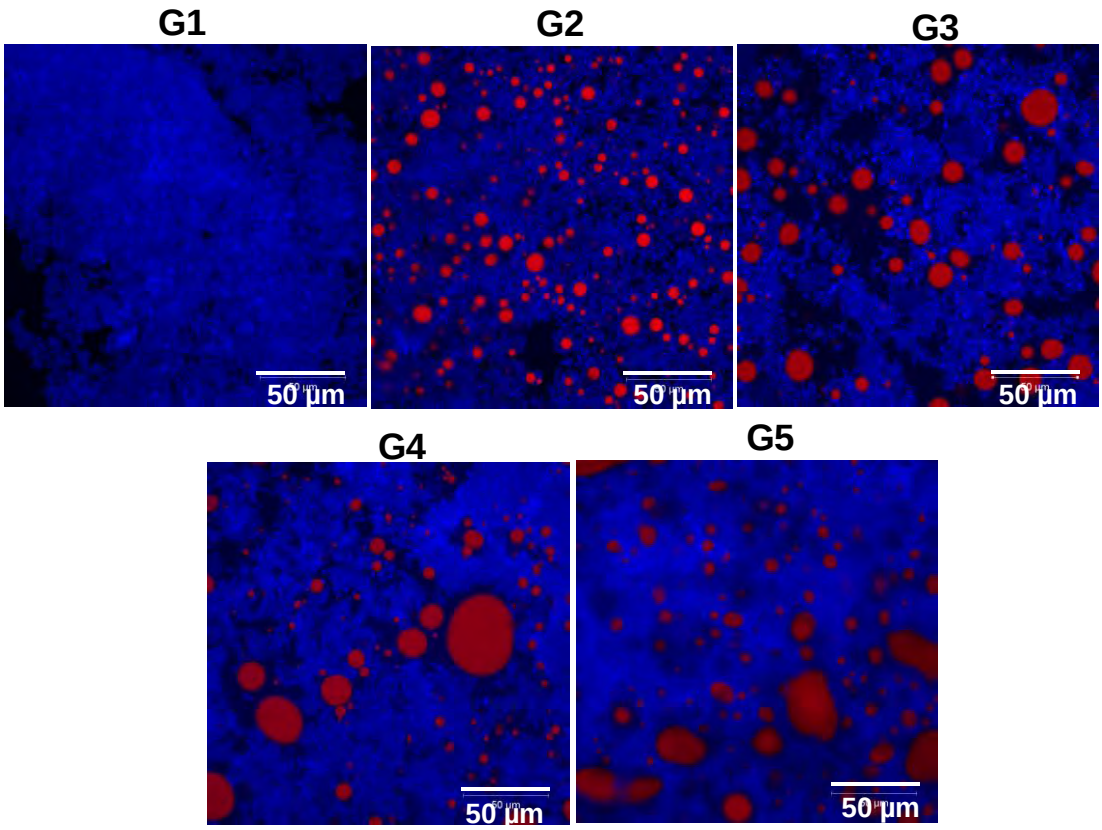

Source: own authorship.

The emulsion droplets were dispersed in the polymeric matrix and only a limited level of droplet aggregation was observed. However, with the increase of the emulsion ration from G2 to G5 in the gels, there was probably a breakdown of the physical barrier at the interface of the Pickering emulsion droplets. This resulted in the aggregation of neighboring droplets, since microscopy showed larger and even deformed droplets at higher concentrations. Thus, with higher oil contents, larger agglomerates of emulsion droplets were formed. This phenomenon may have occurred due to the low availability of water for starch gelatinization and formation of the gel network for this samples. This demonstrates that the structure of the EFG can be altered by varying the oil concentration.

Similar results were reported by Lyu, Sala and Scholten (2023), which produced corn and potato starch gels filled with emulsion stabilized by whey protein isolate (WPI), with oil fractions ranging from 5 to 15% (w/w). These authors indicated that with 5% oil content, the emulsion droplets were dispersed in the polymeric matrix and little droplet aggregation was observed, a different behavior when the oil content was increased to 10 and 15%, with greater occurrence interconnectivity of the emulsion droplets and leading to aggregation and network formation.

5.3.2.3. Scanning electron microscopy (SEM)

The surface and fracture microstructures of EFG with different emulsion ratio are shown in Figure 4. Differences were found in the microstructures of the gel networks as the oil concentration decreased in the formulation, both on the surface and in the transversal area of the samples (Figure 4). During starch gelazination, changes occured in the granules, such as swelling of the granules, melting of crystallites, separation of amylose and amylopectin, and disentanglement of entanglements between starch molecules (KEETELS; VLIET; WALSTRA, 1996). Thus, the amylose and amylopectin chains are leached from the granules after starch gelatinization/retrogradation. These molecules are highly hydrophilic and form hydrogen bonds with water. Thus, these interactions influenced the formation of the gel network, as well as the presence of the emulsion within the matrix.

Figure 4 - Scanning electron microscopy of up side (scale bar = 200 µm) (a); and fracture surfaces (scale bar = 500 µm) (b) of EFG with different emulsion ratio (0, G1, 25%, G2, 50%, G3, 75%, G4 and 100%, G5).

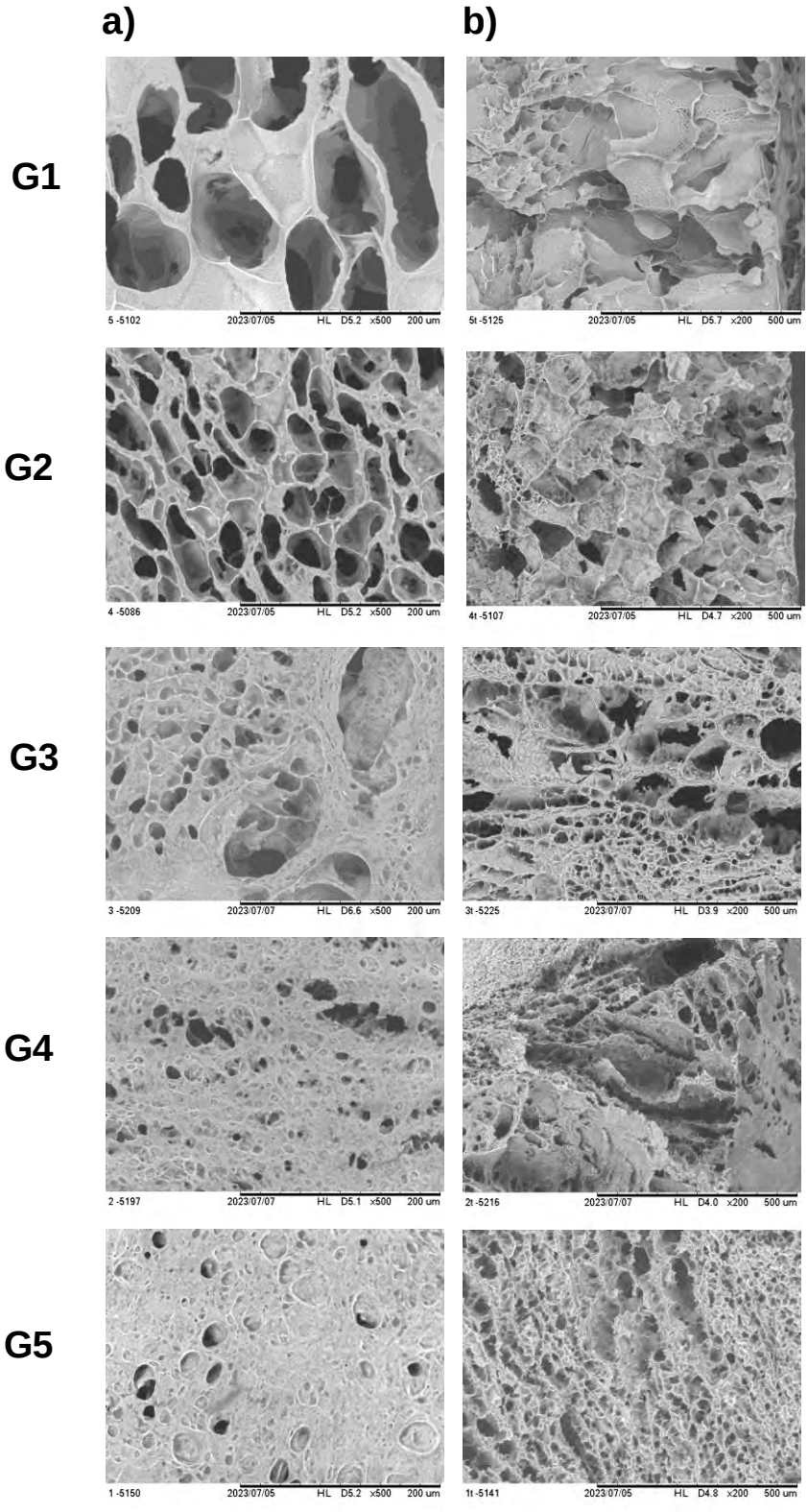

Source: own authorship.

SEM micrographs of non-filled gel and the gels with the lowest concentration of emulsion (G2) revealed a porous honeycomb structure, which can be attributed to the freezing process, where ice crystal destroyed the gel network, leading to the enlargement of the gel pores. The size and number of pores in the gel network decreased with increasing oil concentration, indicating that the incorporation of the emulsion into the formulation produced a smaller, more compact, and less porous network structure. The same phenomenon was observed in the CLSM images. This is because as the emulsion concentration increases, the interaction between molecules also increases proportionally, indicating an active filling behavior (a phenomenon that will be better discussed in section 5.3.2.5).

Bu *et al.* (2023) reported similar results for emulsion-filled (oil:aqueous phases ratio of 4:6 w/w) pea starch-based gels. However, these authors varied the starch concentration in the matrix (14.3 - 45.4%), observing porous honeycombs in gels with lower starch concentrations (14.3%) and smaller pores in more concentrated formulations (45.4%).

5.3.2.4. Water holding capacity and syneresis measurement

The gel systems' capacity to retain water and resist its release or expulsion from the gel network under external pressure (e.g., centrifugation or compression) was assessed through water holding capacity (WHC) (Figure 5a). This assessment also indicated the stability of the gel structures. (LI *et al.*, 2021). The quinoa starch non-filled gel (G1) showed the smallest WHC value (~25%). With the increase in the amount of emulsion incorporated in the EFG formulations (G2 – G5), there was an increase in WHC (53 – 81%), which may be due to increased interactions between Pickering emulsions and the starch matrix, mainly through hydrogen bonding interactions. In addition, in the EFG with the highest concentration of emulsion, there was less water available, which also contributed to the higher water retention in these systems.

Figure 5 - Water holding capacity (WHC) and syneresis (days 7 and 14) of EFG with different emulsion ratio (0, G1, 25%, G2, 50%, G3, 75%, G4 and 100%, G5). Values followed by the same lower-case letters do not differ significantly ($p<0.05$).

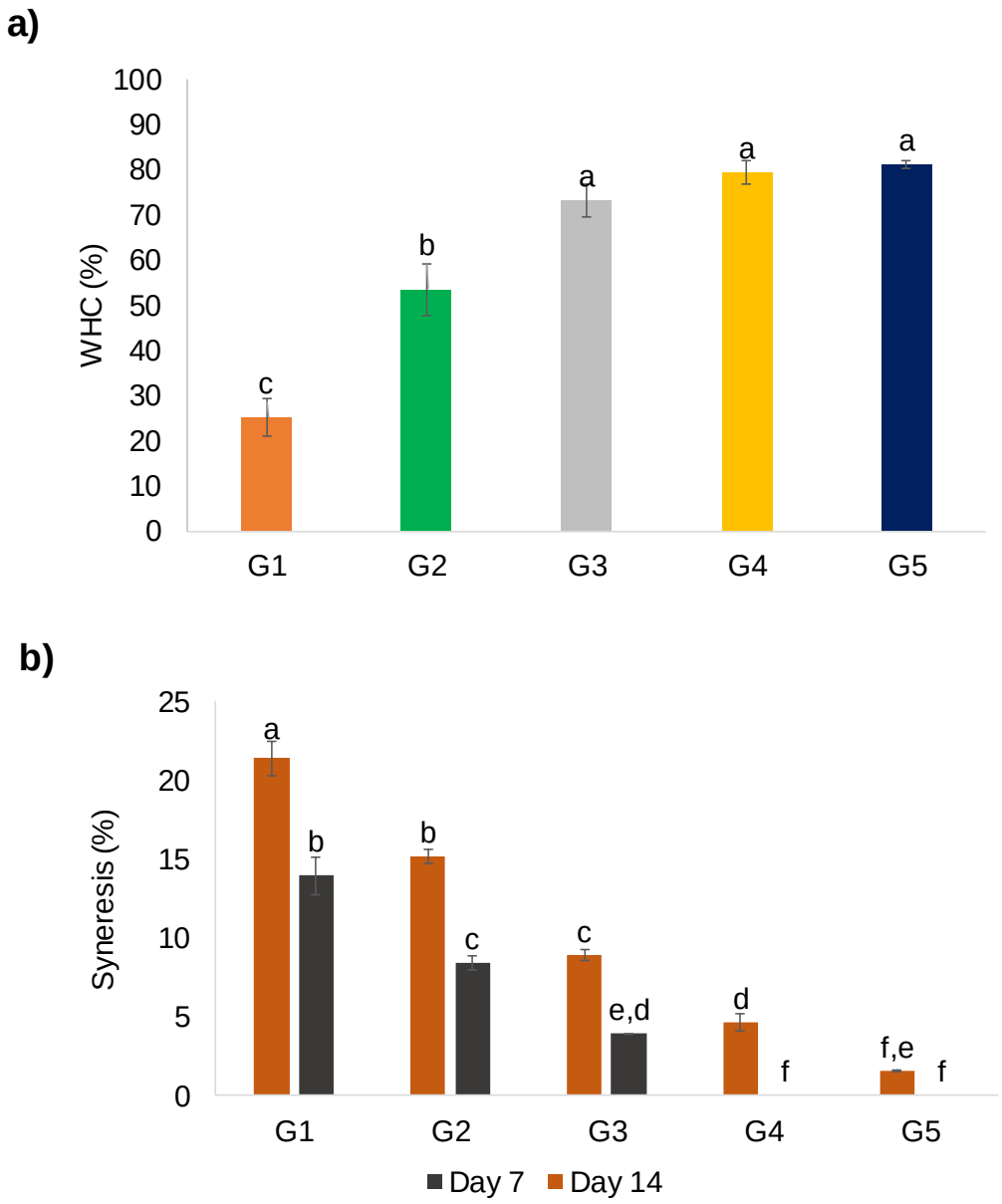

Source: own authorship.

HMT-modified starch nanoparticles, used to stabilize the droplet interface, tend to have a large amount of hydroxyl groups available on the surface of the nanostructure. This occurs due to the nanoprecipitation process combined with the modification of starch by HMT. In addition, the rough surface of the nanoparticle increases the hydrogen bonding interactions between the starch nanoparticle chains, water, and the starch chains of the gel matrix.

The increase in WHC indicates that water was strongly trapped in the gel network with higher emulsion concentration. Furthermore, the oil droplet, an integral part of the gel matrix, can reduce the effective pore size of the gel network and clog the microchannel, leading to a reduction in water release during centrifugation (DUN *et al.*, 2020).

Similar results have been reported by other authors. Li *et al.* (2021) produced gels based on chitosan hydrochloride-carboxymethyl starch, filled with Pickering emulsions and reported that the addition of emulsions with higher fractions of the oil phase decreased WHC, relating this behavior to the increase in interactions between the oil droplets in the emulsion and the starch in the gel network. Dun *et al.* (2020) produced whey protein isolate (WPI) stabilized emulsions which were incorporated into the rice starch gel matrix and reported that the emulsion also inhibited the reduction of WHC from the starch gel, and the inhibitory effect increased with increasing of the oil phase content of the emulsion (1 - 5%). However, it is important to remember that proteins, in general, have higher values of zeta potential and are able to have electrostatic interactions, while starch nanoparticles, as used in this study, showed low surface charges (RAMOS *et al.*, 2023b).

The syneresis rate was used to describe the stability of emulsion filled gels over a certain period of storage, reflecting the suitability of it applying in food, mainly for demand for low fat products. There was not any syneresis on the first of storage, therefore, only values from day 7 and 14 of storage were presented. Syneresis is associated with the phenomenon of starch retrogradation, which is the reassociation of amylose and amylopectin in gelatinized starch with the consequent expulsion of water from the system. Amylose is responsible for the short-term retrogradation of starch, while amylopectin acts on long-term retrogradation (ANBARANI; ALI RAZAVI; TAGHIZADEH, 2021). Thus, the 7-day syneresis values may be more associated with amylose retrogradation, while the 14-day syneresis values with amylopectin retrogradation.

As seen in Figure 5b, the rate of syneresis of the EFG increased with the reduction of the proportion of emulsion incorporated in the formulation (G5 – G2), with values from 0 - 14% for day 7 and from 1.6 to 15.2% for day 14 of storage. The non-filled gel, as expected, presented the highest syneresis of all tested samples (14%, day 7; 21.4%, day 14). The syneresis values of the gels

corroborated the WHC results, which were inversely proportional. This phenomenon is expected, since both parameters are mainly influenced by the interaction between components within the matrix. The oil droplets act as active fillers in the emulsion gels, which contributes to the reduction of the pore size of the gels (LI *et al.*, 2021). Thus, it can be concluded that the droplets of the Pickering emulsions were trapped in the three-dimensional network of the gels during the formation of the emulsion gels.

5.3.2.5. Uniaxial compression test

The uniaxial compression test on the EFG to reach 25% strain was used to compare the mechanical properties of these samples (Table 3). As the proportion of emulsion increased, the Young's modulus (Eg) and the hardness of the gels increased significantly, indicating that the EFG with a higher proportion of emulsion was more resistant. The non-filled gel had a drastically lower Young's modulus (~1.55 KPa) and hardness value (~0.07 N) when compared to the EFG (G2 – G5) which ranged from ~5.34-9.82 KPa and ~1.14 – 2.54 N, respectively, in order of increase of the proportion of the emulsion.

Table 3 – Young's modulus (Eg) and Hardness of EFG with different emulsion ratio (0, G1, 25%, G2, 50%, G3, 75%, G4 and 100%, G5). Values followed by the same lowercase letters in the same column and the same uppercase letters in the same line (same parameter) do not differ significantly ($p<0.05$).

Sample	Eg (kPa)	Hardness (N)
G1	1.55 ± 0.32^{d}	0.07 ± 0.00^{d}
G2	5.34 ± 0.09^{c}	1.14 ± 0.10^{c}
G3	7.01 ± 0.24^{b}	1.78 ± 0.06^{b}
G4	9.92 ± 0.65^{a}	2.64 ± 0.05^{a}
G5	9.82 ± 0.40^{a}	2.54 ± 0.10^{a}

Source: own authorship.

The changes in Eg and hardness observed in the present study indicate that the emulsion droplets acted as active fillers in the EFG. The hardness of a sample reflects the force required to achieve deformation to a certain degree. In addition, greater hardness indicates a denser and more rigid microstructure of

gels, which corroborates the results of SEM and WHC. This microstructure is associated with an increase in the droplet network and a decrease in porosity with increasing oil content in the system, caused by the active filling effect of the emulsion. (MU *et al.*, 2023). According to Dickinson (2012), a gel filled with an emulsion has a higher hardness than that presented by an equivalent non-filled gel, which is an indicator of the strong reinforcement provided by the emulsion oil droplets to the semisolid. However, the nature of the interactions within the system determines whether or not the droplets are bound to the gel network (active or inactive particles) (GEREMIAS-ANDRADE *et al.*, 2017). The active filler particles are bound to the gel matrix due to the interactions that occur between the gel matrix macromolecules and the stabilizer or surfactant molecules, generally increasing the rigidity of the gel. Inactive filler particles, on the other hand, do not bind to the gel matrix and have low chemical and physical affinity with the matrix macromolecules, causing a reduction in rigidity (VLIET, 1988).

Furthermore, the mechanical properties of EFG depend on the physicochemical properties of the gel matrix and the emulsion droplets, the size, volumetric fraction and distribution of the emulsion droplets, as well as the resistance and interactions between the emulsion droplets and the gel matrix (GEREMIAS-ANDRADE *et al.*, 2017). Generally, for active fillers, the higher the volume fraction of oil, the higher the gel strength observed. Futhermore, the aggregation of the emulsion droplets can lead to a further increase in gel rigidity. In our study, this phenomenon was observed in the CLSM analyses. Thus, the greater rigidity of the gel with higher oil content was probably the result of a combination of the increase in the volume fraction and the increase in the level of aggregation of the droplets.

Similar results have been reported. Mu *et al.* (2023) produced potato starch gels filled with emulsions stabilized by sodium caseinate and also reported an increase in hardness (from 0.75 to 1.75 N) of the gels with increasing oil content (0 - 50%), indicating a denser and more rigid microstructure of these gels.

5.3.2.6. Rheological analysis

Small amplitude oscilattory shear (SAOS)

The storage (G′) and loss (G″) moduli of EFG were determined as function of the oscillatory stress allowing the determination of the threshold of the linear viscoelastic region (LVR) can be observed for all samples, up to stress close to 14 Pa (Figure 6a). Furthermore, G' was greater than G″ in all samples, indicating indicating a market elastic solid-like response. Moreover, increasing emulsion ratio in the EFG showed significantly broader LVR, higher G’ values, and higher critical stress (crossover point of G’ and G”) over applied stress, suggesting high gel strength. Esse resultado corrobora com as propriedades mecânicas do gel (compression uniaxial test). So, emulsion ratio influencia a viscoelasticidade da EFG. These results demonstrated Pickering emulsion endows elastic, soft solid-like materials. The moduli (G’ and G”) was higher for samples with a higher proportion of oil, which indicates a more resistant to shear stress structure compared to the starch non-filled gel. Furthermore, for all samples, the moduli G' and G" crossed at the end of the test, which indicates weak gel behavior, typical of starch gel (AHMED; DHULL; CHANDAK, 2023). Frequency sweep and creep-recovery tests were therefore performed within LVR.

Figure 6 - Storage (G') and loss (G”) moduli as a function of shear stress (Pa) (a) and frequency (b); tan(δ) as a function of frequency (c); and G’ at 1 Hz (d) of the EFG with different emulsion ratio (0, G1, 25%, G2, 50%, G3, 75%, G4 and 100%, G5). Values followed by the same lower-case letters do not differ significantly ($p<0.05$).

a)

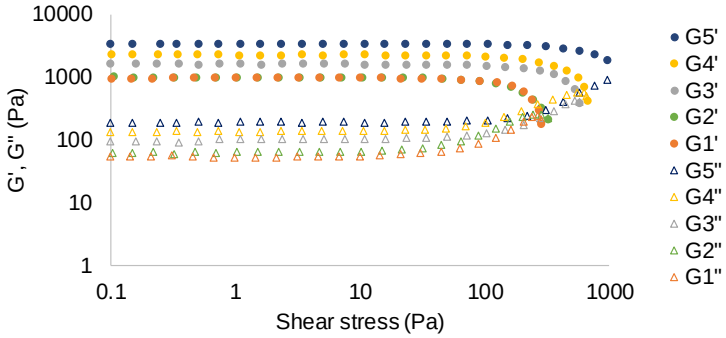

b)

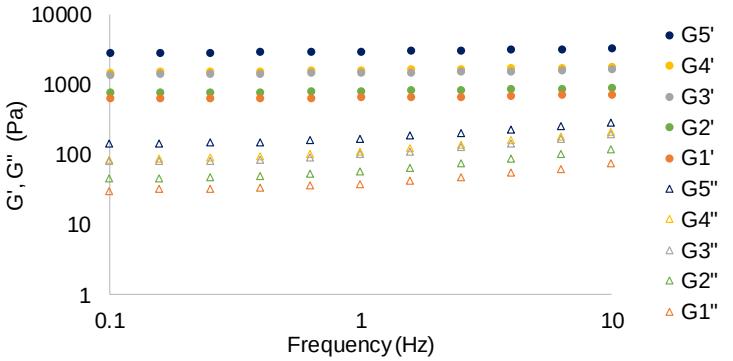

c)

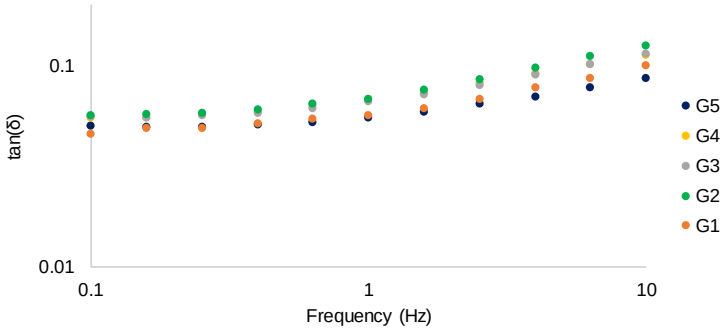

d)

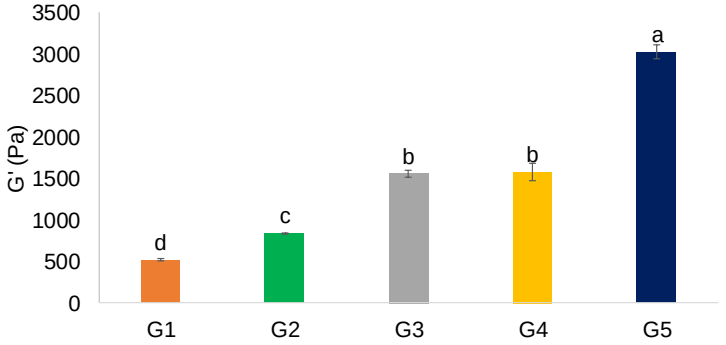

Source: own authorship.

The storage (G′) and loss (G″) moduli of the EFG as a function of frequency allowed to observe that all samples showed G' > G" (Figure 6b), without crossing over the moduli. However, a frequency dependency was observed for these modules, which indicates a weak gel behavior and elastic character of the samples (STEFFE, 1996). All samples showed that G′ and G″ slightly increased with frequency, which suggests a solid-like behavior (AHMED; DHULL; CHANDAK, 2023). In this study, the EFG networks are mainly based on non-covalent cross-links (hydrogen interactions), which were mainly responsible for the frequency dependence. Thus, the amylose/amylopectin chains of starch directly depend on the available relaxation time, and as the frequency increases, their entanglement points can act as temporary knots, thus increasing the elasticity of the EFG with increasing frequency (ZHANG *et al.*, 2023).

The gels with higher proportions of emulsion (G5 and G4) showed higher G' and G" values than G2 and G1, indicating that the increase in the proportion of emulsion contributed to the formation of a structure with greater resistance to shear. This behavior can be explained by the fact that the emulsion acts as an active filler to improve the elastic and viscous behavior of the gel, which provided better support for the emulsions against oscillation. Figure 6d shows the G' values at 1Hz, which confirmed that higher emulsion ratio produced more shear resistant gels (higher G' values). Thus, it can be proven that the properties of gels filled with emulsion confer their microstructural organization dependent on the amount of emulsion used in their formulation. Mu *et al.* (2023) reported similar results, where they obtained an increase in G' and G" with increasing oil content (0 - 50%) in potato starch gels filled with emulsion stabilized with sodium caseinate, suggesting the active filler effect of O/W emulsions in the gel.

In addition, the tan(δ) showed a tendency to increase as a consequence of the increasing of frequency, staying under 0.12 (Figure 6c). This behavior is characteristic of predominantly elastic materials, due to presence of the network. Zhao *et al.* (2023) produced gel filled with rice starch-based emulsion and also reported that G' was always larger than the G" in their gels, with tanδ < 0.3. This behavior can be further confirmed by the slope of the tanδ x frequency curve, which provides evidence about the nature of the viscoelastic fluid, for example, true gels exhibit a slope of zero, while weak gels exhibit a positive slope (BHARDWAJ; SANDHU; SAXENA, 2019).

The parameters of the Power-law models, *k′* and n′ (Eq. 6) and *k″* and n″ (Eq. 7) were calculated by non-linear regression (R^2>0.92) (Table 4). *k*’ and *k*” describe the general range of elastic and viscous properties of the samples, whereas n′ and n″ represent the frequency dependence of G′ and G″, respectively (YU *et al.*, 2020). These frequency dependences are closely related to the structural stability of gels, with high values of n′ and n″ representing low structural stability in general.

Table 4 - Power Law model coefficients obtained for frequency curves (G’ and G”) of EFG with different emulsion ratio (0, G1, 25%, G2, 50%, G3, 75%, G4 and 100%, G5). Values followed by the same lower-case letters in the same column do not differ significantly (p<0.05).

Oil fractions (%)	k' (Pa.s)	n'	R^2	k'' (Pa.s)	n''	R^2
18.2	3037.5 ± 79.1^{a}	0.03 ± 0.00^{a}	0.9893	179.3 ± 9.9^{a}	0.16 ± 0.00^{b}	0.9248
13.7	1589.9 ± 110.2^{b}	0.04 ± 0.00^{a}	0.9872	115.2 ± 9.7^{b}	0.20 ± 0.01^{a,b}	0.9471
9.1	1571.2 ± 44.1^{b}	0.04 ± 0.00^{a}	0.9788	112.4 ± 1.1^{b}	0.19 ± 0.01^{a,b}	0.9253
4.6	840.8 ± 7.9^{c}	0.03 ± 0.00^{a}	0.9612	64.6 ± 0.2^{c}	0.21 ± 0.00^{a}	0.9233
0.0	554.3 ± 25.7^{d}	0.02 ± 0.01^{a}	0.9075	35.7 ± 0.7^{d}	0.21 ± 0.02^{a}	0.9498

Source: own authorship.

k' was always greater than *k*'', which confirms the weak gel behavior. As the emulsion ratio increased, the values of *k*’ and *k*” also increased proportionally (*k*’ = 554 - 3057 Pa.s^{-n}, and *k*” = 36 - 179 Pa.s^{-n}), which confirms the increase in resistance and viscoelasticity for EFG with higher emulsion concentration. Regarding n', the incorporation of the emulsion did not affect this parameter in the EFG. On the other hand, n'' showed a tendency to decrease with the increase in the emulsion ratio, indicating the formation of a more stable system, which can be explained by the stronger interactions between matrix and emulsion droplets. Mu *et al.* (2023) reported similar results for potato starch gels filled with emulsion stabilized with sodium caseinate, where both K' and K'' gradually increased with increasing oil content (0 - 50%).

Creep-recovery properties

The Creep-recovery curves of EFG are shown in Figure 7, as well as the applied modeling curves. All samples fitted well (R^2>0.99) to the fractional derivative model used. The viscoelastic behavior of complex systems is mainly determined by oscillatory rheological measurements, but the internal structure of a system and the changes in its structure caused by the modification of its composition can also be analyzed by creep-recovery studies. Creep curves have similar viscoelastic performance, but were different in maximum strain. The macromolecular network formed in the gel without emulsion (G1) tends to be more deformable since the emulsion occupies spaces in the formed gel network. Thus, non-filled gel is more easily stretched than EFG (G2 – G5). Among the EFG, the G2, was more flexible, an expected behavior, since it has less emulsion in its formulation. The greater deformation can be attributed to the fact that the molecular network formed in the sample tends to be more fragile so the gel is more susceptible to strain deformation (ZHAO *et al.*, 2023).

Figure 7 - Creep-recovery behaviors (compliance (%/Pa) x time (min), data and fit model fractional derivative) for EFG with different emulsion ratio (0, G1, 25%, G2, 50%, G3, 75%, G4 and 100%, G5).

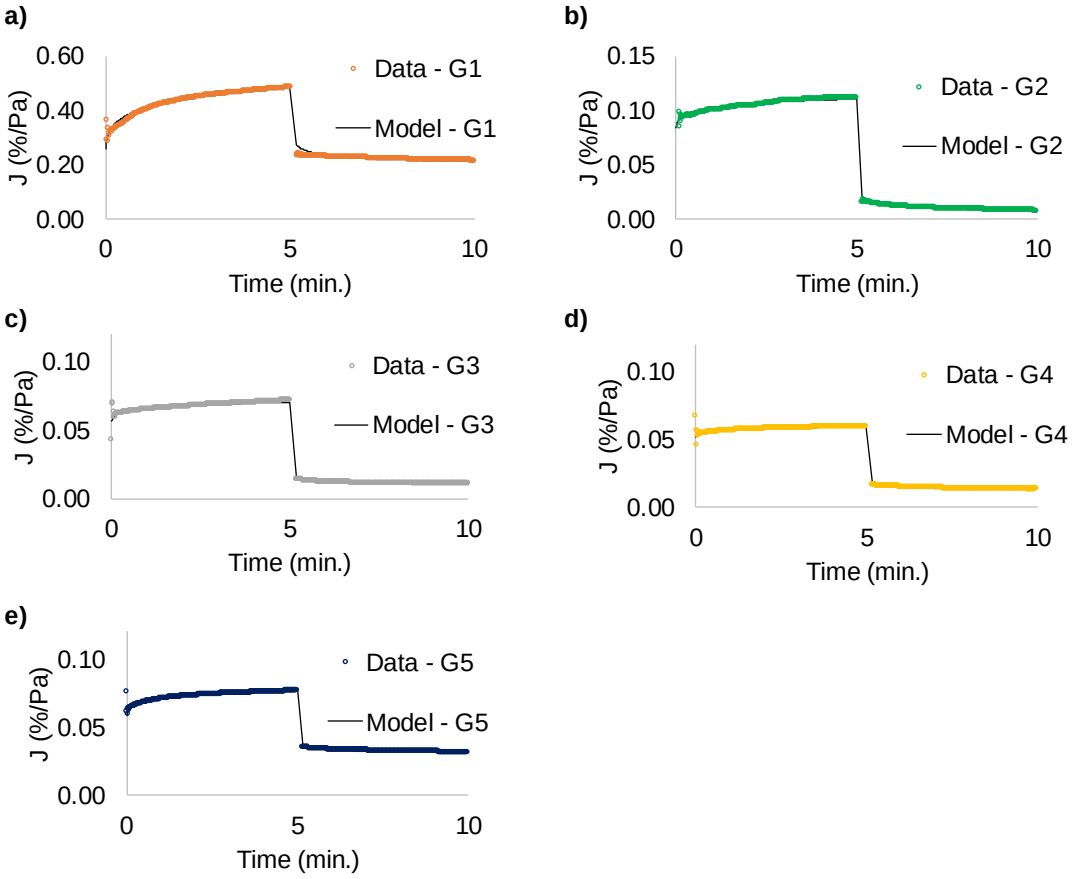

Source: own authorship

The α parameter (Eq. 9), calculated by non-linear regression (Table 5), allowed to observe that EFG (G2 – G5) presented lower α values than the non-filled gel (G1). The parameter α varies between 0 and 1. The closer the parameter is to 1, the more viscous the material is, with α = 1 for a perfectly viscous material and α = 0 for a perfectly elastic material (SPOTTI *et al*., 2017). Thus, the EFG are significantly more elastic than the gel without emulsion. These results corroborate those presented for the frequency sweep (section 5.3.2.6). However, unlike the frequency tests, the creep test parameters indicated that the elasticity of the EFG was not altered by the different emulsion ratio in the formulation (G2 – G5). This difference can be explained due to the different tests proposed in the two methodologies, where one provides the analysis of the behavior during oscillatory shear of the EFG and the other of the behavior during the application of a stress and during its recovery. These results indicate that the internal

structure of the EFG was similar, although the viscous behavior under oscillation was different.

Table 5 - Creep-recovery fitting parameters for model (Eq. 9) fractional derivative of EFG with different emulsion ratio (0, G1, 25%, G2, 50%, G3, 75%, G4 and 100%, G5). Values followed by the same lower-case letters in the same column do not differ significantly ($p<0.05$).

Sample	Derivative order (α)	Creep constant (λ1σo)	Recovery constant (λ2σo)	λ1–λ2	R^2
G1	0.097 ± 0.016^{a}	4.724 ± 0.151^{a}	3.142 ± 0.320^{a}	0.132	0.995
G2	0.039 ± 0.013^{b}	1.263 ± 0.092^{b}	1.282 ± 0.188^{b}	-0.002	0.997
G3	0.039 ± 0.001^{b}	0.802 ± 0.035^{c}	0.648 ± 0.053^{b}	0.012	0.999
G4	0.038 ± 0.017^{b}	0.707 ± 0.045^{c}	0.680 ± 0.213^{b}	0.002	0.999
G5	0.043 ± 0.004^{b}	0.794 ± 0.048^{c}	0.552 ± 0.059^{b}	0.020	0.998

Source: own authorship.

Materials that are permanently deformed generally have a higher resistance to recovery and therefore a lower value of λ2 than λ1. This behavior occurred for all tested gel samples, with the exception of the sample G2. The λ2 parameter can have values between 0 and λ1, indicating an infinite resistance (without recovery, λ2=0), or a recovery equal to the creep (λ2=λ1) (SPOTTI *et al.*, 2017). Thus, the λ1 -λ2 analysis is useful to compare how materials recover. In general, smaller differences between these parameters indicate materials with greater recovery capacity as observed in EFG (G2 -G5), with λ1 -λ2 an average of 0.008, while non-filled gel showed a higher value of 0.132. The emulsion droplets in the gel matrix insert a softer and, at the same time, more resistant material into the system, and thus, as previously discussed, it promotes increased interactions between the chains, which allows a greater possibility of EFG recovery.

Brito-Oliveira *et al.* (2022) produced gels of soy protein isolate (SPI), xanthan gum (XG) and locust bean gum (LBG), loaded with emulsion stabilized by Tween 80 and Span 80, with 4.5 % (w/w) of oil phase, and reported satisfactory adjustments to the fractional model ($R^2 = 0.913$). The λ1 -λ2 values (0.110 - 0.011) were similar to those reported in our study, with a reduction in this parameter for

EFG compared to non-filled gel. However, the α (0.16 - 0.20) for these authors was higher than that found in this study, indicating more viscous gels. This variation is due to the different types of emulsifiers, matrix material, oil fractions and methodologies employed in the production of EFG. In our case, it is expected that the EFG produced from Pickering-type emulsions present a more elastic material, due to the flexible behavior of the particles at the interface of the droplet and the starch matrix.

Conclusion

EFG were developed with different proportions of curcumin loaded Pickering emulsion. Intermediate emulsion concentrations were shown to have greater color and curcumin stability. Increasing the proportion emulsion significantly improved the texture properties of the EFG, such as hardness, as well as the water holding capacity, the G' and G" values and allowed the formation of a more compact network, filling the spaces in the gel networks. The emulsion droplets stabilized with modified cassava starch nanoparticles acted as active fillers in a native quinoa starch gel, allowing the design of a solid and smooth network encapsulating several oil droplets with an encapsulated lipophilic bioactive. Thus, we can state that these emulsion-filled gels could certainly find applications in the food and personal care industries for the delivery of lipophilic molecules.

Acknowledgments

The authors thank:

- This study was financed in part by the Coordenação de Aperfeiçoamento de Pessoal de Nível Superior - Brasil (CAPES) - Finance Code 001.
- The access to equipment and assistance provided by the National Institute of Science and Technology on Photonics Applied to Cell Biology (INFABIC) at the State University of Campinas; INFABIC is co-funded by the Research Support Foundation of the State of São Paulo (FAPESP) (2014/50938-8) and National Council for Scientific and Technological Development (CNPq) (465699/2014-6).

References

AACC. **American Association of Cereal Chemists. Approved Methods of the AACC (10th Methods)**Saint Paul, Minnesota: AACC, 1995. .

ADITYA, N. P. *et al.* Curcumin and genistein coloaded nanostructured lipid carriers: In vitro digestion and antiprostate cancer activity. **Journal of Agricultural and Food Chemistry**, v. 61, n. 8, p. 1878–1883, 2013.

AHMED, J.; DHULL, S. B.; CHANDAK, A. Rheology and rheological measurements of starch. **Advances in Food Rheology and Its Applications** Second Edition, 2023.

ANBARANI, N. M.; ALI RAZAVI, S. M.; TAGHIZADEH, M. Impact of sage seed gum and whey protein concentrate on the functional properties and retrogradation behavior of native wheat starch gel. **Food Hydrocolloids**, v. 111, n. August 2020, p. 106261, 2021.

BHARDWAJ, M.; SANDHU, K. S.; SAXENA, D. C. Experimental and modeling studies of the flow, dynamic and creep recovery properties of pearl millet starch as affected by concentration and cultivar type. **International Journal of Biological Macromolecules**, v. 135, p. 544–552, 2019.

BORRIN, T. R. *et al.* Curcumin-loaded nanoemulsions produced by the emulsion inversion point (EIP) method: An evaluation of process parameters and physico-chemical stability. **Journal of Food Engineering**, v. 169, p. 1–9, 2016.

BRITO-OLIVEIRA, T. C. *et al*. Cold-Set Gelation of Commercial Soy Protein Isolate: Effects of the Incorporation of Locust Bean Gum and Solid Lipid Microparticles on the Properties of Gels. **Food Biophysics**, v. 13, p. 226–239, 2018.

BRITO-OLIVEIRA, T. C. *et al.* Modeling creep / recovery behavior of cold-set gels using different approaches. **Food Hydrocolloids**, v. 123, n. September 2021, p. 107183, 2022.

BU, X. *et al.* Fabrication of starch-based emulsion gel beads by an inverse gelation technique for loading proanthocyanidin and curcumin. **Food**

Hydrocolloids, v. 137, n. November 2022, 2023.

CHANG, Y. Y. *et al.* Effect of gums on the rheological characteristics and microstructure of acid-induced SPI-gum mixed gels. **Carbohydrate polymers**, v. 108, n. 1, p. 183–191, 8 ago. 2014.

CIEŚLA, K.; SARTOWSKA, B.; KRÓLAK, E. SEM studies of the structure of the gels prepared from untreated and radiation modified potato starch. **Radiation Physics and Chemistry**, v. 106, p. 289–302, 2015.

DAMMAK, I.; SOBRAL, P. J. do A. Investigation into the physicochemical stability and rheological properties of rutin emulsions stabilized by chitosan and lecithin. **Journal of Food Engineering**, v. 229, p. 12–20, 2018a.

DAMMAK, I.; SOBRAL, P. J. do A. Formulation optimization of lecithin-enhanced pickering emulsions stabilized by chitosan nanoparticles for hesperidin encapsulation. **Journal of Food Engineering**, v. 229, p. 2–11, 2018b.

DAMMAK, I.; SOBRAL, P. J. do A. Curcumin nanoemulsions stabilized with natural plant-based emulsifiers**. Food Bioscience**, v. 43, n. August, p. 101335, 2021.

DICKINSON, E. Emulsion gels: The structuring of soft solids with protein-stabilized oil droplets. **Food Hydrocolloids**, v. 28, n. 1, p. 224–241, 2012.

DUN, H. *et al.* Influence of O/W emulsion on gelatinization and retrogradation properties of rice starch. **Food Hydrocolloids**, v. 103, p. 105652, 1 jun. 2020.

DUN, H. *et al.* Influence of an O/W emulsion on the gelatinization, retrogradation and digestibility of rice starch with varying amylose contents. **Food Hydrocolloids**, v. 113, n. October 2020, p. 106547, 2021.

FENG, T. *et al.* Emulsion-based delivery systems for curcumin: Encapsulation and interaction mechanism between debranched starch and curcumin. **International Journal of Biological Macromolecules**, v. 161, p. 746–754, 15 out. 2020.

GEREMIAS-ANDRADE, I. M. *et al.* Rheological and mechanical characterization of curcumin-loaded emulsion-filled gels produced with whey protein isolate and xanthan gum. **Lwt**, v. 86, p. 166–173, 2017.

ISO. Determination of amylose content. **Norme ISO 6647, Cereals, pulses and derived products**, p. 4, 1987.

KAMWILAISAK, K. *et al.* Rheology, stability, antioxidant properties, and curcumin release of oil-in-water Pickering emulsions stabilized by rice starch nanoparticles. **International Journal of Biological Macromolecules**, v. 214, n. March, p. 370–380, 2022.

KEETELS, C. J. A. M.; VLIET, T. va.; WALSTRA, P. Gelation and retrogradation of concentrated starch systems: 2. Retrogradation. **Food Hydrocolloids**, v. 10, n. 3, p. 355–362, 1996.

LI, G.; ZHU, F. Rheological properties in relation to molecular structure of quinoa starch. **International Journal of Biological Macromolecules**, v. 114, p. 767–775, 2018.

LI, S. *et al.* Pickering emulsion gel stabilized by octenylsuccinate quinoa starch granule as lutein carrier : Role of the gel network. **Food Chemistry**, v. 305, p. 125476, 2020.

LI, X. M. *et al.* Investigation of the fabrication, characterization, protective effect and digestive mechanism of a novel Pickering emulsion gels. **Food Hydrocolloids**, v. 117, n. September 2020, p. 106708, 2021.

LIU, G. *et al.* Insights into the changes of structure and digestibility of microwave and heat moisture treated quinoa starch. **International Journal of Biological Macromolecules**, v. 246, n. 29, p. 125681, 2023.

LYU, Z.; SALA, G.; SCHOLTEN, E. Melting properties of vegan cheese: Effect of emulsion and protein addition on the thermal behaviour of starch gels. **Food Hydrocolloids**, v. 144, n. May, p. 108917, 2023.

MAO, L. *et al.* Design of gel structures in water and oil phases for improved delivery of bioactive food ingredients. **Critical Comments on Food Science and Nutrition**, v. 60, p. 1651–1666, 2020.

MU, R. *et al.* Improvement of extrudability and self-support of emulsion-filled starch gel for 3D printing: Increasing oil content. **Carbohydrate Polymers**, v. 301, n. PA, p. 120293, 2023.

NIU, H. *et al.* The interfacial behavior and long-term stability of emulsions stabilized by gum arabic and sugar beet pectin. **Carbohydrate Polymers**, v. 291, n. February, p. 119623, 2022.

ONG, L. *et al.* The effect of pH at renneting on the microstructure, composition and texture of Cheddar cheese. **Food Research International**, v. 48, n. 1, p. 119–130, 2012.

RAMOS, G. V. C. *et al.* Encapsulation of curcumin in Pickering emulsions stabilized with modified starch nanoparticles. **Food Hydrocolloids**, (submitted article), 2023a.

RAMOS, G. V. C. *et al.* Dual modification of cassava starch by physical treatments for production of Pickering stabilizers. **Journal of Polymers and the Environment**, (submitted article), 2023b.

RAVIADARAN, R. *et al.* Optimization of palm oil in water nano-emulsion with curcumin using microfluidizer and response surface methodology. **Lwt**, v. 96, n. March, p. 58–65, 2018.

SANT'ANNA, V. *et al.* Tracking bioactive compounds with colour changes in foods - A review. **Dyes and Pigments**, v. 98, n. 3, p. 601–608, 2013.

SPOTTI, M. J. *et al.* Whey protein gelation induced by enzymatic hydrolysis and heat treatment: Comparison of creep and recovery behavior. **Food Hydrocolloids**, v. 63, p. 696–704, 2017.

STEFFE, J. F. **RHEOLOGICAL METHODS IN FOOD PROCESS ENGINEERING**. second ed. Michigan: Freeman Press, 1996.

TORRES, O. *et al.* Novel starch based emulsion gels and emulsion microgel particles : Design , structure and rheology. **Carbohydrate Polymers**, v. 178, n. September, p. 86–94, 2017.

VELÁSQUEZ-CASTILLO, L. E. *et al.* Quinoa starch nanocrystals production by acid hydrolysis: Kinetics and properties. **International Journal of Biological Macromolecules**, v. 143, p. 93–101, 2020.

VLIET, T. Van. Rheological properties of filled gels . Influence of filler matrix interaction. **Colloid and Polymer Science,** v. 524, p. 518–524, 1988.

WANG, C. *et al.* Substituent distribution changes the pasting and emulsion properties of octenylsuccinate starch. **Carbohydrate Polymers**, v. 135, p. 64–71, 2016.

WANG, R. *et al.* Characterization of Pickering emulsion by SCFAs-modified debranched starch and a potent for delivering encapsulated bioactive compound. **International Journal of Biological Macromolecules**, v. 231, p. 123164, 15 mar. 2023.

WANYI, W. *et al.* Comparison of emulsifying characteristics of different macromolecule emulsifiers and their effects on the physical properties of lycopene nanoemulsions. **Journal of Dispersion Science and Technology**, v. 41, n. 4, p. 618–627, 2020.

XU, T. *et al.* Formation, stability and the application of Pickering emulsions stabilized with OSA starch/chitosan complexes. **Carbohydrate Polymers**, v. 299, n. September 2022, p. 120149, 2023.

YU, B. *et al.* The effects of acetylated distarch phosphate from tapioca starch on rheological properties and microstructure of acid-induced casein gel. **International Journal of Biological Macromolecules**, v. 159, p. 1132–1139, 2020.

ZHANG, L. *et al.* Enzymatically modified quinoa starch based pickering emulsion as carrier for curcumin: Rheological properties, protection effect and in vitro digestion study. **Food Bioscience**, v. 49, n. July, p. 101933, 2022.

ZHANG, R. *et al.* Enhanced freeze-thawing stability of water-in-oil Pickering emulsions stabilized by ethylcellulose nanoparticles and oleogels. **Carbohydrate Polymers**, v. 312, n. March, p. 120814, 2023.

ZHAO, X. *et al.* Role of gelation temperature in rheological behavior and microstructure of high elastic starch-based emulsion-filled gel. **Food Hydrocolloids**, v. 135, n. July 2022, p. 108208, 2023.

ZHU, F. Starch based Pickering emulsions: Fabrication, properties, and applications. **Trends in Food Science & Technology**, v. 85, p. 129–137, 1 mar. 2019.

ZHU, F. Quinoa starch. **Chemistry and Technology**, p. 69–91, 2023.

6. CAPÍTULO 6: CONCLUSÕES GERAIS

6.1. Conclusões gerais

A modificação combinada do amido de mandioca por HMT e nanoprecipitação (método antissolvente), resultou em partículas (HSNP) com capacidade de estabilizar emulsões O/A. No processo de produção das nanopartículas HSNP foram utilizadas somente técnicas verdes (modificações físicas) Essas modificações resultaram em características e propriedades (superfície rugosa, baixa carga superficial, baixa cristalinidade, maior hidrofobicidade e tamanhos nanométricos) que viabilizaram a estabilização da emulsão *Pickering* por até 14 dias. Na produção das emulsões, concentrações menores que 3% (g SNP/100g de emulsão) não foram suficientes para estabilizar esse sistema, independentemente do tipo de SNP. As emulsões foram estabilizadas com 4 g de HSNP/ 100 g de emulsão e essa estrutura foi selecionada para encapsular a curcumina. A microestrutura das emulsões confirmou que as HSNP se alocaram na interface da gota de óleo, formando uma barreira física com uma forte resistência à desestabilização. A tensão interfacial e o potencial zeta confirmaram que o método de estabilização do sistema era *Pickering*, já que apresentava uma rápida tendência de equilíbrio da tensão e baixos valores de carga superficial. A análise quantitativa da curcumina encapsulada mostrou uma retenção de aproximadamente 100% ao longo de um período de 60 dias de armazenamento, o que demonstra o potencial do sistema desenvolvido em termos de proteção e encapsulação do bioativo. Os géis à base de amido de quinoa carregados de emulsão (EFG) foram desenvolvidos com diferentes quantidades de emulsão *Pickering* na formulação. A análise de cor foi feita como um indicativo da estabilidade da curcumina nos EFG e as formulações com a proporção de 75 e 50% de emulsão se mostraram mais estáveis. A análise de microestrutura por MEV, a avaliação da capacidade de retenção de água, o teste de compressão e as análises reológicas mostraram que os géis com maiores proporções de emulsão na formulação apresentaram uma estrutura mais densa e menos porosa e uma maior interação entre as moléculas de amido a as gotas de óleo, apresentando um comportamento mais elástico do que os

géis com menor proporção de emulsão, que apresentaram um caráter mais viscoso. Isso demonstra que as gotas de emulsão estabilizadas com nanopartículas de amido desempenharam o papel de partícula ativa no gel de amido, explorando possibilidades de construção de diferentes *designs* dos EFG, visando encapsulação e proteção de bioativos.

6.2. Sugestão Para Trabalhos Futuros

- Avaliar o efeito de outros tipos de modificação combinado do amido de mandioca, como o aquecimento em micro-ondas, que é uma técnica de modificação física, rápida e verde, seguida da nanoprecipitação, para aplicação como estabilizantes de emulsão;

- Avaliar o efeito de diferentes óleos e condições de stress (pH, temperatura de armazenamento, força iônica do meio) para o mecanismo de adsorção da nanopartícula de amido de mandioca modificado na interface óleo-água;

- Verificar a incorporação de outros bioativos nas emulsões *Pickering*, avaliando sua estabilidade e as características da emulsão;

- Analisar a digestibilidade das emulsões *Pickering* em condições simuladas do sistema gastrointestinal (*in vitro*);

- Realizar testes de estabilidade dos géis carregados de emulsão ao longo do tempo em diferentes condições, como diferentes temperaturas, pH e intensidades de luminosidade.

- Analisar a digestibilidade dos géis carregados de emulsão em condições simuladas do sistema gastrointestinal *(in vitro*);

- Fazer a aplicação dos géis carregados de emulsão em matrizes alimentícias, como pudins e flans, por exemplo.